Functional studies towards the role of a polymorphism in the human connexin37 gene in atherosclerosis

Derouette, Jean-Paul

UNIVERSITE DE GENEVE

Département de zoologie
et de biologie animale — FACULTE DES SCIENCES
Professeur Jean-Louis Beny

Département de médecine interne — FACULTE DE MEDECINE
Professeur Brenda Kwak

UNIVERSITE DE BERNE

Institut de physiologie — FACULTE DES SCIENCES
Professeur Robert Weingart

Functional studies towards the role of a polymorphism in the human connexin37 gene in atherosclerosis

THESE
présentée à la Faculté des sciences de l'Université de Genève
pour obtenir le grade de Docteur ès sciences, mention biologie

par

Jean-Paul, Jean-François, Alain Derouette
d'Onex (GE)
(Suisse)

Thèse n° 4030
Editeur ou imprimeur
Genève
2008

RESUME EN FRANÇAIS

L'athérosclérose et ces conséquences, sont les premières causes de mortalité dans les pays industrialisés. Dans la majorité des cas, ces constatations cliniques sont consécutives à une rupture ou une érosion d'une plaque d'athérome avec formation d'un thrombus obstruant la lumière de l'artère.

L'hypertension, le tabac, le diabète, l'hypercholestérolémie, les forces hémo-dynamiques du flux sanguin ou encore des facteurs génétiques sont parmi les causes les plus importantes favorisant le développement de l'athérosclérose. L'ensemble de ces facteurs induisent une dysfonction endothéliale chronique qui facilite l'adhésion des lymphocytes T, des monocytes et leur transmigration dans les parois artérielles. Suite à cette infiltration, les monocytes se différentient et s'activent en macrophages qui se chargent en lipides pour devenir des cellules spumeuses, formant ainsi la partie grasse de l'athérome. Au niveau du site de la lésion, ces cellules vont sécréter des molécules inflammatoires capables d'induire la migration des cellules musculaires lisses de la média vers l'intima vasculaire où elles vont proliférer et sécréter la matrice extracellulaire pour former la partie fibreuse de l'athérome. Une littérature scientifique abondante démontre que des facteurs autocrines et paracrines (cytokines, et facteurs de croissance) jouent un rôle important dans la pathogénèse de l'athérosclérose. A part ces facteurs, il a été récemment montré que la communication cellulaire via les jonctions communicantes (jonctions gap) joue un rôle important dans l'initiation et la progression de la maladie athéromateuse. Les jonctions gap sont des structures membranaires permettant la communication directe entre deux cellules adjacentes via l'échange de petits métabolites et d'ions. Ainsi les jonctions gap jouent un rôle majeure dans des processus biologiques tels que la croissance cellulaire, le développement, la

conduction des signaux nerveux, la synchronisation du muscle cardiaque, la régulation cellulaire ou l'homéostasie tissulaire.

Les jonctions gap sont constituées de protéines transmembranaires, les connexines (Cx), qui appartiennent à une famille multi-génique dont 21 membres sont répertoriés. Ces protéines se différencient surtout par leur poids moléculaire et leur séquence C-terminale. Ces variations permettent de les répertorier selon une nomenclature dérivée de leur poids moléculaire (p. ex. la Cx de 37kDa est la Cx37). Les connexines d'un même poids moléculaire s'assemblent pour former un hexamère, qui une fois à la membrane plasmique sera le connexon ou hemi-channel. Deux connexons, issue de cellules adjacentes s'accouplent pour former un canal jonctionnel. Chaque canal jonctionnel possède une signature individuelle définie par ses propriétés de conductance électrophysiologique caractérisée et par ses propriétés de perméabilité et de sélectivité ionique. L'implication de trois Cx vasculaires majeures, Cx37, Cx40 et Cx43 a été récemment démontré lors de la progression de la pathologie athéromateuse. De plus, un polymorphisme pour la Cx37 humaine (hCx37) a été mis en relation avec la fréquence d'observation de cas cliniques de plaque d'athérosclérose (PA) dans les coronaires et le risque d'infarctus du myocarde (IM).

Le but de ce travail de thèse est de déterminer :

1. les propriétés électro-physiologiques, conductance et perméabilité, du polymorphisme de la Cx37 qui pourraient expliquer les différences fonctionnelles observées cliniquement.
2. si le polymorphisme de la Cx37 pourrait impliquer des interactions différentielles avec d'autres protéines, et en particulier le cas de l'enzyme des cellules endothéliales qui synthétise oxyde nitrique.
3. et l'implication de la Cx37 dans les plaques athéromateuse avancées.

Pour répondre à ces questions, des cellules endothéliales humaines (EAHy926) et murines (bEnds.3) ainsi que des cellules épithéliales humaines (HeLa) et des neuroblastes murins (N2a) ont été utilisées. Dans le premier chapitre de ce travail, les cellules HeLa, naturellement déficientes en Cx, ont été transfectées avec la séquence codante pour le polymorphisme hCx37-P319 ou hCx37-S319 de manière à ce qu'elles expriment également cette protéine au niveau membranaire. Ces clones cellulaires stables ont montré des propriétés adhésives différentes (hCx37-P319 moins adhésif) ainsi qu'une excrétion différentielle d'ATP (hCx37-P319 sécrètent plus d'ATP) en milieu pauvre en calcium. De plus, les cellules transfectées avec la hCx37-P319 ont montré une plus grande conductance macroscopique des hémi-canaux ainsi qu'une augmentation dans la conductance d'un canal intercellulaire (300pS pour la hCx37-P319 et 200pS pour la hCx37-S319). Cette différence dans les propriétés électro-physiologiques pourrait ainsi constituer un mécanisme potentiel (effet antiadhésif pour le polymorphisme hCx37-P319) permettant d'expliquer les différences observées cliniquement pour les prédictions des PA et des IM.

Dans le second chapitre, nous avons identifié des motifs peptidiques potentiels qui se lient à la partie carboxyle terminal de la Cx37 (Cx37CT) grâce à la technique de « phage display ». Nous avons ainsi identifié deux séquences consensus au motif adhérant du type: WHK…[K,R]XP et FHK…[K,R]XXP, le premier étant plus fréquent pour la forme hCx37-P319 et le second plus fréquent pour la forme hCx37-S319. Parmi toutes les séquences obtenues, la séquence WHRTPRLPPPVP a été retenue car elle possède une homologie avec la séquence de la NO synthétase endothéliale (eNOS). Cette interaction entre la Cx37-CT et l'eNOS a été confirmé par des techniques in vitro, telles que le « cross-linking » et le « surface plasmon resonance ». De plus, des analyses électro-physiologiques des différents canaux hCx37 révèlent une augmentation des conductances respectives des canaux formés par hCx37-S319 ou par hCx37-P319 en présence d'une séquence peptidique qui simule le site de

liaison d'eNOS à la hCx37. L'interaction et la co-localisation entre les protéines Cx37 et eNOS ont aussi été confirmées in vitro par co-immunoprécipitation et microscopie par immunofluorescence. Par ailleurs, une augmentation de la production de NO a été observée dans les cellules bEnd.3 qui ont été incubées avec un ARN anti-sens pour la Cx37. Ces résultats montrent pour la première fois une interaction fonctionnelle entre eNOS et Cx37, interaction qui pourrait jouer un rôle physiologique dans les vaisseaux et être altérée dans la pathologie de l'athérosclérose.

Dans le troisième chapitre, l'étude du rôle de la Cx37 dans des plaques avancées d'athérome a été réalisée à l'aide de souris knock-out ApoE–/– et Cx37–/–ApoE–/–, qui ont reçues un régime riche en cholestérol pendant 18 semaines. L'artère thoraco-abdominale descendante de ces animaux a été utilisée pour réaliser une analyse de type « microarrays ». Pour confirmer la présence de certaines protéines révélées lors de l'analyse type « microarrays », une analyse histologique/morphométrique des valves aortiques de l'artère ascendante a été réalisée. Avant la modification du régime alimentaire, nous avons montré que des gènes impliqués dans la communication cellulaire et dans la réponse immuno-inflammatoire étaient exprimés différemment entre les deux souches de souris. Après 18 semaines de régime, l'expression de gènes impliqués dans la calcification et la dégradation de la matrice extracellulaire était modifiée. En effet, l'analyse histologique/morphométrique de la plaque d'athérome a montré une augmentation de la calcification et une diminution de la matrice extracellulaire chez la souris Cx37–/–ApoE–/–. En conclusion, il semble que les souris déficientes en Cx37 présentent une altération de l'expression de certains gènes conduisant à un phénotype pro-inflammatoire et démontre que cette Cx peut être impliqué dans la calcification de la paroi vasculaire.

L'ensemble de ces résultats obtenus sur l'implication de la Cx37 et de ses polymorphismes dans l'athérosclérose suggère des implications cliniques telles que l'utilisation de molécules influençant l'expression ou la fonction de cette connexine.

SUMMARY

Atherosclerosis is a chronic inflammatory disease that follows a “response-to-injury scenario”. The first obligatory event is endothelium dysfunction or injury resulting in increased expression of various cell adhesion molecules and secretion of chemo-attractants to recruit specific leukocytes. The many risk factors that are implicated in the first step of atherogenesis are all linked by their common ability to promote inflammatory reactions. Monocytes will adhere to the dysfunctional endothelium and then transmigrate to penetrate into the arterial intima. In the intima, monocytes proliferate, mature and accumulate lipids, eventually progressing into macrophage foam cells, which is a hallmark of atherosclerosis.

A genetic polymorphism in the human connexin37 (Cx37) gene at position 1019 gene has been reported as a potential prognostic marker for atherosclerosis; the polymorphism represents a variation in one nucleotide (C-to-T), which results in a change of a proline into a serine at amino acid 319 in the C-terminus of Cx37 (Cx37CT). Members of the connexin protein family (21 genes) form gap junction channels and hemichannels with unique properties including the distinctive unitary conductance and permeability for various signalling molecules. The expression pattern of Cx37 is altered in mouse and human atherosclerotic lesions, disappearing from the endothelium of advanced plaques while being detected in macrophages recruited to the lesions. This alteration in Cx37 expression during atherogenesis will likely change the communication between atheroma-associated cells as well as between these cells and the extracellular space. Our group has recently demonstrated that Cx37 hemichannels control the initiation of atherosclerotic plaque development by regulating ATP-dependent monocyte adhesion in atherosclerosis-susceptible apolipoprotein E-deficient mice. Nevertheless, little is known about how the Cx37 polymorphism might affect ATP release and cell adhesion. Moreover, the role of Cx37 in advanced atherosclerosis

has not been studied this far. The aim of my PhD work was to gain further insight into the participation of Cx37 in advanced atherosclerosis and into the biophysical and interactive properties of Cx37 hemichannels or gap junction channels.

In the first chapter, we searched for the electrophysiological properties and the functional consequences of the Cx37 polymorphism. Therefore, we measured the electrical properties of Cx37 hemichannels (HCs) and gap junction channels (GJCs) with voltage-clamp methods. To this end, we have transfected hCx37-P319, hCx37-S319 or empty pIRES-eGFP vector cDNA into communication-deficient HeLa cells. The analysis of voltage-sensitive HC current yielded a bell-shaped function (normalized conductance at steady state), indicating a double gating process. We observed differences in macroscopic conductances of polymorphic hemichannels. Experiments on cell pairs revealed differences in unitary conductances of polymorphic gap junction channels. In addition, we found that Cx37-P319 cells released more ATP and were less adhesive than Cx37-S319 cells. We conclude that the differences in biophysical properties between polymorphic HCs may be responsible for inequality in ATP release between Cx37-P319 and Cx37-S319 cells, which results in differential cell adhesion.

In the second chapter, we identified potential binding motifs for Cx37-P319-CT and Cx37-S319-CT. Using a high throughput phage display, we retrieved 2 consensus binding motifs for Cx37CT: WHK…[K,R]XP and FHK…[K,R]XXP, the first one being more frequent for Cx37-P319 and the second more frequent for Cx37-S319. One of the motifs (WHRTPRLPPPVP) showed a high homology with the endothelial nitric oxide synthase (eNOS). *In vitro* binding of this peptide to both forms of Cx37CT was confirmed by cross-linking and surface plasmon resonance. Electrophysiological analysis of Cx37 single channel activity in transfected N2a cells showed that eNOS-like peptides increased the frequency of occurrence of conductances higher than 300 pS. eNOS co-immunoprecipitated with Cx37 in human endothelial cells (ECs) transfected with the Cx37 polymorphs and in a mouse EC line

(bEnd.3). Immunofluorescence microscopy showed a co-localization of these proteins at membranes in bEnd.3 cells. A dose-dependent increase in NO production was observed in bEnd.3 cells treated with Cx37-antisense. Overall, our data show for the first time a functional interaction between eNOS and Cx37. This interaction may be relevant for the control of vascular physiology both in health and in disease.

In the third chapter, we used a micro-array based approach to investigate the molecular role of Cx37 in advanced atherosclerosis. For this purpose, advanced atherosclerosis was induced in $ApoE^{-/-}$ and $Cx37^{-/-}$ $ApoE^{-/-}$ mice by feeding them a cholesterol-rich diet for 18 weeks. Aortic mRNA was extracted from $ApoE^{-/-}$ and $Cx37^{-/-}ApoE^{-/-}$ mice before (at age of 10 weeks) and after cholesterol-rich diet (at age of 28 weeks) to perform micro-array analysis. At 10 weeks of age, 100 genes were significantly differentially expressed implicated in stress-responsive genes and inflammatory molecules, possibly contributing to enhanced atherosclerotic plaque development in $Cx37^{-/-}ApoE^{-/-}$ mice. In addition, we identified 95 genes that were significantly perturbed after the cholesterol-rich diet and that mostly included genes involved in calcium handling metabolism and matrix degradation, some of which were further confirmed at protein level. Furthermore, Von Kossa staining revealed increased calcium deposits in atherosclerotic lesions of $Cx37^{-/-}ApoE^{-/-}$ mice. In conclusion, we suggest that Cx37 deficiency alters the global differential gene expression profiles in young mice towards a pro-inflammatory phenotype, which are then further influenced in advanced atherosclerosis.

The work presented in this PhD thesis demonstrates that the Cx37 polymorphism modifies the electrophysiological properties of the channels formed by it, which provides a possible explanation for the association between the Cx37 polymorphism and risk on myocardial infarction observed in epidemiological studies. In addition, a functional interaction between Cx37CT and eNOS has revealed, which might play a role in the

physiological regulation of blood vessel tone as well as in development of disease. Finally, we have demonstrated that Cx37 also affects the advanced atherosclerotic lesion with possible implications on plaque vulnerability. All together, it might be worth to aim future research on developing and testing molecules that affect Cx37 expression or function in purpose of clinical use.

RESEARCH COMMUNICATIONS

1.1 PUBLICATIONS

Pfenniger A, **Derouette JP**, Verma V, Lin X, Foglia B, Coombs W, Roth I, Satta N, Dunoyer-Geindre S, Sorgen P, Taffet S, Kwak BR, Delmar M. **Gap Junction Protein Cx37 Interacts With Endothelial Nitric Oxide Synthase in Endothelial Cells.** Arterioscler Thromb Vasc Biol. 2010 Jan 15.

Derouette JP, Wong C, Burnier L, Morel S, Sutter E, Galan K, Brisset AC, Roth I, Chadjichristos CE, Kwak BR. **Molecular role of Cx37 in advanced atherosclerosis: a micro-array study.** Atherosclerosis. 2009 Sep; 206(1):69-76.

Derouette JP, Desplantez T, Wong CW, Roth I, Kwak BR, Weingart R. **Functional differences between human Cx37 polymorphic hemichannels.** J Mol Cell Cardiol. 2009 Apr; 46(4):499-507.

Chadjichristos CE, Morel S, **Derouette JP**, Sutter E, Roth I, Brisset AC, Bochaton-Piallat ML, Kwak BR. **Targeting connexin 43 prevents platelet-derived growth factor-BB-induced phenotypic change in porcine coronary artery smooth muscle cells.** Circ Res. 2008 Mar 28; 102 (6): 653-60. Epub 2008 Jan 31.

Wong CW, Christen T, Roth I, Chadjichristos CE, **Derouette JP**, Foglia BF, Chanson M, Goodenough DA, Kwak BR. **Connexin37 protects against atherosclerosis by regulating monocyte adhesion.** Nat Med. 2006 Aug; 12 (8): 950-4. Epub 2006 Jul 23.

Chadjichristos CE, **Derouette JP**, Kwak BR. **Connexins in atherosclerosis.** Adv Cardiol. 2006; 42: 255-67. Review.

Chanson M, **Derouette JP**, Roth I, Foglia B, Scerri I, Dudez T, Kwak BR. **Gap junctional communication in tissue inflammation and repair.** Biochim Biophys Acta. 2005 Jun 10; 1711(2): 197-207. Epub 2004 Oct. 30. Review.

1.2 IMPORTANT COMMUNICATIONS

July 2008: Oral presentation (20min) at the French Gap Junction Meeting in Poitiers: Enhanced calcification in advanced atherosclerotic lesions of Cx37-deficient mice.

October 2007: Oral presentation (15min) at the 13ème Swiss Cardiovascular Biology and Clinical Implications Meeting: Functional differences between human Cx37 polymorphic hemichannels.

September 2007: Oral presentation (10min) at the Swiss Physiology Annual Meeting: Functional differences between human Cx37 polymorphic hemichannels. And a poster session at the 4th European Meeting on Vascular Biology and Medecine (EMVBM).

August 2007: Oral presentation (20min) at the International Gap Junction Meeting in Copenhagen: Functional differences between human Cx37 polymorphic hemichannels.

October 2006: First prize (Asher-Hess Prize, 2006) at the Swiss Physilogy Annual Meeting, poster session plus short talk. Human connexin37 polymorphic hemichannels: are they functionally different?

August 2003: poster presentation at the International Gap Junction Meeting in Cambridge (UK): Reduction of connexin43 expression by statins in human vascular cells and mouse atherosclerosis lesions.

LIST OF ABBREVIATIONS

ADP	adenosine diphosphate
ATP	adenosine triphosphate
AF	aldehyde-fuchsine
AHA	American Heart Association
ApoB	apolipoprotein B
ApoE	apolipoprotein E
$ApoE^{-/-}$	ApoE-deficient
AQP0	aquaporin-0
ATP	adenosine triphosphate
BH_4	tetrahydrobiopterin
CaM	calmodulin
CK1	casein kinase 1
(h)Cx	(human) connexin
Cx37CT	connexin 37 C-terminal domain
CL	connexin cytoplasmic loops
ECs	endothelial cells
eNOS	endothelium nitric oxide synthase
ECM	extracellular matrice
EV	empty vector
E1 and E2	connexin extracellular loops
GJIC	gap junctional intercellular communication
GJC	gap junction channels
FGF	fibroblast growth factor

HE	hematoxylin-eosin
HMG-CoA	3-hydroxy-3-methylglutaryl-CoA
IPA	Ingenuity Pathway Analysis (software)
IL	interleukin
IGF-1	insulin growth factor-1
JAM	Junctional Associated Molecule
K_D	Dissociation constants
LDL	low density lipoprotein
LDLR($^{-/-}$)	low density lipoprotein receptor (deficient)
LPS	lipopolysaccharide
LOX-1	lectin-like receptor for ox-LDL
LY	Lucifer Yellow
MAPK	mitogen activated protein kinase
MMP	matrix metalloproteinase
M1–M4	four cytoplasmic membrane domains
MW	molecular weights
NB	Neurobiotin
PBS	phosphate-buffered saline
PDGF-BB	platelet-derived growth factor-BB
PPs	protein phosphatases
RPTP	receptor protein tyrosine phosphatases
SMCs	smooth muscle cells
SPR	surface plasmon resonance
TNF	tumor necrosis factor

TABLE OF CONTENT

1. GENERAL INTRODUCTION

Cardiovascular diseases are currently the major cause of death and disability in western countries [1]. Their numbers are also increasing in developing countries. Atherosclerosis is an inflammatory disease [2] of medium and large arteries, and its consequences, such as stroke and myocardial infarction, represent the major cause of death worldwide.

1.3 STRUCTURE AND FUNCTION OF HEALTHY BLOOD VESSELS

The cardiovascular system is a continuous, completely closed structure which comprises the heart and the blood vessels. It is divided into the systemic (peripheral) and the pulmonary circulations.

The architecture of the vasculature depends on functional requirements at different locations. To withstand the pulsatile and higher blood pressures in arteries, arterial walls are generally thicker than their venous counterparts (Figure 1). Arterial wall thickness gradually diminishes as the vessels become smaller, but the ratio of the wall thickness to lumen diameter becomes greater. In order to keep a constant blood flow through the entire system, the ratio of the pressure to cross-sectional area of the vessel must be kept constant. The brain, liver and digestive tract, kidneys, and skeletal muscles receive most of the blood that is pumped out of the heart. Veins have a larger overall diameter, a larger lumen, and a thinner wall than their corresponding arteries.

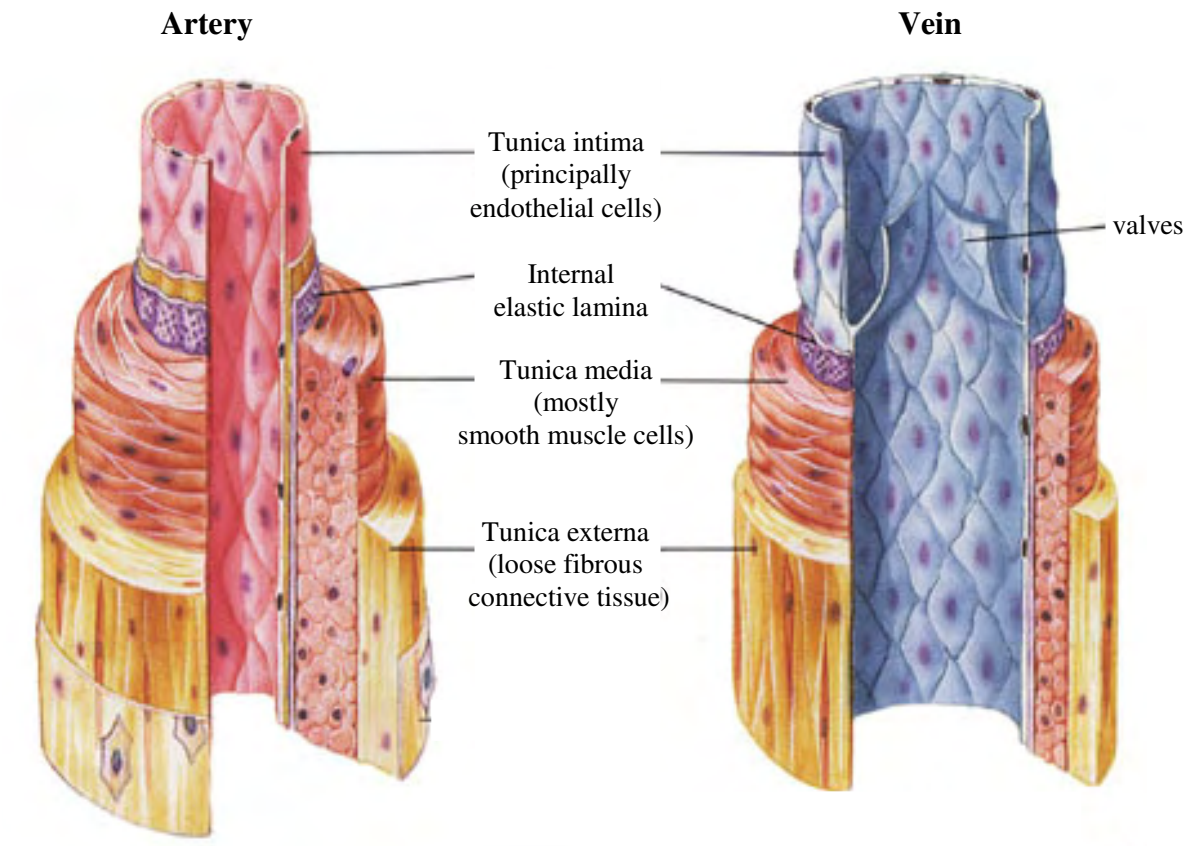

Figure 1: Schematic representation of the main components of an artery (left) and vein (right). Adapted from: Fox & Stuart, Human Physiology, 4th edition, 2002.

Arteries are divided into three types, based on their size and structural features:

1. large or elastic arteries, including the aorta and its large branches such as femoral arteries;
2. medium-sized or muscular arteries comprising, for example, coronary arteries, also referred to as distributing arteries;
3. small arteries, less than 1.9 mm diameter, which generally cross tissues and organs.

The basic constituents of the walls of blood vessels comprise from inside to outside endothelial cells (ECs), smooth muscle cells (SMCs) and fibrous tissue (extra cellular matrix

(ECM), including elastic elements, collagen, and proteoglycans). They are arranged in three concentric layers (Figure 2):

1. The intima is formed by a monolayer of ECs that covers the luminal surface of every vessel, the internal elastic lamina and a very thin layer of sub-endothelial connective tissue. The endothelium is continuous with the endocardium in the heart. The normal properties of the endothelium include low permeability (continuous and with many tight junctions), alignment of cells with a smooth surface and with anti-adhesive properties in order to reduce flow friction to the minimum as well as anti-coagulant properties [3].
2. The media, which is usually the thickest layer in arteries, is mainly composed of SMCs concentrically disposed within elastin layers. They vary their level of intrinsic contraction depending on the needs of the organ they irrigate. This is regulated by the sympathic/parasympathic nerve system as well as local endothelial and tissue-derived factors. Small changes in arterial diameter have a substantial impact on blood pressure.
3. The adventitial layer, also called externa, is rich in collagen fibers that are loosely intertwined. In large arteries, nerves, lymphatic vessels as well as small blood vessels run through it. These vessels, also called vasa vasorum, feed the external tissue from the large vessels; the internal part of the vessel being directly fed from the blood going through it.

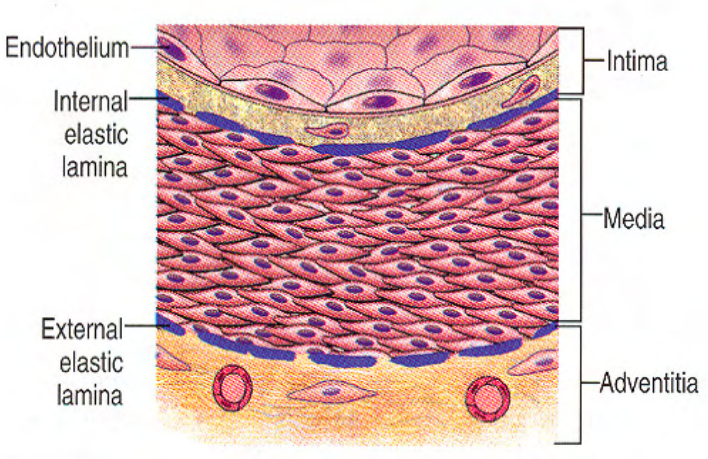

Figure 2: The normal vascular wall.

A schematic representation of the main components of the vascular wall, seen here in a muscular artery. From: Robbins and Cotran, Pathologic basis of disease, 7th edition, 2004.

The relative amount and configuration of the basic constituents vary along the arterial system owing to local adaptations to mechanical or metabolic needs. In the elastic arteries, the media is rich in elastic fibers, disposed in fairly compact layers separated by layers of SMCs. They are dampening the pulsatile pressure that results from the intermittent ejection of blood from the heart (Windkessel function). The dampening is a function of arterial compliance ($\Delta V/\Delta P$ at a given pressure), which is determined in large part by the relative proportion of elastin fibers versus smooth muscle and collagen in the vessel wall. In muscular arteries and arterioles, the media is predominantly composed of SMCs arranged circularly or spirally. Elastin is limited to the internal and external membranes. Small arteries and arterioles represent the primary resistance vessels; changes in the state of contraction of the medial SMCs cause dramatic adjustments of lumen diameter that regulate systemic arterial blood pressure and blood flow within organs. As arterioles become smaller in diameter (<10 µm), they lose their smooth muscle. Vessels that have no smooth muscle and are composed of only ECs and a basement membrane are called capillairies.

Some pathologic conditions involve arteries of a particular size range. For example, atherosclerosis affects large elastic and muscular arteries, hypertension affects primarily small

muscular arteries and arterioles, and specific types of vasculitis are associated with certain vascular segments [4].

1.4 PATHOGENESIS OF ATHEROSCLEROSIS

1.4.1 General

Atherosclerosis and its devastating clinical complications are the underlying cause of about 50% of all death in westernized societies [5]. Consequently, it is the first cause of all morbidity and mortality in the adult population. The disease has an early asymptomatic onset. Lesions are already present in most young adults, but it usually takes decades to evolve into complicated lesions responsible for acute myocardial infarction, brain ischemia or aortic aneurysm. Epidemiological studies have revealed several important environmental and genetic risk factors associated with atherosclerosis, such as hypercholesterolemia, hypertension, smoking, diabetes, hemodynamics and immune reactions [6, 7]. New research tools such as genetically modified mouse models of the disease have resulted in improved understanding of the molecular mechanisms that connect altered cholesterol metabolism and other risk factors to the development of atherosclerotic plaques. It is now well-accepted that atherosclerosis is not simply an inevitable degenerative consequence of ageing, but rather a chronic inflammatory condition that may run into an acute clinical event by plaque rupture and thrombosis [8, 9].

The name, atherosclerosis has been proposed in 1904 by Dr. Marchand who described the association of an atheroma and a sclerosis in artery walls [10]. Atheroma, in Greek "*Athéré*", stands for the jelly part, rich in lipids, in the center of the lesion, also named lipid core, which is also characterized by the presence of necrotic cells. Sclerosis, "*Skléros*" stands for hard in Greek and refers to the fibrous cap, a skeleton of the plaque made of SMCs surrounded by dense extracellular matrix such as collagen, elastin and proteoglycans. The respective parts,

atheroma and sclerosis, vary from one atherosclerotic plaque to another, thus influencing the evolution of the lesion as well as the associated clinical complications.

Atherosclerosis is a process of multi-factorial origin that progresses very slowly and already starts during adolescence. Atherosclerotic lesions grow into nodular plaques in the vascular wall of large arteries, creating a reduction of the vascular lumen called stenosis. An American Heart Association (AHA)-based classification divides them in six categories (Figure 3):

1. Early lesions, characterized by the presence of cholesterol-engorged macrophages, called "foam cells" in the sub-endothelium. In human, they can be found in the aorta in the first decade of life, in the coronary arteries in the second decade, and in the cerebral arteries in the third or fourth decade.
2. Fatty streak lesions, mainly characterized by intra-cellular lipid accumulation
3. Intermediate lesions, in which lipid-rich necrotic debris (small extra-cellular lipid pools) and smooth muscle foam cells are observed. Necrosis is possibly due to the cytotoxic effect of oxidized low-density lipoprotein (LDL) taken up by macrophages via their scavenger receptors.
4. Atheroma lesions, with a core of extra-cellular lipid, which will evolve either in type 5 or in type 6:
5. Fibrous plaques with a fibrous cap consisting of a high number of SMCs and extra-cellular matrix that enfold a rich lipid core.
6. Complicated advanced lesions with calcification within the plaque [11] and ulceration at the luminal surface.

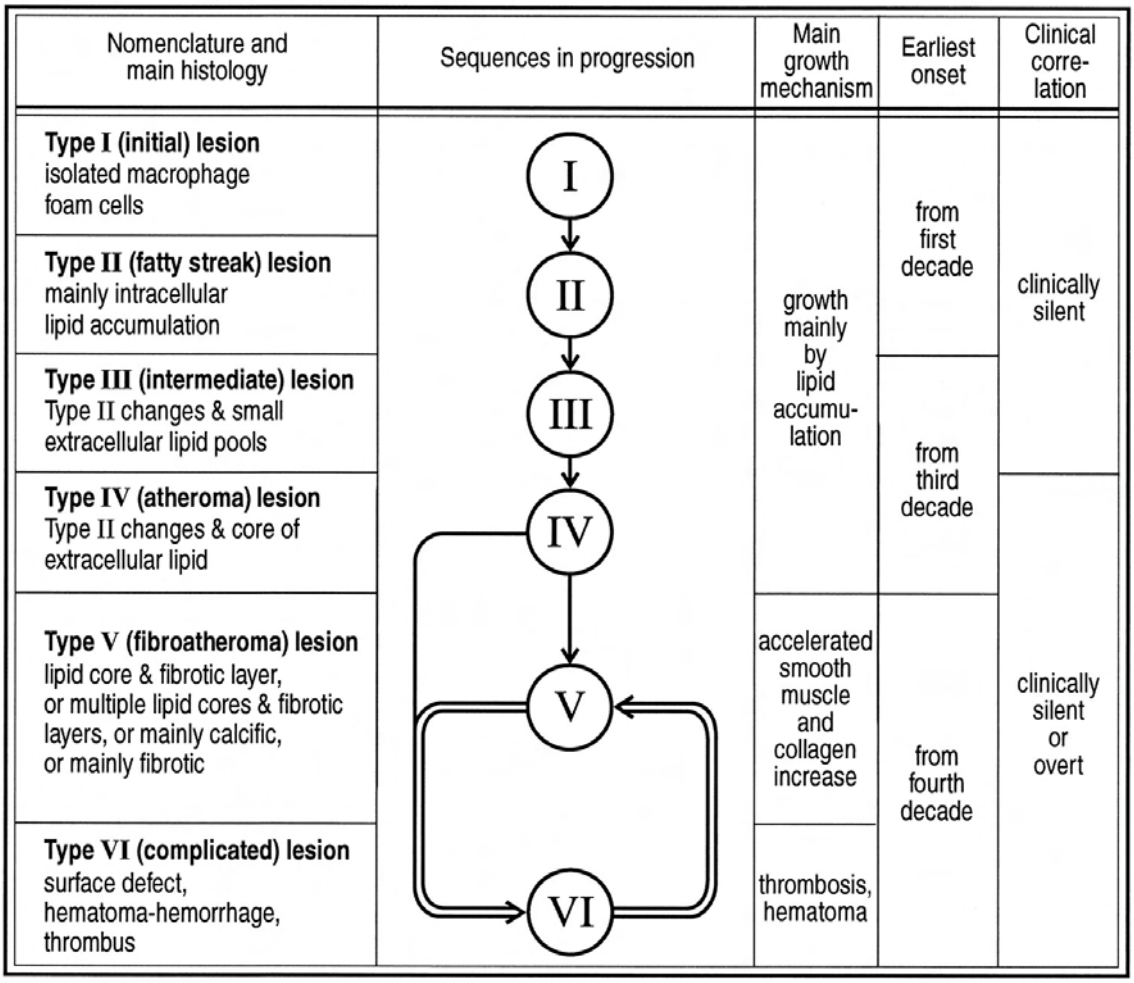

Figure 3: Six different stages of atherosclerosis.

Flow diagram in center column indicates pathways in evolution and progression of human atherosclerotic lesions. Roman numerals at the left of the flow diagram indicate histologically characteristic types of lesions. The direction of arrows indicates sequence in which characteristic morphologies may change. From type I to type IV, changes in lesion morphology occur primarily because of increasing accumulation of lipid. The loop between types V and VI illustrates how lesions increase in thickness when thrombotic deposits form on their surfaces. Thrombotic deposits may form repeatedly over varied time spans in the same location and may be the principal mechanism for gradual occlusion of medium-sized arteries. From: Naghavi M, *et al.,* (Circulation. 2003). [12]

It is common to observe plaques at different stages of development in the same patient suffering from atherosclerosis. Usually, early and intermediate lesions are not associated with clinical symptoms. It is important to understand that the extreme pathological consequences of atherosclerosis, i.e. complete artery obstruction with cellular ischemia and necrosis of the

organ, are often not due to the stenotic process itself. Instead it is frequently induced by the rupture of the fibrous cap, resulting in contact between circulating inactive coagulation factors and activating compounds of the inner atherosclerotic plaque (mainly tissue factor), which triggers blood clotting resulting in occlusion of the vessel lumen.

Vascular calcification is also increasing with age and, as it has been shown in human coronary arteries, this process starts already in the second decade of life, just after fatty streak formation [13]. Previous studies have shown that the severity of coronary calcification is closely related to atherosclerotic plaque burden and rate of cardiac events [14]. In the past few decades, coronary calcification has been considered passive and degenerative. With recent clinical and basic research, however, there is increasing recognition that coronary calcification is an active, regulated process [15].

In this context, understanding of the vulnerability of atherosclerotic lesions to rupture has emerged as being much more important than plaque size and stenosis severity itself (Figure 4). Plaques containing a large core of soft lipid-rich atheromatous 'gruel' and thin fibrous cap are particularly dangerous, whereas plaques with a thick fibrous cap seem to be much more resistant to rupture. Thus, there are four major determinants to characterize the vulnerability of atherosclerotic lesions to rupture [16]:

1. the size and consistency of the atheromatous core;
2. the structure, thickness of the fibrous cap covering the core which is tightly related to the SMC content;
3. inflammation and repair within the cap;
4. 'Cap fatigue' due to long-term repetitive cyclic shear stress.

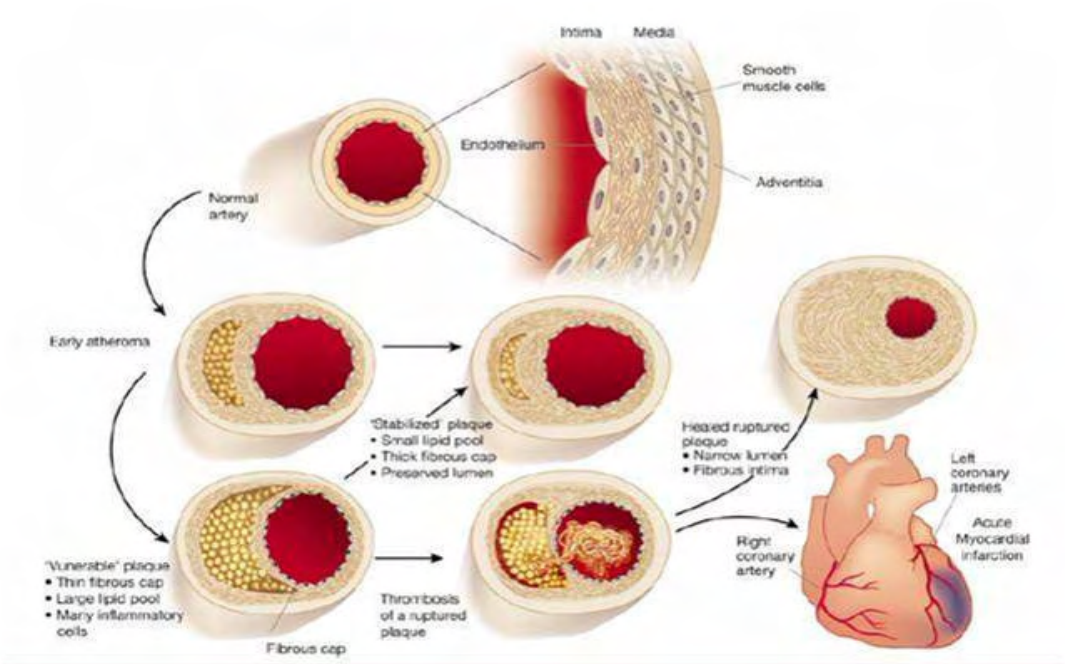

Figure 4: Schematic drawing illustrating the possible evolution of an atherosclerotic lesion to myocardial infarction. From: Libby P, et al. (Nature, 2002) [17].

Size of the atheromatous core is critical for the stability of individual plaques. Aortic plaques containing a core occupying more than 40% of the plaque area are considered particularly vulnerable and at high risk of rupture and thrombosis [18]. The consistency of the core, which is probably also important for the stability of a plaque, depends on temperature and lipid composition. Liquid cholesteryl esters soften the gruel, while crystalline cholesterol has the opposite effect [19]. Based on animal experiments [20], lipid-lowering therapy in humans is expected to deplete plaque lipid with an overall reduction in the liquid and mobile cholesteryl esters and a relative increase in the solid and inert crystalline cholesterol, theoretically resulting in a stiffer and more stable plaque.

The ***thickness***, cellularity, matrix, strength, and stiffness of fibrous caps vary widely. Cap thinning and reduced collagen content increase the plaques' vulnerability to rupture [21]. Caps of eccentric plaques are often thinnest and heavily infiltrated with foam cells at their shoulder regions, where they most frequently rupture [22]. Collagen is important for the tensile strength of tissues, and ruptured fibrous caps contain fewer SMCs (the collagen-synthesizing

cells in plaques) and less collagen than intact caps [23, 24]. The causes of low SMC content in ruptured caps are not completely understood, but SMCs may vanish as a result of apoptotic cell death, which has been shown to occur in fibrous caps [25].

Cap inflammation and repair: Ruptured fibrous caps are usually heavily infiltrated by macrophage foam cells [26]; their activation state indicates ongoing inflammation at the site of plaque disruption [27]. Macrophages are capable of degrading extracellular matrix (ECM) by secreting proteolytic enzymes such as plasminogen activators and matrix metalloproteinases (i.e., collagenase or MMP-2, gelatinase or MMP-9 and stromeolysins or MMP-3), which may weaken the fibrous cap, thus predisposing it for rupture [28] (Figure 5).

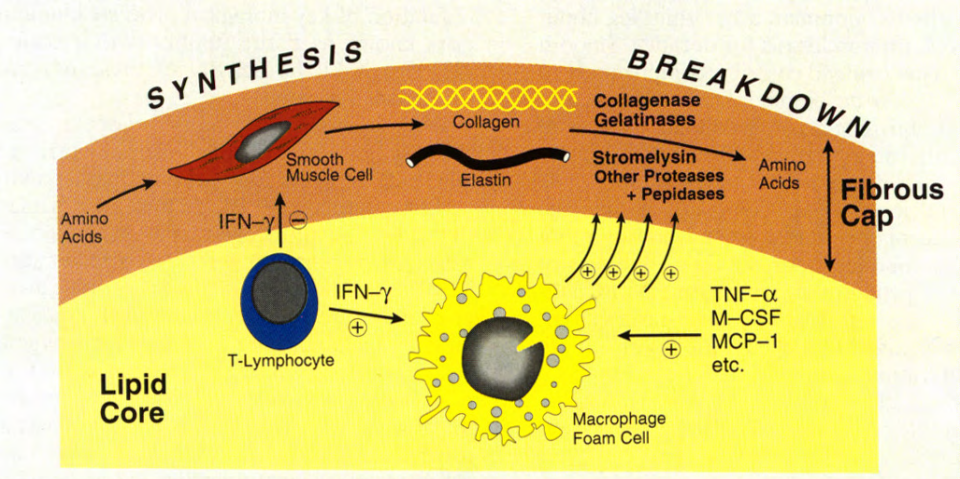

Figure 5: The balance between synthesis and breakdown of the fibrous cap determines the vulnerability of atherosclerotic lesions. From: Libby P, et al. (Circulation, 1995) [29].

Cap fatigue When a material is exposed to a steady load that does not cause immediate fracture, the material may weaken if the load is applied repeatedly. Consequently, repetitive stress may lead to sudden fracture of tissue due to fatigue. Cyclic stretching, compression, bending, flexion, shear and pressure fluctuation are factors that may fatigue and weaken a fibrous cap causing spontaneous rupture. If fatigue plays a role, lowering the frequency and magnitude of loading should in theory reduce the risk of plaque disruption [30].

Beyond the concept of vulnerable plaque, it is important to identify patients in whom plaque rupture is likely to result in a clinical event. In these patients, additional factors such as thrombogenic blood and electrical instability of myocardium are responsible for the final outcome. Thus, the concept of "vulnerable patients" (Figure 6) has been proposed by Libby and colleagues, explaining that plaques with similar histological characteristics may result in different clinical presentations because of blood coagulability (vulnerable blood) or myocardial susceptibility to develop fatal arrhythmia (vulnerable myocardium). The latter may depend on a current or previous ischemic condition and/or a nonischemic electrophysiological abnormality [12]. The term "cardiovascular vulnerable patient" is proposed to define individuals' susceptible to acute coronary syndrome or sudden cardiac death based on combined plaque, blood, and myocardial vulnerability (for example, 1-year risk ≥5%). Such a comprehensive risk-stratification tool capable of predicting acute coronary syndromes as well as sudden cardiac death would be very useful in preventive cardiology.

Figure 6: The risk of a vulnerable patient is affected by a combination of vulnerable plaques, vulnerable blood and/or vulnerable myocardium. A comprehensive assessment must consider all of the above. From: Naghavi M., et al. (Circulation, 2003) . [12]

The overwhelming clinical importance of atherosclerosis has stimulated research to better understand its cause. The "response-to-injury hypothesis" is the presently accepted concept of atherosclerotic plaque development. It considers atherosclerosis as a chronic inflammatory response of the arterial wall to an initial endothelial injury or dysfunction [31].

1.4.2 Atherosclerosis as an inflammatory disease

Four different cell types participate in the growth of atherosclerotic lesions: ECs, SMCs [32], monocyte-macrophages and T lymphocytes [30].

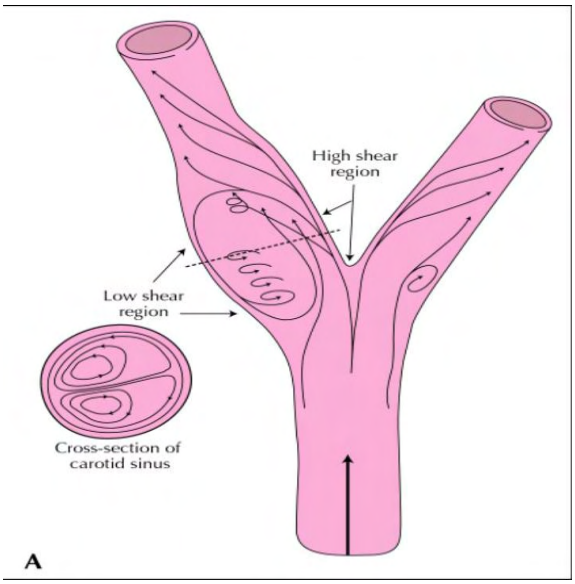

Figure 7: Schematic drawing illustrating the different patterns of shear stress observed at an arterial (carotid) bifurcation. From: Braunwald E., Essential Atlas of Heart Disease, 2nd edition, 1985. [33]

Differences in vascular geometrics result in laminar or turbulent flow patterns and preferred sites of atherosclerotic lesion formation within the arteries are at areas of non-laminar dynamic flow [34] (turbulent flow), either in curves or after a bifurcation as shown in Figure 7. Indeed, turbulent shear stress in combination with other injuring agents/events [25] might induce endothelium activation and dysfunction (Figure 8.1). These injuring

agents/events are often related to well-known cardiovascular risk factors such as [35] hypertension, hypercholesteremia, smoking and hyperglycemia. An important consequence of endothelium activation is that it promotes the attraction, adhesion and trans-endothelial migration of inflammatory cells such as monocytes and T lymphocytes (Figure 8.2). In addition, these risk factors transcriptionally upregulate a lectin-like receptor for ox-LDL (LOX-1) which will increase endothelial permeability and allow LDL particles to enter the vascular wall [36]. Next, LDL particles will accumulate in the intima and enhance the local inflammatory process. Furthermore, platelets may adhere to focal areas of endothelial denudation or to adherent inflammatory cells.

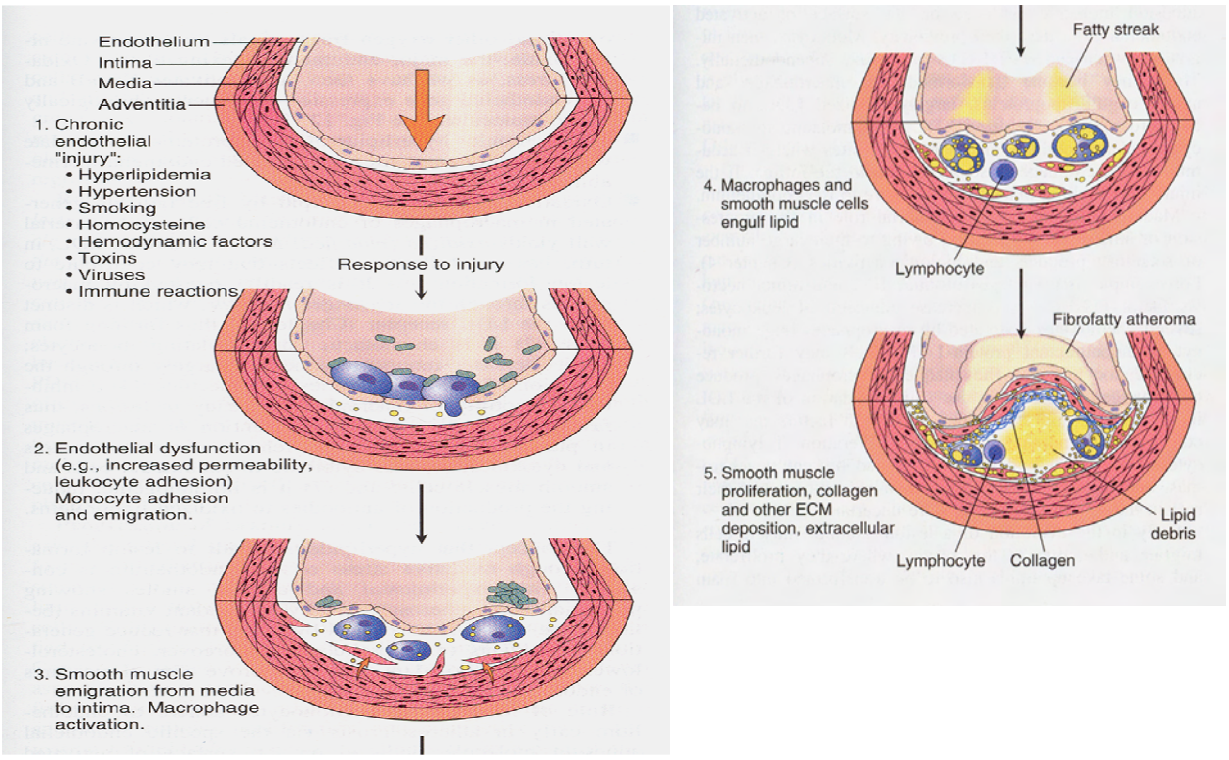

Figure 8.1 to 8.5: Schematic representation of the "response-to-injury hypothesis". From: Robbins and Cotran, Pathologic basis of disease, 7th edition, 2004.

Later, SMCs join the disease. Release of cytokines and growth factors from activated platelets, macrophages or ECs induce migration of SMCs from the media towards the intima

(Figure 8.3). SMCs and macrophages engulf lipids (Figure 8.4). Growth factors such as PDGF-BB (platelet-derived growth factor-BB), FGF (fibroblast growth factor), IGF-1 (insulin growth factor-1) or angiotensin further influence SMC proliferation in the intima. Their production of ECM leads to intimal accumulation of collagen and proteoglycans and further growth of the atherosclerotic lesion (Figure 8.5).

1.5 EXPERIMENTAL ANIMAL MODELS USED IN ATHEROSCLEROSIS

Definition of atherogenic mechanisms in humans is hindered by the complexity and chronicity of the disease process, combined with the inability to sequentially characterize lesions in an individual patient because of shortcomings in non-invasive detection modalities. Therefore, there has been a dependence on animal models to define mechanistic pathways in the development of the disease [37]. In the past, the most frequently used model of atherosclerosis was the hypercholesterolemic rabbit, resulting from serial inbreeding [38]. Both the plaque formation itself and its consequences on vascular function have been extensively studied in this model. Nevertheless, rabbits require high-cholesterol diets to develop atherosclerotic disease, and there are no rabbit models of metabolic syndrome. Other inbred rodent models included hamsters and Guinea pigs. Even avian models (pigeons, quail, and swine) as well as dogs and cats or pigs [39] have been used since the 1950s [40]. Mice and rats are naturally rather resistant to atherosclerosis. Due to the knock-out technology, specific genetically altered strains have been induced to respond to cholesterol feeding with atherosclerosis and since 1992 the Apolipoprotein E-deficient ($ApoE^{-/-}$) and the low-density lipoprotein receptor-deficient ($LDLR^{-/-}$) mice became the two most commonly used mouse models of atherosclerosis [41]. Being deficient in proteins essential for lipoprotein trafficking, both mouse models exhibit hypercholesterolemia and develop rapidly atherosclerosis

throughout the arterial tree in response to a high cholesterol diet (cholesterol levels up to 4-5 times higher than normal values) [42, 43]. The plaques that develop are very reproducible and display some architectural features comparable to human lesions [44]. Therefore, over the last decade, the mouse has become the preferred species used to create models of atherosclerosis.

In recent years, there has been some evidence of spontaneous plaque rupture in mouse atherosclerotic lesions [45]. This evidence includes intraplaque hemorrhage and fibrin deposition, loss of fibrous cap continuity, buried fibrous caps and thrombi extending to a necrotic core [46]. Although these histological studies represent a major advance in the concept of plaque rupture, in most cases the rupture did not cause complete vessel occlusion and could not be indicated from the animal's death but rather from an extensive search for the above-mentioned signs of plaque rupture. Consequently, to date there is no easy-to-use and reproducible mouse model that exhibits lesion rupture or erosion to mimic events that precedes the acute cardiovascular event in humans.

Many molecules with key roles in atherogenesis have been identified in recent years from studies performed on mouse models. This has been mainly accomplished by interbreeding an atherosclerosis-susceptible mouse strain with mice that are knock-out or transgenic for genes important in paracrine intercellular signaling, such as adhesion molecules, chemokines, and growth factors. In the laboratory where the studies described in this Thesis have been conducted, the main scientific interest is on the role of another form of direct cell-to-cell communication involving gap junctions in the development of atherosclerotic disease [47].

1.6 CONNEXINS, CONNEXONS AND GAP JUNCTION CHANNELS

1.6.1 General

1.6.1.1 Connexin gene family

At the International Gap Junction Conference in Elsinore, Denmark this past August 2008, a discussion and vote was held to decide on an official system for naming human and mouse connexin genes [48]. A majority has been in favour of a system that incorporates the recognized subgroups of the connexin family that are based on sequence comparisons. Subsequent to that meeting, a group of connexin researchers with expertise in bioinformatics held discussions to finalize the subgroup assignments of the known connexin genes based on the available data. The resulting official human and mouse ortholog connexin gene symbols are now listed on the websites of the human and mouse genome committees (see table1).

Approved Symbol	Approved Name	Previous Symbols	Aliases	Chromosome	Accession Numbers	RefSeq Ids	Mouse Ortholog
GJA1	GJP, alpha 1, 43kDa	ODDD, GJAL	CX43, ODD, ODOD, SDTY3	6q22-q23	BC026329	NM_000165	MGI:95713
GJA1P1	GJP, alpha 1, 43kDa pseudogene 1			5q21.3	M65189	NG_003029	
GJA3	GJP, alpha 3, 46kDa	CZP3	CX46	13q12.11	AF075290	NM_021954	MGI:95714
GJA4	GJP, alpha 4, 37kDa		CX37	1p35.1	M96789	NM_002060	MGI:95715
GJA5	GJP, alpha 5, 40kDa		CX40	1q21.1		NM_181703	MGI:95716
GJA6P	GJP, alpha 6, pseudogene			Xp22			MGI:95717
GJA8	GJP, alpha 8, 50kDa	CAE1, CZP1, CAE	CX50	1q21.1	U34802	NM_005267	MGI:99953
GJA9	GJP, alpha 9, 59kDa	GJA10	CX59, CX58	1p34	AF179597	NM_030772	
GJA10	GJP, alpha 10, 62kDa		CX62	6q15-q16	AF296766	NM_032602	MGI:1339969
GJB1	GJP, beta 1, 32kDa	CMTX1, CMTX	CX32	Xq13.1	X04325	NM_000166	MGI:95719
GJB2	GJP, beta 2,	DFNB	CX26, NSRD1	13q11-q12	M86849		MGI:95720

	26kDa	1, DFNA 3					
GJB3	GJP, beta 3, 31kDa	DFNA 2	CX31	1p34	BC012918	NM_024009	MGI:95721
GJB4	GJP, beta 4, 30.3kDa		CX30.3	1p35-1p34		NM_153212	MGI:95722
GJB5	GJP, beta 5, 31.1kDa		CX31.1	1p34-p35	BC004379	NM_005268	MGI:95723
GJB6	GJP, beta 6, 30kDa	DFNA 3, ED2	EDH, HED, CX30	13q12	AJ005585		MGI:107588
GJB7	GJP, beta 7, 25kDa		CX25, bA136M9.1	6q15	AJ414563		
GJC1	GJP, gamma 1, 45kDa	GJA7	CX45	17q21.31	U03493	NM_005497	MGI:95718
GJC2	GJP, gamma 2, 47kDa	GJA1 2	CX47, CX46.6	1q41-q42	AF014643	NM_020435	MGI:2153060
GJC3	GJP, gamma 3, 30.2kDa	GJE1	CX30.2	7q22.1	AF503615	NM_181538	MGI:2153041
GJD2	GJP, delta 2, 36kDa	GJA9	CX36	15q13.1	AB037509		MGI:1334209
GJD3	GJP, delta 3, 31.9kDa	GJC1	CX31.9, GJA11, Cx30.2	17q21.1	AF514298		MGI:2384150
GJD4	GJP, delta 4, 40.1kDa		CX40.1, FLJ90023	10p11.22	AJ414564	NM_153368	MGI:2444990
GJE1	GJP, epsilon 1, 23kDa		CX23, ENSG00000203733	6q24.1			MGI:1923993

Table1: adapted from http://www.genenames.org/genefamily/gj.php. GJP is gap junction protein. Cx37, subject of this thesis, is highlighted in blue.

Thus, the GJP gene family consists of 21 members (Table 1) and gap junction channels are composed of oligomers of connexin proteins, called connexons. Generally, the protein name is composed by the predicted molecular weight in kilo Dalton. An alternative protein name system is based on the exon/intron structure. The majority of the connexins have one of the two coding structures which depend on splicing mechanisms. The *Alpha* GJP name is used when the entire coding region is present within a single exon (Figure 9B upper part). The *Beta* name represents a group with the coding region contains an intron within and (Figure 9B down part). Three more classes have emerged, *Gamma*, *Delta* and *Epsilon* (Table 1) which have different splicing mechanisms. Interestingly, the connexins from the *Alpha*

subgroup have developed from a common origin, i.e. they are on the same branch of a phylogenic tree (Figure 9A, α in green), and that the *Beta* subgroup can be found on another branch of the tree by a sequence divergence of 10% (Figure 9A, β, in blue) [55].

Because of their long evolutionary history, gap junctions have been drafted into diverse functional roles subserving changing multicellular needs [49]. These intercellular connections have co-evolved with metazoans and are found joining animal cells in virtually all phyla, named innexins as protein units in invertebrates. Plant cells are similarly connected using different structures, the plasmodesmata.

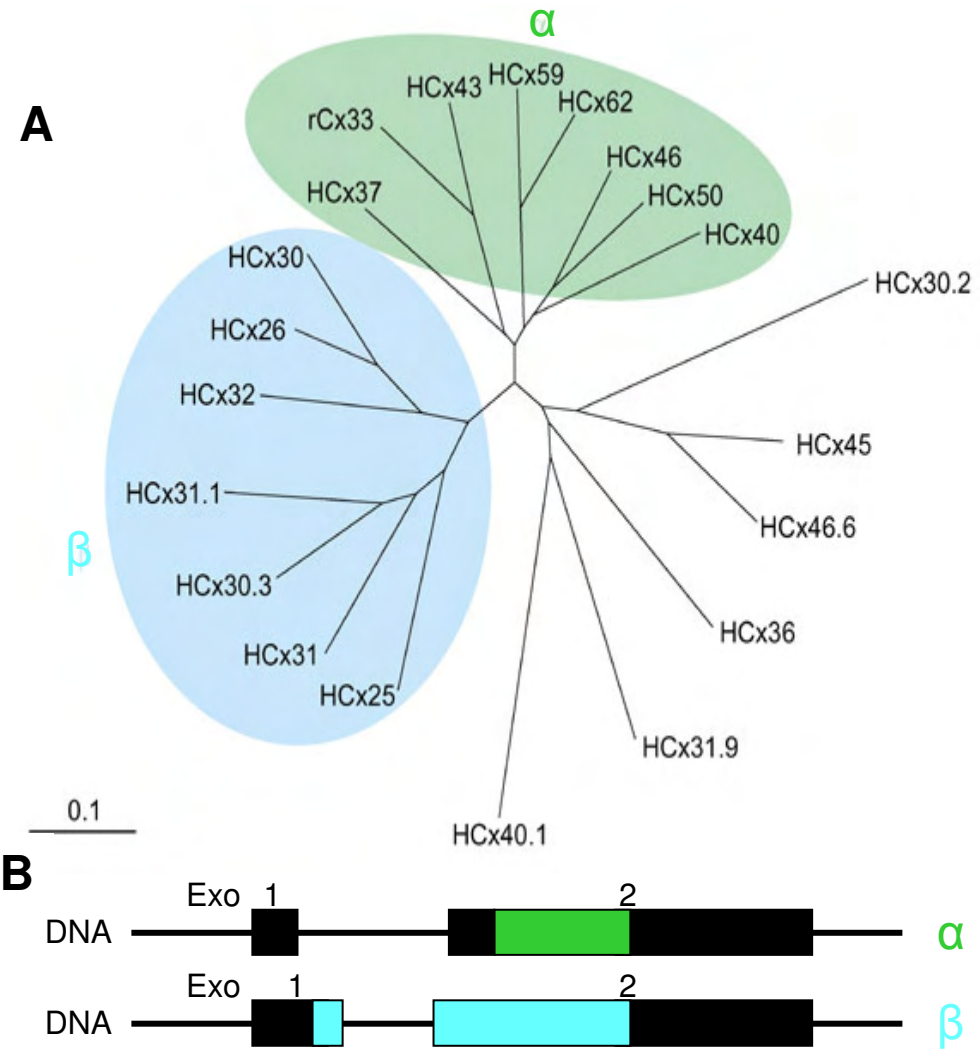

Figure 9: A) The connexin family can be broadly separated into three main subgroups, the historical α (green) and β (blue) and a more divergent non-α non-β branch. The divergent sequence portions (the intracellular loop

and the carboxy-terminal domain) were removed from the multiple alignments. The distance matrices were then analyzed by the neighbor-joining method of Saitou and Nei *(*Mol Biol Evol., 1987) [50], producing an unrooted molecular phylogenetic tree. From: Bruzzone R (Genome Biology, 2001) [51]. **B**) Alpha and Beta subgroups also differ in the gene structures. *Alpha* has a unique coding sequence inside exon2 whereas *Beta* has a coding sequence separated by one intron. Adapted from: Sohl and Willecke (Cardiovasc Res, 2004) [52].

1.6.1.2 Structure

The 21 members of the connexin gene family are integral membrane proteins (Figure 10). The transmembrane topology of a generic connexin polypeptide creates four membrane domains (M1–M4), one cytoplasmic (CL) and two extracellular (E1 and E2) loops, and the N- and C-termini facing the cytoplasm [53, 54]. Analysis of the various connexins indicates that one of the transmembrane domains, M3, has an amphipathic character, suggesting that it contributes to the lining of the channel pore. The two extracellular loops (E1 and E2) are thought to be involved in the docking between connexons in adjacent cells. A set of three cysteine residues with a characteristic arrangement exists in each of the extracellular loops [55]. These cysteines are thought to maintain the rigid tertiary structure that enables two opposing connexons to dock with each other. The regions between the transmembrane domains M2 and M3, as well as the C-termini of the connexins, are highly variable among the different connexins and are, therefore, considered important for unique regulatory properties of the various gap junction channels.

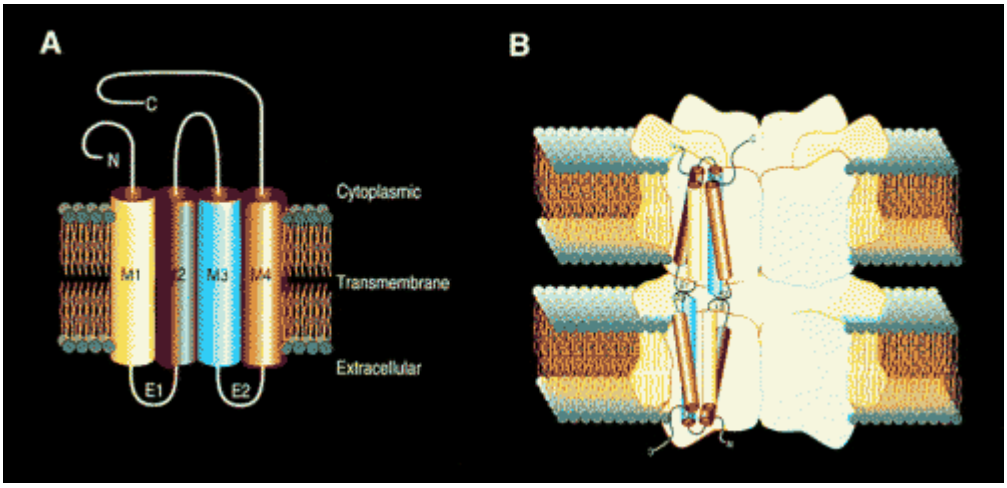

Figure 10: Molecular Models for Connexin Topology. **A)** Topological model for the connexins. The cylinders represent transmembrane domains (M1–M4). The loops between the first and second, as well as the third and fourth, transmembrane domains are predicted to be extracellular (E1 and E2, respectively). **B)** Model of the transmembrane domains of six connexin subunits in an oligomeric arrangement to form the hydrophobic spacing (pore) for the gap junction channel. From: Kumar and Gilula (Cell, 1996) [55].

In 1999, Yeager's group exploited the natural tendency of gap junction channels to aggregate into plaques within cell membranes to obtain detailed information on the molecular organization of a gap junction channel (Figure 10B). They made well-ordered two-dimensional crystals of recombinant gap junction channels and obtained high resolution images of such crystals at different tilt angles by electron microscopy. Finally, these crystallographic data was be merged to yield a 3D map [56] at high resolution—about 6 Angstroms (Å) (Figure 11). These experiments revealed that the four transmembrane domains, of within each connexin subunit, are made of α-helical folding. The six subunits oligomerize to form a connexon or a hemichannel. The six protruding peaks on the extracellular surface of one connexon fit perfectly into the six valleys on the extracellular surface of the adjacent connexon, forming thus a tight seal called the full intercellular channel.

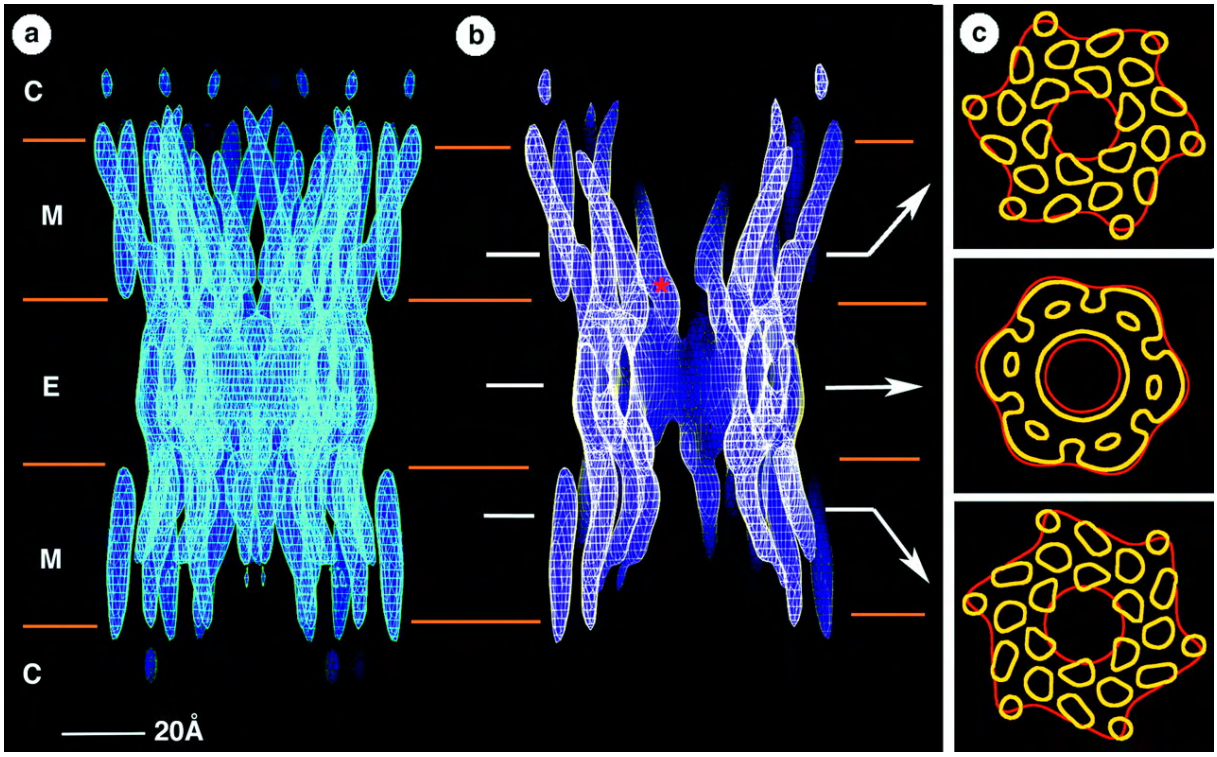

Figure 11: Molecular organization of a gap junction channel. It shows a side view of the three-dimensional map model of a gap junction channel based on an image reconstruction using data obtained from Fourier microscopy of rat liver connexons. (a) A full side view is shown, and (b) the density has been cropped to show the channel interior. The approximate boundaries for the membrane bilayers (M), extracellular gap (E), and the cytoplasmic space (C) are indicated. The white arrows identify the locations of (c) the cross sections that are parallel to the membrane bilayers. The red contours in (c) are at 1σ above the mean density and include data to a resolution of 15 Å. These contours define the boundary of the connexon and can be compared to previous low-resolution structural studies of liver and heart gap junctions. The yellow contours at 1.5σ above the mean density include data to a resolution of 7.5 Å. The roughly circular shape of these contours within the hydrophobic region of the bilayers is consistent with 24 transmembrane α helices per connexon. From: Unger VM *(*Science, 1999) [56].

The assembly of gap junction channels is a multi-step process. It starts with the biosynthesis of the connexin proteins on endoplasmic reticulum membranes, followed by oligomerization of compatible subunits into hexameric hemi-channels (connexons) [57]. Then, delivery of the connexons to the plasma membrane, head-on docking of compatible connexons in the extracellular space at distinct locations, arrangement of channels into

dynamic, spatially and temporally organized GJ channel aggregates [58] (so-called GJ plaques). Finally, coordinated removal of channels into the cytoplasm is followed by their degradation.

Some tissues and cells express more then one connexin and consequently gap junctions and individual gap junction channels may consist of multiple types of connexins. As depicted in Figure 13, one gap junction hemichannel or connexon may be constituted of one connexin isoform only (homomeric) or be of mixed origin (heteromeric). After docking of two hemichannels various GJCs are possible: both hemichannels are formed of the same connexon (homotypic) or different connexons (heterotypic); or the two hemichannels are each formed from the mixed hemichannels (heteromeric). Since different connexins have different structural properties, it is reasonable to assume that connexons that contain multiple connexins (heteromeric connexons) will have unique physiological properties. Thus, the specific communication pathways that exist between cells in an organ are likely to be influenced by the utilization of different connexins [59].

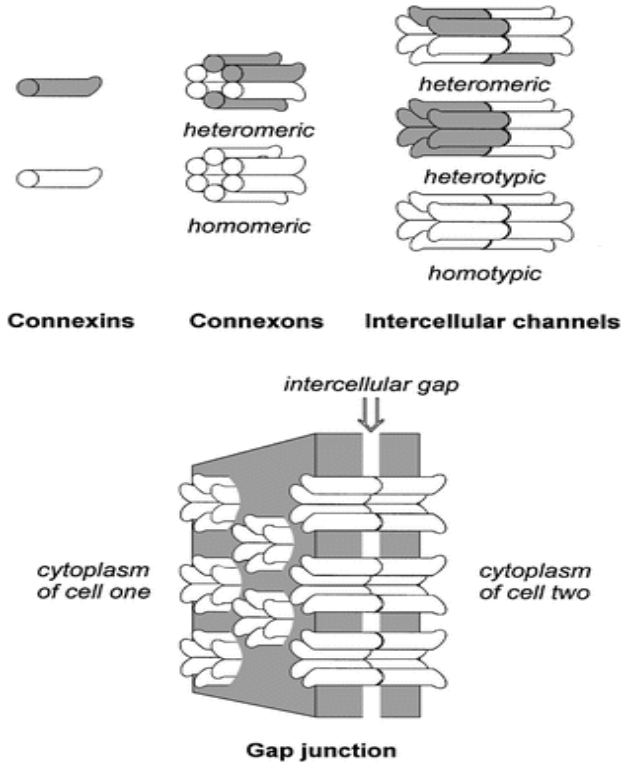

Figure 13: Organization of connexins into connexons, intercellular channels, and gap junctions. Connexin proteins oligomerize into connexons that are homomeric if they have one type of connexin or heteromeric if they contain multiple connexins. Connexons from adjacent cells align to form complete intercellular channels that span two plasma membranes. Each cell can contribute different types of connexons—giving rise to either homotypic, heterotypic, or heteromeric intercellular channels—that cluster in specialized membrane regions called gap junctions. From: White and Paul, Annual Review of Physiology, 1999 [60].

1.6.1.3 Gap junctions in physiology

Gap junction channels allow the transfer of ions, metabolites and messenger molecules smaller than ~1 kDa between connected cells, providing mechanisms for coordinating the activities of groups of cells [61, 62]. It has been suggested that these activities fall into five general classes: speed, synchrony, switching, symbiosis and stimulus/suppression [63].

In the heart, for example, gap junctions permit the rapid cell-to-cell transfer of action potentials ensuring coordinated contraction of the cardiomyocytes [64]. Gap junctions are also present in the nervous system, where electrical synapses are used in neuronal pathways requiring maximum speed, synchronous neuronal firing and switching between neuronal pathways [65].

In renal vasculature, cells are coupled and express connexins in a vessel and cell-specific pattern. Renal connexins likely play an important role in renal autoregulatory mechanisms (Bayliss effect, tubuloglomerular feedback) and in the control of vasomotor responses. Coupling of endothelial and vascular SMCs in the afferent arterioles has been described and may also contribute to the communication of neighboring nephrons, called "nephron coupling" [66].

Cell-to-cell communication has been shown to coordinate cell growth; this is of particular importance during carcinogenesis. Indeed, most tumour cells have a reduced ability to communicate among themselves and/or with surrounding normal cells, suggesting the importance of intact GJIC in growth control. When connexin genes are transfected into such

cells, normal cell growth control is often recovered [67]. In addition, certain dominant-negative mutant connexin genes can reverse such tumour suppression [68]. These results suggest that connexin genes may function as tumour suppressing genes. Although experimental studies revealed two connexin gene mutations in chemically induced rat tumours [69], so far no connexin gene mutations have been found in human tumours. Alternatively, epigenetic inactivation of connexin genes or aberrant location of connexion proteins may be mechanisms by which intercellular communications is disturbed in certain tumours [68]. Aberrant localization of connexins may result from lack of an appropriate cell-cell recognition apparatus and anomalous phosphorylation of connexins.

In summary, GJCs play a major role in physiology by regulating many different cellular aspects within tissues and organs. Consequently, disregulation of connexin expression, location, function and regulation may lead to various human pathologies.

1.6.1.4 Modulation of gap junctions

Gap junctions are under the control of multiple mechanisms, which may lead to a change in cell-to-cell coupling with a wide spectrum of time courses (milliseconds to hours). Examples of such mechanisms are: the transcription rate of connexins genes, the stability and translation rate of connexins, the insertion and removal in the cell membrane, assembly into gap junction channels, protein interactions of connexins with other molecules as well as channel gating [70]. My project involved the latter two types of modulation, which are described in more detail below.

1.6.1.4.1 Protein partners of connexins

Many of the signalling pathways and regulatory systems in mammalian cells are controlled by proteins with multiple interaction domains that mediate specific protein-protein

and protein-phospholipid interactions. Protein-protein interactions are key elements in building functional protein complexes. These interactions are typically mediated by special domains of the polypeptide chain, of which PDZ (Postsynaptic density-95/Discs large/Zonulaoccludens-1) motifs are of the most commonly found. The protein-protein interactions may act as "molecular switches", changing the properties of the gap junction channel in response to modifications in the channels microenvironment. Several proteins have been reported able to interact with different connexins [71] (see Figure 14). They can be divided in various functional classes:

1) Calmodulin (CaM): calcium has a long history as a modulator of GJIC [72] and might have an indirect action via its interaction with calmodulin. Some experiments demonstrated that CaM could bind and modulate the chemical gating sensitivity of GJ channels composed of Cx32 [73]. Also, CaM was shown to interact with Cx50 presumably by the cytoplasmic loop (CL), to form a CaM, CT and CL protein complex [74].
2) Membrane-junction associated proteins, including transmembrane proteins (Claudins, Occludins, and Junctional Associated Molecule or JAM) were found to interact i.e. with Cx32 [75]; cytoplasmic scaffolds (including ZO-1, ZO-2, ZO-3) are frequently associated through their respective PDZ to Cxs [76] and numerous actin-interacting proteins (i.e. cingulin and vinculin) .
3) Adherens junction-associated proteins: Cadherins and the adherens junctions were originally hypothesised to be important only for bringing cells in close enough contact to allow for the formation of GJ between the cells. Now, with the understanding that many of the protein members of the adherens junction complex are signal transduction molecules, it appears that adherens junctions may also transduce signals which may include the status of cell–cell coupling.

Interistingely, β-catenin acts as a component of cell–adhesive junctions and it was found to co-localise and co-immuno-precipitate with Cx43 in neonatal rat cardiomyocytes [77].

4) Membrane channels and receptors: The first catalytic domain of receptor protein tyrosine phosphatases (RPTPμ) has been found to interact with the C-tail on Cx43 in diverse cell systems [78]. Also, aquaporin-0 (AQP0), which belongs to the water channel proteins, was found to interact with two binding sites within the intracellular loop region of Cx45.6 [79].
5) Enzymes: The C-tail of several Cxs (e.g. Cx43) contains consensus phosphorylation sites for several protein kinases (PKs) [80]. Indeed, Cxs transiently interact, as substrates, with several phosphorylation/ de-phosphorylation catalysers, including tyrosine and serine/threonine PKs (e.g. Src, protein kinases A (PKA), C (PKC) and G (PKG), mitogen activated protein kinase (MAPK), cdc2 and casein kinase 1 and 2 (CK1 and 2)) and protein phosphatases (PPs) [81].
6) Cytoskeletal proteins: An association between Cx43 and the tip of actin filaments in embryonic rat astrocytes was suggested. F-actin-binding proteins play a role in connecting extra- and intracellular stimuli to cytoskeleton modelling and reorganization [82].
7) Proteins involved in intracellular trafficking: both Caveolin [83] and Ubiquitin [84] were found to interact with Cx43.

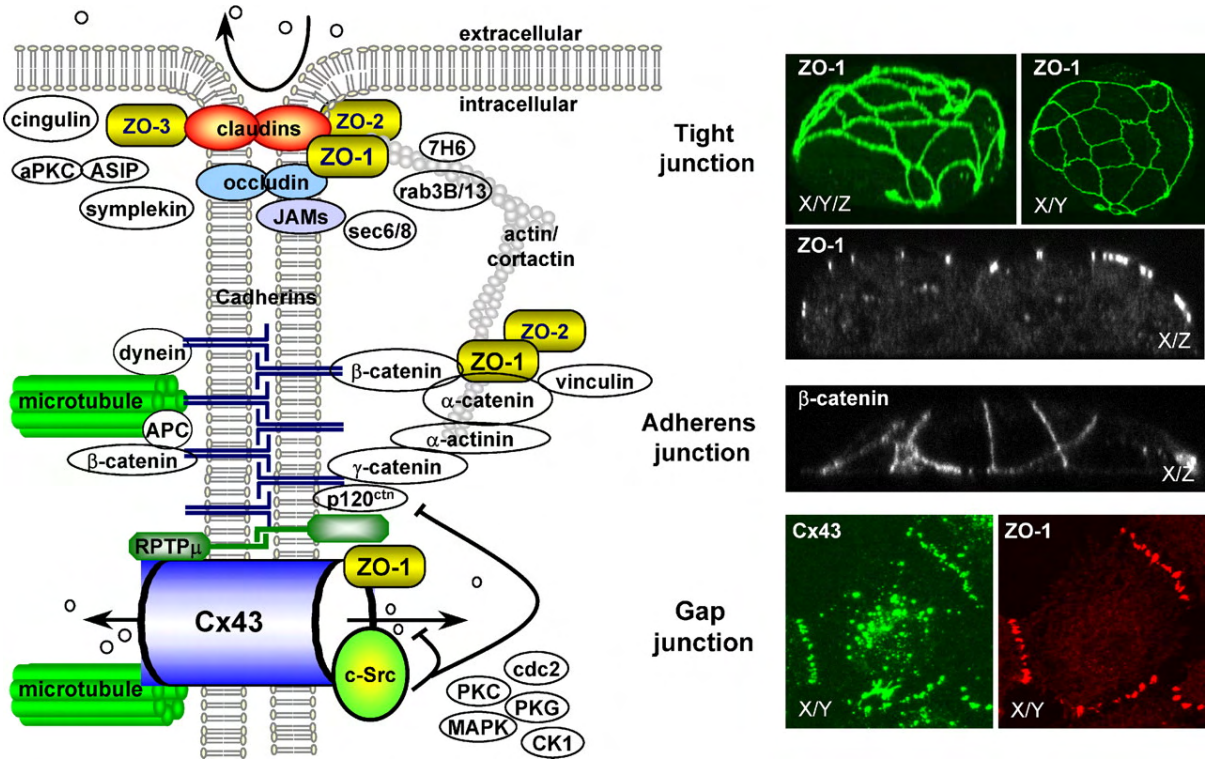

Figure 14: Molecular and cellular organisation of cell–cell junctions. Left: Cx43-associating proteins are depicted. See recent reviews for a complete picture of all known proteins associated with adherens and tight junctions. See text for details. Right: Confocal scanning light microscopy. Tight junctions form a network, which is only present in cell–cell contacts that face the apical contact sites of cells (20 MDCK cells; a three dimensional reconstruction (left; courtesy of Lauran Oomen), a projection (right) and an X/Z section are shown). Adherens junctions zip cells together (MDCK cells; middle panel). Gap junction plaques show a typical punctate staining (Rat-1 fibroblast; bottom panel). Figure and legend from: Giepmans BN (Cardiovascular, Research 2004) [70].

1.6.1.4.2 Channel gating

Gap junction channels are not simple tubes connecting the cytoplasm of neighboring cells, but like other membrane ionic channels they are gated, the channel is in the open or close state (gating kinetics). Assuming that these openings and closings occur stochastically, macroscopic gap junctional conductance (g_j) is determined by the number of channels comprising the gap junction (n) multiplied by the conductance of each individual channel (γ_j) and the open-state probability (P_o) of the channels.

Variations in g_j can thus result from a change in the number of functional channels present between two cells, a change in the unitary conductance of the channels, and a change in the mean time that each channel is the open and closed state. Earlier studies have shown that g_j might be affected by intracellular pH and/or intracellular [Ca^{2+}] [85, 86], second messengers/phosphorylation [87], transjunctional and transmembrane voltage [72, 88], and lipophilic substances [89, 90]. The sensitivity to these factors varies widely among gap junctions in different tissues [91]. Cell-to-cell coupling can be investigated by dual voltage-clamp or dye transfer experiments.

Patch clamp technique

Single or multiple membrane channel current properties, such as kinetics or V(j)-sensitive conductance are gained from current measurements by patch clamp (electrophysiology). Erwin Neher and Bert Sakmann developed the patch clamp technique in the late 1970s and early 1980s. They received the Nobel Prize in Physiology or Medicine in 1991 for their work. The technique can be applied to a wide variety of cells but is often used in the study of excitable cells such as neurons, cardiac cells, muscle fibers and cell lines (e.g. HeLa cells) transfected with the membrane channel of interest.

In order to gain perform **whole-cell recording** measurements, a small suction is applied to the inside of a glass pipette (tip size=1µm) to establish a gigaohm seal between the tip of the glass pipette in order to establish an electrical contact between the pipette solution and the cytoplasm of the cell. This configuration then enables to record the membrane potential and membrane currents. The pipette solution approximates the ionic contents of the cytoplasm. This procedure, together with voltage clamping, allows the measurements of the multipulchannel or single channel currents, depending on the recording conditions. In order to measure currents from gap junction hemichannels, a single suction pipette is used fixed on to

a single cell. In order to measure currents from gap junction channels, two suction pipettes are required separately fixed onto to the two cells of a cell pair.

Micro injections

Whereas in this method described above, currents (i.e. passing of ions) are measured, the dye transfer method is used to measure molecular permeability properties (i.e. passing of molecules) through gap junction channels using dyes of different electrical charges and molecular weights (MW), as Lucifer Yellow (LY) (charge: -2; MW: 443Da), or Neurobiotin (NB) (charge: +1; MW: 287 Da) and other molecules. Different types of gap junction channels display different diffusing properties. For example, cells expressing gap junctions composed of Cx37 are impermeable to LY (when dissolved with LiCl) but are permeable to NB [62]. Usually, two ways are used to measure the incidence of dye coupling: 1) it can be expressed as a ratio between the number of injected cells showing dye transfer to one or more neighbouring cells and the total number of cells injected in an experiment, or 2) as a number circles of neighbouring cells showing dye transfer. This microelectrode-based technique can also be applied *in situ* [92].

1.6.2 Expression and co-expression of connexins in the vascular system

In several tissues, the physiological role of gap junctions has been elucidated by the discovery of mutant connexins associated with genetic diseases and by the generation of mice with targeted ablation of specific connexin genes. The observed phenotype ranges from specific tissue dysfunction to embryonic lethality [93]. A summary is given in Table 2.

	Cx37	**Cx40**	**Cx43**	**Cx45**
Protein sequence identity mouse vs. human	0.91	0.85	0.98	0.98
Transcript sizes	1.7 kb	3.5 kb	3.0 kb	2.2 kb
Cell types with major	ECs, oocytes	some	ubiquitous	ECs, neurons,

expression		cardiomyocytes, ECs, some SMCs		SMCs, some cardiomyocytes
Cell-type specific expression in cardiovascular system	ECs	some cardiomyocytes, ECs, some SMCs	cardiomyocytes, SMCs	cardiomyocytes, SMCs
Main unitary conductance	300 pS	200 pS	60–100 pS	20–40 pS
Phenotype(s) of Cx-deficient mice	female sterility	atria arrhythmias hypertension	cardiac malformations	defective vascular development
Human disease	polymorphism associated with atherosclerosis	polymorphisms associated with sudden cardiac death and hypertension	mutations lead to oculodentodigital dysplasia syndactyly type IIIo	n.a.

Table 2: Distinctive features of mouse and human cardiovascular connexin genes. Adapted from: Söhl and Willecke (Cardiovasc. Res, 2004). [52]

1.6.2.1 Gap junctions in the vessel wall

Cx37, Cx40 and Cx43 are generally reported to be expressed in the vascular wall [94, 95]. The distribution of Cx within the vessel wall is, however, known to be species and vessel specific [96]. ECs and SMCs have distinctive but overlapping Cx expression patterns. In general, Cx43 expression is limited to SMCs [97], although it can be detected scarcely between ECs [98, 99]. Cx40 and Cx37 expression is detected in the endothelium throughout the vascular tree [100], and Cx40 is observed in the SMCs of small elastic (coronary) and resistance arteries [95, 101]. Recently, additional connexins, i.e. Cx45, Cx37 and Cx31.9 have been reported to be expressed in subpopulations of vascular SMCs [102].

Current knowledge about vascular gap junctions is growing rapidly. These communication pathways have been implicated in a variety of vascular functions, such as coordination of vasomotor responses, regulation of angiogenesis, repair of the endothelial lining, and senescence[103, 104]. A role for gap junctions in blood vessel pathology has also been established *in vivo*. Using Cx40 knockout mice, De Wit and colleagues [105] demonstrated that this Cx is required for normal transmission of endothelium-dependent vasodilator responses

and may be involved in the regulation of blood pressure as well. In addition, endothelial-specific deletion of Cx43 causes hypotension and bradycardia in mice [106]. The latter observation, however, remains to be confirmed as similar mice developed by another laboratory do not display a vascular phenotype [107]. Using Cx37-/- mice led to female infertility [108], however these animals did not show an obvious vascular phenotype [109]. In contrast to the single knock-out animals, mice that lack both Cx37 and Cx40 died perinatally and displayed severe abnormalities in vascular morphology [110].

1.6.2.2 Indirect support that gap junctions may be implicated in atherogenesis

Much literature provides indirect support to the notion that Cx may play a role in the development of atherosclerosis. First, important changes in the pattern of vascular Cx expression have been observed during atherosclerotic plaque formation [111]. Secondly, disturbances local fluid dynamic factors and inflammatory molecules have been shown to affect Cx expression or direct intercellular communication [99]**.** Finally, changes in Cx expression or gap junction coupling have been associated with important risk factors of the disease [112].

1 Cx expression displays dynamic changes during atherosclerotic plaque development, these changes are summarized in Figure 15 [102]. Briefly, monocytes express little Cx37. Once recruited to the early atheroma, the macrophages enhance their expression of Cx37. SMCs migrate from the media into the intima and intimal SMCs display increased Cx43 expression. ECs in early lesions continue to express Cx37 and Cx40. In an advanced atheroma, we should differentiate the shoulder region of the lesion from the central region. In the shoulder regions, the endothelium starts to express only Cx43 whereas in the central region no endothelial connexin expression can be detected. SMCs in the intima of advanced lesions gradually decrease their expression

of Cx43 [97]. Macrophage foam cells still express Cx37 but also Cx43 when close to the lipid core. Based on the changes in connexin expression during atherosclerotic plaque development, it is tempting to hypothesize that gap junctional communication might not only play a role in the recruitment of inflammatory cells across the endothelial monolayer but may play a role in their differentiation as well. In addition, gap junctional communication might play a role in SMC migration and proliferation.

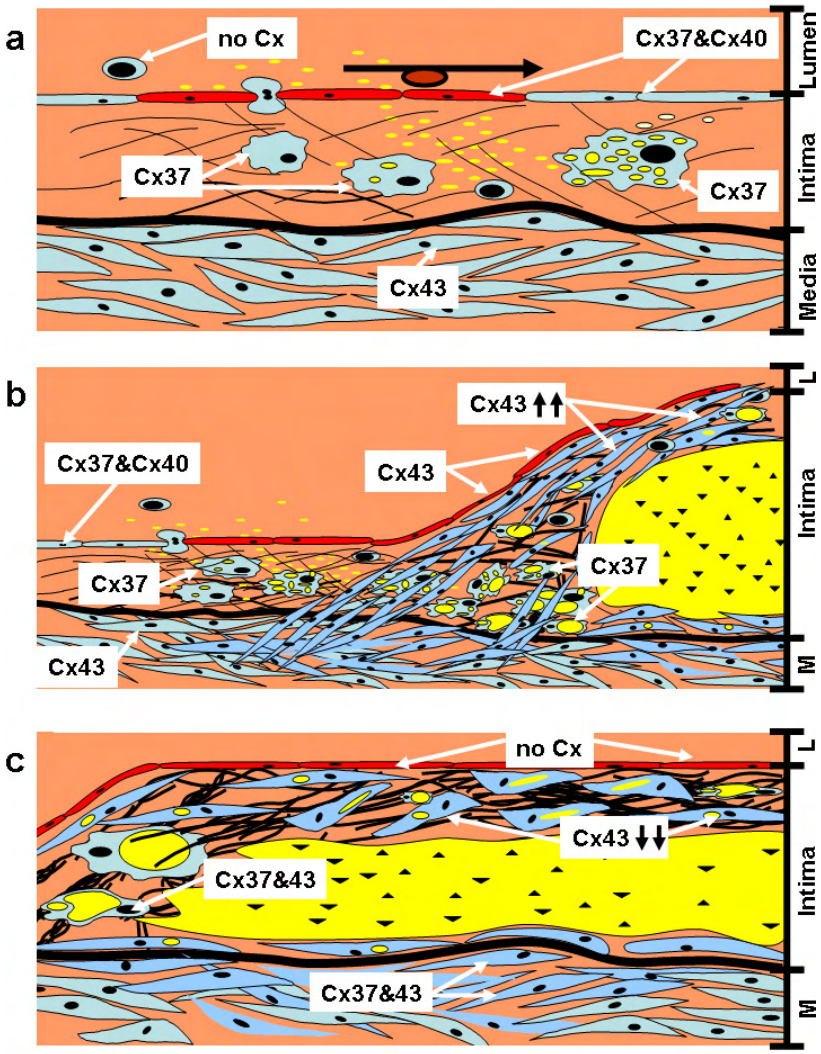

Figure 15: Connexin expression in atherosclerotic plaques Schematic drawing of an artery containing an atherosclerotic lesion is shown. Expression patterns of the 3 vascular connexins are indicated for the non-diseased part of the vessel (A), the shoulder of the plaque (B), and the center of the advanced lesion (C) From: Chadjichristos et al. (Adv Cardiol., 2006) [102].

2 In a study examining rat aorta and its bifurcation, high levels of Cx43 in the endothelium were exclusively localized in areas facing turbulent blood flow [99]. Several *in vitro* studies also show a positive correlation between Cx43 expression and mechanical load or disturbed flow patterns [113, 114]. Taken together, these studies suggest a causal link between endothelial Cx43 expression and hemodynamic conditions that may be relevant to focal vulnerability to atherosclerosis.

3 Hypertension and hypercholesteremia are important risk factors for atherosclerosis. Increased Cx43 expression and gap junction communication has been described in aortas from hypertensive rats [115, 116]. Exposing cell cultures to LDL or cholesterol resulted in increased gap junction channel assembly or protection against heptanol-induced closure of Cx43-built gap junction channels [117, 118].

Altogether, these studies have stimulated the research in the laboratory on how vascular Cx participate in atherosclerosis, especially using the LDLR- or ApoE-deficient mouse models.

1.6.2.3 Cx43 in mouse atherosclerosis

In an earlier study of the laboratory, the role of Cx43 in atherogenesis was examined [112]. Thus, atherosclerosis-susceptible $LDLR^{-/-}$ mice with mice heterozygous for a Cx43 null mutation ($Cx43^{+/-}$ mice). The Cx43 knock-out mutation ($Cx43^{-/-}$) in mice is lethal [119], however, in $Cx43^{+/-}$ mice the amount of Cx43 is reduced by half [120]. Male $LDLR^{-/-}$ mice with normal ($Cx43^{+/+}LDLR^{-/-}$) or reduced ($Cx43^{+/-}LDLR^{-/-}$) levels of Cx43 of 10 weeks old were fed a cholesterol-rich diet for 14 weeks. In these animals, lesion development was reduced by about 50% both at the level of the aortic roots and in the descending aortas in comparison to $Cx43^{+/+}LDLR^{-/-}$ littermate controls [112]. In addition, the composition of atherosclerotic plaques in $Cx43^{+/-}LDLR^{-/-}$ mice was strikingly different from $Cx43^{+/+}LDLR^{-/-}$ mice. Lesions of $Cx43^{+/-}LDLR^{-/-}$ mice had smaller lipid-cores and fewer macrophages. In addition, the lesions

had thicker fibrous caps containing more SMC and interstitial collagen. Thus, reducing Cx43 levels in mice seems to favour potential plaque stabilizing processes rather than affecting plaque size alone. The scenario by which reduced Cx43 ultimately leads to this dual benefit remains to be identified. Possible mechanisms involve Cx43-mediated effects on endothelium dysfunction, leukocyte migration or proliferation on the one hand as well as Cx43-mediated effects on SMC function on the other hand [121].

1.6.2.4 Connexin37 in atherosclerotic disease

As described before, the expression profile of Cx37 is altered in mouse and human atherosclerotic plaques. Notably, Cx37 is no longer found in the endothelium covering advanced plaques but detected in macrophages recruited to the lesions [111, 47]. Also, a polymorphism in the human Cx37 gene (C1019T) has been reported as a potential prognostic marker for atherosclerotic plaque development [122, 94, 47] and myocardial infarction [123, 124]. Therefore, we recently investigated the effect of Cx37 deletion ($Cx37^{-/-}$) on atherogenesis in $ApoE^{-/-}$ mice [47]. Again, we induced atherosclerosis in $Cx37^{+/+}ApoE^{-/-}$ and $Cx37^{-/-}ApoE^{-/-}$ mice by feeding them a high-cholesterol diet and demonstrated that atherosclerotic lesion development was accelerated in mice lacking Cx37, both in the descending aortas and aortic sinuses. Knowing that recruitment of leukocytes is a prerequisite for atherosclerotic lesion formation, we next investigated whether the increased atherosclerosis in $Cx37^{-/-}ApoE^{-/-}$ mice was caused by accelerated monocyte migration across the endothelium. Criss-cross *in vivo* adoptive transfer assays revealed that the presence of Cx37 in monocyte/macrophages but not in the endothelium contributed to decreased recruitment of these leukocytes to atherosclerotic lesions. To explore whether Cx37 could control the earliest step of the leukocyte recruitment paradigm, we then compared adhesion of $Cx37^{+/+}ApoE^{-/-}$ and $Cx37^{-/-}ApoE^{-/-}$ monocyte/macrophages to an activated mouse EC monolayer. Indeed, an increased number of

Cx37-deficient monocytes or macrophages adhered. It is known that individual monocytes and macrophages cannot form gap junctions, thus we speculated that cell adhesion may be regulated by the activity of Cx37 hemichannels. We further demonstrated in primary monocytes, macrophages and a macrophage cell line transfected with Cx37 cDNA that Cx37 hemichannel activity inhibited leukocyte adhesion. This anti-adhesive effect was mediated by ATP release into the extracellular space [47]. Thus, Cx37 hemichannels may control the initiation of atherosclerotic lesion development by regulating monocyte adhesion.

In contrast to the mouse, the human connexin37 gene exhibits a C1019T polymorphism resulting in a non-conservative amino acid alteration (serine or proline at codon 319) in the regulatory intracellular C-terminus of the protein. To determine whether this Cx37 polymorphism encodes for hemichannels that might differentially regulate cell adhesion, we have transfected Cx37–1019C, Cx37–1019T, or empty pIRES-eGFP vector cDNA into H36.12j macrophages. We then performed stringent bulk-sorting of eGFP-expressing cells to assure for similar protein expression levels. Consistent with the previous experiments, Cx37-deficient H36.12j cells showed increased adherence to an activated endothelial monolayer as compared to Cx37-expressing cells. In addition, we found that cells expressing the Cx37–P319 protein were less adhesive than cells expressing Cx37–S319. Finally, the reduction in adhesiveness of Cx37-expressing monocytes was canceled by extracellular apyrase, indicating that these effects were likely mediated by ATP. Thus, the Cx37 C1019T polymorphism encodes for hemichannels that differentially control monocyte adhesiveness. We therefore hypothesize that amino acid alteration at codon 319 likely alters the biophysical properties of Cx37 hemichannels, thereby affecting ATP-dependent cell adhesion.

1.7 UNRESOLVED QUESTIONS / AIMS OF THIS RESEARCH

The studies presented in this thesis were performed to find answers to the following specific questions:

- **Part one:** What are the basic biophysical properties of hCx37-319S and hCx37-319P hemichannels? And can such differential properties explain differences in adhesion?
- **Part two:** Do hCx37-319S and Cx37-319P interact with different proteins? And what are the effects of such interactions on cell function?
- **Part three:** Does Cx37 expression affect the composition and morphology of advanced atherosclerotic lesions?

In the chapters these questions will be addressed as follows:

Chapter 2: To get more insight into the molecular role of this polymorphism in atherosclerotic development, we will determine whether gap junction channels and hemichannels made of Cx37-1019C or Cx37-1019T transfected in communication incompetent HeLa cell show altered physiological regulation of hemichannel and full channel properties. It will be demonstrated by patch clamp experiments on single cells and cell pairs, ATP measurements and adhesion assays.

Chapter 3: To determine whether the polymorphism for Cx37-319S or Cx37-319P modified interaction with proteins, we identified potential binding motifs using high throughput phage display. A particular peptidic sequence was identified which showed high homology to a region of endothelium nitric oxide synthase (eNOS). The binding was confirmed *in vitro* by cross-linking, plasma resonance and nuclear magnetic resonance. Finally, the binding and co-localisation of Cx37 and eNOS was confirmed in ECs.

Experiments on transfected cells revealed that the binding affected both electrophysiological properties of Cx37 channels (Cx37 function) as well as NO-release (eNOS function).

To get more insight into the role that Cx37 may play in advanced atherosclerotic lesions, we performed in Chapter 4 a "wide and unbiased micro-array search" for genes that may be inherently differently expressed (before diet) or that are differentially expressed in advanced atherosclerotic lesions (after 18 weeks diet) in $Cx37^{+/+}ApoE^{-/-}$ versus $Cx37^{-/-}ApoE^{-/-}$ mouse aortas. We then searched for 'patterns' in RNA changes by dividing them in functional groups. Finally, some changes were confirmed by immunostaining and histology on atherosclerotic lesions.

2 FUNCTIONAL DIFFERENCES BETWEEN HUMAN Cx37 POLYMORPHIC HEMICHANNELS

Resubmitted in JMCC at the 5th of August, 2008

Functional differences between human Cx37 polymorphic hemichannels

Jean-Paul Derouette[1], Thomas Desplantez[2], Cindy W. Wong[1], Isabelle Roth[1], Brenda R. Kwak[1]* and Robert Weingart[2]*

[1]Division of Cardiology, Department of Internal Medicine, Faculty of Medicine, University of Geneva, CH-1211 Geneva, and [2]Institute of Physiology, University of Bern, CH-3012 Bern, Switzerland

*Authors contributed equally to the study

Running head: Properties of human Cx37 polymorphic hemichannels
The manuscript contains 7'284 words and 7 figures.
The abstract contains 242 words.

Address of correspondence:

Brenda R. Kwak, PhD
Foundation for Medical Research
Division of Cardiology
Geneva University Hospitals
64 avenue de la Roseraie
CH-1211 Geneva
Switzerland
Tel: (41 22) 382.72.37
Fax: (44 22) 382.72.45
E-mail : Brenda.KwakChanson@medecine.unige.ch

2.1 ABSTRACT

A polymorphism in the human Cx37 gene (C1019T), resulting in a non-conservative amino acid change in the regulatory C-terminus of the Cx37 protein (P319S), has been proposed as prognostic marker for atherosclerosis. We have recently demonstrated that Cx37 hemichannels control the initiation of atherosclerotic plaque development by regulating ATP-dependent monocyte adhesion in atherosclerosis-susceptible apolipoprotein E-deficient mice. In this study, we have measured the electrical properties of Cx37 hemichannels (HCs) and gap junction channels (GJCs) with voltage-clamp methods. To this end, we have transfected hCx37-P319, hCx37-S319 or empty pIRES-eGFP vector cDNA into communication-deficient HeLa cells. In clones expressing similar levels of Cx37, exposure of single cells to low-Ca^{2+} solution induced a voltage-sensitive HC current. The analysis yielded a bell-shaped function $g_{hc}=f(V_m)$ (g_{hc}: normalized conductance at steady state; V_m: membrane potential) with a maximum around V_m=-30 mV. The peak g_{hc} of Cx37-P319 was 3-fold larger than that of Cx37-S319 HCs. Experiments on cell pairs revealed that Cx37-P319 GJCs exhibited a 1.5-fold larger unitary conductance than Cx37-S319 GJCs. Hence, the larger peak g_{hc} of the former may reflect a larger conductance of their HCs. Using the same clones, we found that Cx37-P319 cells released more ATP and were less adhesive than Cx37-S319 cells. The reduction in adhesiveness of Cx37-expressing cells was prevented by extracellular apyrase. We conclude that the differences in biophysical properties between polymorphic HCs may be responsible for inequality in ATP release between Cx37-P319 and Cx37-S319 cells, which results in differential cell adhesion.

Keywords
atherosclerosis; genetic polymorphism; connexin; Cx37; hemichannel; electrophysiology

2.2 INTRODUCTION

Coronary artery disease is the most common form of heart disease resulting primarily from atherosclerosis [125, 126]. The cellular and molecular mechanisms underlying atherosclerosis remain widely unknown. The complex nature of atherosclerotic disease demands the development of novel technologies that enable discovery of new biomarkers for early disease detection and risk stratification, which may predict clinical outcome. Compelling evidence, mostly from epidemiological studies, suggests a genetic basis for atherosclerotic heart disease and acute myocardial infarction [127-129]. Although numerous candidate genes have been implicated as potential cardiovascular risk factors, only few have been firmly established. Factors complicating identification of prognostic markers often are the small sample size or multiple subgroup comparisons in epidemiological studies. However, disguise of the molecular function of the gene product may also play a role.

To date, several gene polymorphism-association studies have detected a link between a single nucleotide polymorphism in the human connexin37 (Cx37) gene and coronary artery disease as well as myocardial infarction [122-124, 130, 131]. Connexins are members of a family of proteins encoded by 21 different mammalian genes that are expressed in a wide variety of tissues [52]. Cx37 is expressed in the vascular endothelium as well as in monocytes and macrophages [47, 111]. Interestingly, these three cell types are key players in atherogenesis. In the early phases of atherosclerosis, blood monocytes are recruited to the sites of injury in response to chemotactic factors. Monocytes adhere to the dysfunctional endothelium and transmigrate across endothelial cells to penetrate the arterial intima. In the intima, monocytes proliferate, mature and accumulate lipids to progress into macrophage foam cells [132, 133].

The life cycle of connexins (Cx) begins with the non-covalent oligomerization of 6 Cx monomers into annular structures called connexons [134, 135]. After assembly, connexons are delivered in vesicular carriers travelling along microtubules from the Golgi to the cell

periphery. Once inserted into the plasma membrane, the connexons move laterally to reach the margins of channel clusters and dock with their counterparts in the neighbouring cells to form intercellular channels, the gap junction channels (GJC), which assemble to gap junctions. Cxs, connexons and GJCs are involved in numerous processes contributing to the maintenance of normal cell growth and differentiation [61]. Particularly, connexons can function as hemichannels (HC) in transmembrane signalling whereas GJCs mediate the direct exchange of ions and small molecules (second messengers, metabolites, linear peptides, siRNA) between cells in contact [136].

Cx genes show 40% sequence identity, i.e. the amino acid sequences of their transcripts are highly conserved. A Cx exhibits 4 α-helical transmembrane domains (M1-M4), 2 extracellular loops (E1 and E2), a short cytoplasmic loop (CL), and cytoplasmic NH_2- and COOH-termini (NT and CT, respectively). The CT, which varies significantly in both length and composition, is nearly unique to each type of Cx. For most Cxs studied so far, the CT is a substrate for specific kinases and/or protein partners, acting as a regulatory domain to modulate the activity of GJCs in response to appropriate biochemical stimuli [137, 138]. The atherosclerosis-related C1019T polymorphism results in a non-conservative amino acid change in the CT of Cx37; a proline residue at codon 319 (P319) produced by the 1019C allele is replaced by a serine residue (S319) generated by the 1019T allele.

We have recently demonstrated in a mouse model that Cx37 serves as a potential "protector" protein that prevents excessive monocyte recruitment in atherosclerosis [47]. We have also shown that mononuclear cells expressing the human Cx37-S319 polymorph show stronger ATP-dependent adhesion than those expressing P319. Thus, Cx37-P319 polymorphic HCs could function as a protective genetic variant by specifically retarding recruitment of monocytes to human atherosclerotic lesions [139]. The amino acid alteration at codon 319

probably alters the biophysical properties of Cx37 HCs, thereby affecting ATP-dependent cell adhesion.

The aim of this study has been to refine the role of the Cx37 C1019T polymorphism in the context of atherosclerosis. The pertinent question is: can the differential effect of Cx37-P319 and Cx37-S319 on ATP-dependent cell adhesion, recently reported for a mouse model [47], be explained by differences in Cx37 HC properties? Communication-deficient HeLa cells were used for transfection with Cx37-1019C, Cx37-1019T or empty pIRES-eGFP vector cDNA. Clones with equal expression levels of Cx37-S319 and Cx37-P319 were carefully selected by means of FACS sorting and Western blotting. Cells were then used to perform electrophysiological measurements to search for differential properties of HCs. These experiments were complemented by ATP-release studies and cell-adhesion assays.

2.3 MATERIALS AND METHODS

2.3.1 Cell cultures

Transfected human HeLa cell lines expressing hCx37-P319, hCx37-S319 or empty vector pIRES2-eGFP, and wild-type HeLa cells were grown in DMEM medium supplemented with 10% FBS, 50 U/ml penicillin and 50µg/ml streptomycin (Gibco-BRL). Transfected cells were selected with 300 µg/ml G418 (Gibco-BRL). To perform experiments, cells were harvested in DMEM with 10% FBS, seeded onto sterile glass coverslips placed in multi-well culture dishes and used 1-2 days thereafter.

2.3.2 Transfection

hCx37-1019T and hCx37-1019C cDNAs were subcloned into the pIRES2-eGFP mammalian expression vector (Clonetech) using EcoRI and BamHI restriction sites [47]. The vectors were separately transformed into DH5α-competent cells (Invitrogen) and positive kanamycin-resistant clones were isolated according to the manufacturer's protocol. Aliquots of 5 µg plasmid DNA were electroporated into $3 \cdot 10^5$ HeLa cells by means of a Gene pulser II device (Bio-Rad) using the following settings: 350 V and 960 µF during 25 s. Thereafter, the cells were transferred to a six-well tissue-culture plate. They were cultured for 48 h in recovery medium, i.e. DMEM supplemented with 30% FBS, no penicillin and no streptomycin. Subsequently, the cells were selected in DMEM medium supplemented with 10% FBS, 50 U/ml penicillin, 50µg/ml streptomycin (Gibco-BRL) and 300µg/ml G418. After 21 days, individual cells with different levels of eGFP expression were isolated by flow cytometry (FACS Vantage, Becton Dickinson) and clones were grown. The expression of hCx37 was verified by immunostaining and Western blotting. Clones expressing similar amounts of total hCx37-P319 and hCx37-S319 were then selected from the Western blots and used for further

experiments. First, equal expression of Cx37 at the cell membrane was verified in these clones after biotinylation and purification of cell surface proteins using an extraction kit according to the manufacturers' instructions (Pierce Biotechnology). To ensure that protein expression levels remained equal in the selected clones, the cell sorting procedure was repeated regularly.

2.3.3 Immunofluorescence

We plated transfected HeLa cells onto coverslips coated with culture medium, fixed the cells in ice-cold methanol (-20°C) for 5 min and immunolabeled them with Cx37-specific antibodies (Alpha Diagnostics), as described before [47, 111]. Immunofluorescent samples were analyzed on an inverted confocal microscope (Zeiss LSM 510).

2.3.4 Western blotting

Western blotting of protein extracted from transfected HeLa cells was performed as described [47, 140] using antibodies against Cx37 (Alpha Diagnostics) or anti β-actin (Pharmingen), which was used as control for loading.

2.3.5 Solutions

Electrophysiological experiments on single cells were carried out in modified Krebs-Ringer solution containing normal Ca^{2+} [in mM: NaCl 140, KCl 4, $CaCl_2$ 2, $MgCl_2$ 1, CsCl 2, $BaCl_2$ 1, HEPES 5 (pH 7.4), glucose 5, Na-pyruvate 2] or low Ca^{2+} [in mM: $CaCl_2$ 1, EGTA 5 (pCa 7.7)]. Cs^+ and Ba^{2+} were added to block the K^+ channels. Patch electrodes were filled with pipette solution [in mM: KCl 140, NaCl 4, $CaCl_2$ 1, $MgCl_2$ 1, Mg-ATP 3, CsCl 2, $BaCl_2$ 1, TEA-Cl 2, HEPES 5 (pH 7.2) and EGTA 5 (pCa 7.4)]. The osmolarity of these solutions was

measured with an osmometer (3MO; Advanced Instruments, USA) and adjusted to 310 mOsm by adding mannitol. Mibefradil (50 µM; gift from La Roche, Switzerland) was added to the extracellular solutions to block the volume-regulated anion channels [141]. Heptanol (2 mM; Fluka) was added to the bath solution to block HCs or GJCs [141]. Electrophysiological experiments on cell pairs were performed in Krebs-Ringer solution [in mM: NaCl 140, KCl 4, $CaCl_2$ 2, $MgCl_2$ 2, HEPES 5 (pH 7.4), Na-pyruvate 2, glucose 5] and pipettes were filled with a solution containing [in mM: K-aspartate 130, NaCl 10, $CaCl_2$ 1, MgATP 3, HEPES 5 (pH 7.2) and EGTA 10 (pCa ~8)].

2.3.6 Electrophysiology

The electrical properties of Cx37 HCs and GJCs have been studied on transfected HeLa cells. Glass coverslips with adherent cells were transferred to an experimental chamber and superfused with modified Krebs-Ringer solution at room temperature (22-26°C). The chamber was mounted on the stage of an inverted microscope (Diaphot-TMD Nikon, Japan). Patch pipettes were pulled from glass capillaries (GC150F-10; Harvard Apparatus, UK) with a horizontal puller (DMZ-Universal; Zeitz-Instruments, Germany). Filled with solution, the pipettes had DC resistances of 3-6 MΩ (tip diameter: 1-2 µm). A video system allowed a visual inspection of the cells and pipettes during an experiment (CCD camera: Panasonic WV-CD51/6; monitor: JVC TM-916EM). Experiments were carried out on single cells or cell pairs using a single or a dual voltage-clamp technique, respectively, and tight-seal whole-cell recording [141-143]. Patch pipettes were fixed in pipette holders mounted on micromanipulators (MP-258; Sutter Instruments, USA) and connected to amplifiers (EPC 9/2; HEKA Elektronik, Germany). These methods permitted to control the membrane potential of the cells and measure membrane currents. Initially, the membrane potential was clamped to V_m=0 mV. Thereafter, it was changed using a voltage-ramp protocol. The duration of the ramp was

chosen to ensure steady-state currents. Preliminary tests with a voltage-pulse protocol served to define the temporal requirements.

Single cells were used to measure currents by HCs, I_{hc} [143]. A given voltage protocol was first applied in the presence of extracellular solution of normal Ca^{2+} and then in extracellular solution of low Ca^{2+} and the membrane currents, I_m, measured. I_{hc} was then determined as difference between the latter and the former. The solution in the bath was changed by means of a gravity-driven rapid superfusion system positioned close to the cell investigated. Cell pairs were chosen to measure currents by GJCs, I_j [143]. To start with, the membrane potential of cells 1 and 2 was clamped to the same voltage, $V_1=V_2=0$ mV. Thereafter, V_1 was stepped to different levels to establish a gap junction potential, $V_j=V_2-V_1$. The current measured from cell 1 represents the sum of two components, the gap junction current, I_j, and the membrane current of cell 1, I_{m1}; the current measured from cell 2 corresponds to $-I_j$. Currents carried by single GJCs were examined after partial uncoupling with 2 mM heptanol (*cf.* Harris et al. [72]). The voltage and currents signals were stored with a PC for off-line analysis. Current signals were Bessel filtered (1 kHz) and digitised (3.33 kHz). Data acquisition and analyses were done with the software Pulse/Pulsefit (HEKA Elektronik), curve fitting and statistics with SigmaPlot and SigmaStat, respectively (Jandel Scientific, Erkrath, Germany).

2.3.7 ATP release assays

As described before [47], release of cellular ATP was measured by means of an ATP bioluminescent assay kit (FL-AA; Sigma) according to the manufacturers' instructions. For each clone, samples of $3 \cdot 10^5$ cells were incubated in 100 µl of Ca^{2+}-free modified Krebs-Ringer solution at room temperature for 5 min. After centrifugation, the supernatant was

removed and bioluminescent solution added from the assay kit. Three min later, the ATP was measured at room temperature with a luminometer (Lumat LB 9507; EG & G Berthold).

2.3.8 Adhesion assays

Cells were resuspended in DMEM or Ca^{2+}-free modified Krebs-Ringer solution, adjusted to approximately $3 \cdot 10^5$ cells/100 µl, added into the wells of culture plates at room temperature and allowed to adhere for approximately 30 min at 37°C. Non-adherent cells were carefully removed, the attached cells two times rinsed by gently pipetting in PBS and tapping of the plates. Adherent cells in 20 randomly chosen fields were counted under a Zeiss Axiovert S100 microscope (magnification: x200). Each experiment was assessed in duplicate. Experiments were repeated 5 times. To change the concentration of extracellular ATP, we preincubated the HeLa cells with 50 U/ml apyrase (Sigma) in DMEM for 15 min.

2.3.9 Statistics

The data are presented as means ±SEM. Independent experiments were compared by Student's t-test. Differences indicated by an asterisk were considered statistically significant at $P<0.05$.

2.4 RESULTS

2.4.1 Expression of the Cx37 variants

To investigate the biophysical properties of polymorphic Cx37 HCs, communication-deficient HeLa cells were stably transfected with Cx37-1019C, Cx37-1019T or empty pIRES-eGFP vector cDNA. As shown in Fig. 1A, G418-resistant clones were first screened by FACS for clones with similar eGFP expression profiles. Next, Western blotting for Cx37 was performed on these clones to verify the expression levels of total Cx37 protein (Fig. 1B). We then selected Cx37-S319 and Cx37-P319 clones with the same expression level of the protein (Fig. 1B, asterisks) and confirmed after biotinylation and extraction of cell surface proteins that equal amount of the polymorphic Cx37 proteins were localized at the cell surface (Fig. 1C). Finally, Cx37 was visualized in Cx37-S319 and Cx37-P319 clones using confocal microscopy (Fig. 1D). The equal expression levels in the Cx37-S319 and Cx37-P319 clones were carefully maintained by monthly FACS sorting and repeated Western blotting.

2.4.2 Electrophysiological properties of polymorphic Cx37 hemichannels

Hemichannels consisting of the Cx37 variants were studied with the single voltage-clamp method. A voltage-ramp protocol was applied to cells first exposed to bath solution of normal Ca^{2+} (control solution) and then to solution of low Ca^{2+} while the associated membrane current, I_m, was recorded.

Figure 2A shows original records obtained from a cell expressing Cx37-S319. The dashed trace represents the voltage protocol used to measure the membrane current, I_m, at steady-state condition. Starting from a holding potential V_h=0 mV, the membrane potential, V_m, was depolarised to 50 mV for 1.5 s. Subsequently, a slow voltage ramp was applied to reach -100 mV within 10 s (rate of change: 15mV/s). Thereafter, V_m was stepped back to V_h. In control solution, this protocol gave rise to a small and nearly linear background current

(grey trace). In low-Ca^{2+} solution, it elicited an extra current with a prominent inward peak (black trace). Figure 2B repeats the I_m signals already shown in Fig. 2A, but now displayed as current versus membrane potential rather than time. In control solution (grey trace), I_m was inward linear at negative V_m and outward at positive V_m. In low-Ca^{2+} solution (black trace), I_m was significantly larger at negative V_m, exhibiting a pronounced peak around V_m=-40 mV; at positive V_m, it was slightly larger and outward. Figure 2B also shows the current signal obtained in low-Ca^{2+} solution containing 2 mM heptanol (red trace), an inhibitor of HCs and GJCs [72, 142]. Under this condition, the Ca^{2+}-sensitive extra current disappeared, suggesting that the extra current in low-Ca^{2+} solution is carried by Cx37-S319 HCs. This conclusion is consistent with the finding that HeLa cells transfected with empty vector exhibited no extra current in low-Ca^{2+} solution (data not shown).

Figure 3A shows plots of the averaged functions $I_{hc}=f(V_m)$ at steady-state for Cx37-S319 (grey trace) and Cx37-P319 cells (black trace), summarizing the results of nine experiments each. To obtain the underlying data, the ramp protocol was applied to cells of both clones to determine $I_m=f(V_m)$ in the presence of control solution and low-Ca^{2+} solution. The difference between the latter and the former yielded a continuous relationship between I_{hc} and V_m for each cell. The difference function $I_{hc}=f(V_m)$ for each clone were sampled to calculate the group averages. The average functions showed a pronounced inward current with a maximum around V_m=-45 mV. The peak amplitude of the Cx37-P319 clone was larger than that of the Cx37-S319 clone. The bars correspond to means ±SEM calculated at discrete voltages.

To further characterize the properties of the induced HC current, the average $I_{hc}=f(V_m)$ of each clone was transformed into an average conductance function $g_{hc}=f(V_m)$ using the relationship $g_{hc}=I_{hc}/V_m$. Figure 3B shows $g_{hc}=f(V_m)$ for Cx37-S319 (grey trace) and Cx37-P319 (black trace). Both curves were bell-shaped, suggesting the involvement of two V_m-

sensitive gating mechanisms, one operational at large negative voltage, the other at small negative and positive voltage. The statistical analysis revealed a significant difference between both curves (asterisks). The clone Cx37-S319 reached a maximal conductance of 4.8 nS at V_m=-29 mV and clone Cx37-P319 a maximal conductance of 14.2 at V_m=-27 mV, respectively. Hence, the peak g_{hc} of Cx37-P319 was about 3-fold larger than that of Cx37-S319. Owing to disperse numeric ratios of g_{hc}/V_m close to V_m=0 mV, these data were ignored.

Figure 4 compares the normalized averaged plots of $g_{hc}=f(V_m)$ for both clones, using Cx37-P319 as reference. The continuous curves represent the best fit of data to the Boltzmann equation separately applied to the left- and right-hand tail of the bell-shaped curves. The analysis yielded the following values for the Boltzmann parameters $V_{m,0}$ (voltage at which g_{hc} is half-maximally inactivated), $g_{hc,min}$ (minimal value of g_{hc} at large voltage) and z (constant expressing gating charge). Cx37-P319 clone: $V_{m,0}$=-61.5/-3.5 mV, $g_{hc,min}$=0.03/0.08, z=2.3/3.1 (left-hand tail/right-hand tail; Fig. 4A); Cx37-S319 clone: $V_{m,0}$=-50.1/-4.8 mV, $g_{hc,min}$=0.11/0.09, z=2.3/3.6 (Fig. 4B). Hence, while $V_{m,0}$ was slightly larger and $g_{hc,min}$ slightly smaller in the case of Cx37-P319, z was nearly indistinguishable between the polymorphs.

2.4.3 Electrophysiological properties of Cx37 polymorphic gap junction channels

Single GJCs consisting of the Cx37 variants were examined with the dual voltage-clamp method. Experiments were carried out on pairs of HeLa cells, weakly coupled or normally coupled and exposed to 2 mM heptanol to reduce the number of operational GJCs (see, e.g.Bukauskas et al. [144]). Representative single channel recordings of Cx37-P319 and Cx37-S319 are shown in Figs. 5A and 5B, upper panels, respectively. A bipolar pulse protocol establishing a junctional voltage, V_j=±30 mV or V_j=±50 mV for Cx37-P319 and Cx37-S319 channels, respectively, was used to elicit single channel activity. Both types of channels

exhibited fast repetitive transitions between two distinct levels attributable to the fully open state and partially closed state of a channel, i.e. the main state and residual state. The current records, I_j, were then analyzed to determine the channel conductances, γ_j. The values of $\gamma_{j,main}$ and $\gamma_{j,residual}$ were collected and sampled in 10 pS bins. Figures 5A and 5B, lower panel, summarize the resulting frequency histograms of channel conductances. They include data gained at V_j ranging from ±30 to ±130 mV. In the case of both Cx37-P319 and Cx37-S319 GJCs, the $\gamma_{j,main}$ and $\gamma_{j,residual}$ data gave rise to a binomial distributions. The smooth curves are the best fit of data to the sum of two Gaussians. The mean channel conductances extracted were as follows ($\gamma_{j,main}/\gamma_{j,residual}$): Cx37-P319 clone: 290±2.6/76.5±4.9 pS (n=236; 5 cell pairs); Cx37-S319 clone: 195±2.7/51.2 ±2.7 pS (n=379; 4 cell pairs). Hence, the channel conductances of Cx37-P319 GJCs are about 1.5-fold larger than those of Cx37-S319 GJCs.

2.4.4 ATP release through polymorphic Cx37 hemichannels

ATP release from the Cx37 variants was examined in stably transfected clones with equal expression levels. Thus, ATP release was assayed during 5 min in a low-Ca^{2+} solution and compared between control HeLa cells and Cx37-S319 and Cx37-P319 clones. As shown in Fig. 6, Cx37-expressing HeLa cells released more ATP than control cells. In addition, we found that cells expressing the Cx37-P319 released 1.5 times more ATP than cells expressing Cx37-S319.

Considering the number of cells per sample ($3 \cdot 10^5$) and assuming a cell volume of 1 pl, and an $[ATP]_i$ of 2.5 mM [145], the amount of intracellular ATP per sample is 0.75 nMol. Provided in low-Ca^{2+} solution this intracellular ATP equilibrates with the extracellular solution (100 µl), this would lead to an $[ATP]_o$ of 7.5 µM. It represents an upper $[ATP]_o$ for Cx37-P319 to reduce cell adherence. Hence, the 1.5-fold lower luminescence signal of Cx37-

S319 corresponds to an upper $[ATP]_o$ of 5 μM. Partial release of ATP would result in lower levels of $[ATP]_o$.

2.4.5 Adhesive properties of HeLa cells transfected with the Cx37 variants

We have demonstrated previously that the human Cx37-C1019T polymorphism encodes for HCs that differentially control adhesiveness of mononuclear cells. To investigate whether this phenomenon might be generalized to other cell types, not of hematopoietic origin, we have performed adhesion assays on control HeLa cells, Cx37-S319 and Cx37-P319 transfectants. Consistent with the previous experiments, control HeLa cells showed increased adherence to tissue culture plates as compared to Cx37-expressing cells (Fig. 7A). In addition, we found that cells expressing the Cx37-P319 protein were less adhesive than cells expressing Cx37-S319 (Fig. 7A). When the adhesion assays were performed in a low-Ca^{2+} solution, we observed a ~4-fold reduction in the adhesiveness of control HeLa cells. However, similar differences in adhesiveness between control, Cx37-P319 and Cx37-S319 expressing cells were observed under these conditions (Fig. 7B). Finally, the reduction in adhesiveness of Cx37-expressing HeLa cells was canceled by extracellular apyrase (Fig. 7C), indicating that these effects were likely to be mediated by ATP.

2.5 DISCUSSION

Gap junctions have been historically implicated in the control of cell homeostasis, proliferation, differentiation and death [61], all crucial cellular processes in the development of cardiovascular disease. Previous studies from our laboratory with Cx-deficient mice have shown that these proteins play important roles in the development of atherosclerosis and restenosis [47, 112, 146]. The mechanisms by which Cxs mediate these pathological effects are multiple. They may involve changes in Cx expression levels or alterations in GJC properties. However, recent evidence suggests that Cxs, in particular Cx37, are important in leukocyte extravasation by mechanisms independent of cell-to-cell communication [47]. Connexin HCs, located in the plasma membrane, may play a role in autocrine/paracrine signaling and thus could influence intracellular Ca^{2+}, cell adhesion and cell survival by releasing intracellular mediators like ATP , NAD, or glutamate [147-149].

In this study, we have further investigated the characteristics of polymorphic Cx37 channels, a gene variation associated with CAD and MI in human. Cell biological and electrophysiological experiments yielded prominent differences between the polymorphic forms of hCx37, i.e. Cx37-P319 and Cx37-S319. To resume, we observed differences in adhesion of HeLa cells transfected with the polymorphic forms of hCx37 (Fig. 7). Similar to cells of hematopoietic origin [47], tumour cells transfected with Cx37-P319 were less adherent (50% less) than those with Cx37-S319. Moreover, we were able to correlate Cx37-dependent release of ATP with cell adhesion properties. Firstly, by treating Cx37-expressing HeLa cells with apyrase; this reversed the decreased adherence to the basal level observed in HeLa cells transfected with empty vector. Secondly, by measuring ATP released into the extracellular medium; we observed not only a large increase associated with the expression of Cx37, we also found that cells expressing Cx37-P319 released about 50% more ATP than cells expressing Cx37-S319 (Fig. 6). Calculations revealed considerable differences in the upper

limits of the quantity of released ATP (7.5 µM for Cx37-P319 and 5 µM for Cx37-S319). Although these measurements provide evidence for unequal ATP release through Cx37-P319 and Cx37-S319 HCs, they do not provide information on the actual ATP values in the microenvironment of the adhering cell.

It has been demonstrated that ATP release mediated by purinergic receptors (P2Rs) is controlled by HCs in a host of cells, e.g. in connexin-transfected HeLa cells [150]. The release of ATP is facilitated by lowering the external Ca^{2+}, a condition that favors HC opening. Hence, this positive feedback mechanism may also contribute to the release of ATP observed in our cells.

A summary of the current knowledge on GJCs and HCs may facilitate the discussion of the electrophysiology data [151, 152]. GJCs undergo fast and slow transitions. Fast transitions (<1 ms) between the channel main state (fully open) and residual state (partially closed) are governed by transmembrane voltage, V_j. This process is termed V_j-gating. It largely explains the properties of multichannel currents leading to the bell-shaped function $g_{j,ss}=f(V_j)$. Depending on the gating polarity of the connexins, only one HC of a GJC is responding at a given V_j (*cf.* [72]). In contrast, slow transitions (tens of ms) between the channel main state and a closed state (fully closed) are elicited upon exposure to agents such as alkanols, arachidonic acid, H^+ or Ca^{2+}. This behavior is termed chemical gating. At the multichannel level, it results in a substantial decrease of the gap junction conductance. On rare occasions, V_j also evokes slow transitions to the fully closed state, preferentially at large voltages [153]. Fast transitions to the residual state and slow transitions to the fully closed state are also seen in single cells expressing HCs [151, 152]. They reflect two separate voltage-gating mechanisms, i.e. V_j-gating and 'loop'-gating [154]. The former is reminiscent of V_j-gating seen in GJCs, the latter represents a mechanism by which HCs in cell membranes become operational. 'Loop'-gating responds to negative V_m and is modulated by H^+ and Ca^{2+}.

At the multichannel level, measurements on single cells showed that lowering $[Ca^{2+}]_o$ provoked a prominent inward current in both clones (Fig. 2A). In both cases, the function $g_{hc}=f(V_m)$ at steady state was bell-shaped and showed a peak around V_m=-30 mV (Fig. 3B), a value close to the membrane potential of non-excitable cells. Interestingly, the peak g_{hc} of Cx37-P319 was about 3-fold larger than that of Cx37-S319. The extra current was inhibited by heptanol (Fig. 2B), a HC and GJC blocker [72, 142], and was absent in cells transfected with empty vector, suggesting that it is carried by Cx37 HCs. Since most intrinsic channels of the HeLa cells were pharmacologically blocked (see **2.5 Solutions**), it is unlikely that the effect of heptanol emerged from channels others than Cx37 HCs [141, 142].

Our multichannel current data can be interpreted as follows. It has been shown that Cx37 channels are gating with positive voltage [154]. Hence, the V_j-gate of Cx37 HCs is operated when V_m is depolarized and the 'loop'-gate when V_m is hyperpolarized, i.e. depolarization is expected to elicit fast channel transitions to the residual state and hyperpolarization slow transitions to the closed state. Ideally, $g_{hc,min}$ at large positive V_m corresponds to the ratio $\gamma_{hc,residual}/\gamma_{hc,main}$ [144, 155]. However, it was smaller for both Cx37-P319 and Cx37-S319 (0.08 *vs*. 0.26 and 0.09 *vs*. 0.26). This may reflect a contribution of V_j-gating of slow transitions to the closed state at large voltage. In contrast, $g_{hc.min}$ at large negative V_m is expected to approach zero. Yet it settled at 0.03 and 0.11, respectively, indicating that the HCs close incompletely or some remain open. The parameters $V_{m,0}$ and z characterize the voltage-sensitivity of the channel gating. For depolarization, these parameters are virtually identical for Cx37-P319 and Cx37-S319. However, for hyperpolarization, the values of z are identical, but not those of $V_{m,0}$ (-61.5 *vs*. -50.1 mV). This suggests that Cx37-P319 is less voltage sensitive. The reason for this is not clear.

At the single channel level, measurements on cell pairs revealed differences in the conductance of GJCs between Cx37-P319 and Cx37-S319. Signals of single channel currents

of both clones showed two prominent levels corresponding to $\gamma_{j,main}$ and $\gamma_{j,residual}$, and a less prominent level reflecting the channel closed state, preferentially seen at larger V_j (data not shown). Interestingly, $\gamma_{j,main}$ of Cx37-P319 GJCs was about 50% larger than that of Cx37-S319, implying that the HC conductance of Cx37-P319 is also larger than that of Cx37-S319 (e.g. [155]). This conclusion offers an explanation for the larger g_{hc} values of Cx37-P319 HCs and supports the hypothesis that the larger conductance of Cx37-P319 HCs is largely responsible for the increased ATP release. Whether the amino acid alteration in Cx37-CT also influences the open-channel probability and/or the channel permselectivity [156] remains to be determined.

To study the properties of Cx37 HCs, our single-cell experiments were carried out in low-Ca^{2+} solution. As previously shown, a decrease in $[Ca^{2+}]_o$ increases the number of open Cx37 HCs in a dose-dependent fashion [157]. Hence, occasional channel openings may already occur at physiological $[Ca^{2+}]_o$. Because of their large conductance, this could be sufficient for a sizable release of ATP, especially in the case of Cx37-P319 (Fig. 6).

So far, no systematic investigation on $\gamma_{j,main}$ measurements for Cx37 GJCs has been published. Instead, a compilation of data from different studies is available. It presents values for Cx37-P319 and Cx37-S319 ranging from 300-375 and 348-374 pS, respectively [158]. The authors inferred that the conductance of polymorphic channels is indistinguishable. However, disperse and rudimentary data, selective quotation, missing statistics and involvement of different labs and researchers cast doubts on this conclusion. Conceivably, differences in cell types and experimental conditions may also contribute to the discrepancy with our data and conclusion. With regard to $g_{hc}=f(V_m)$ at steady state, it has been shown that some Cxs form HCs with a sigmoidal relationship reflecting V_j-gating of GJCs (e.g. Cx45 [142]), while others form HCs with a bell-shaped relationship with two gating mechanisms, one corresponding to V_j-gating of GJCs, the other representing 'loop gating' attributable to E1 and E2 of the Cxs

and hence inherent to solitary HCs (e.g. Cx30, Cx46, Cx50) [144, 153]. Hence, our Cx37 HCs resemble the second type.

Recently it has been suggested that voltage gating of Cx37 HCs can be explained as block/unblock by divalent cations with no need for an extra voltage gate [157]. A direct comparison of this study with ours is limited due to different preparations (oocytes expressing high levels of Cx37 *vs*. HeLa cells expressing low levels of Cx37) and ionic conditions ($[Ca^{2+}]_o$: ≥20 μM *vs*. 20 nM). As to experimental data, distinct discrepancies are apparent. For example, at large negative voltage, HCs in oocytes are open in low Ca^{2+} solution, however in HeLa cells they are closed. Moreover, HCs in oocytes are weakly sensitivity to heptanol (10 mM: 68% inhibition), yet in HeLa cell they are strongly sensitive (2 mM: 100% inhibition). Beyond data discrepancies, the model by Puljung and coworkers, although appealing, is not easy to reconcile with the established concept of GJC and HC operation [151, 152] and the large body of underlying data. Considering the wide spectrum of GJC and HC responses to voltage and ions such as H^+ and Ca^{2+}, the exclusion of further gating mechanisms such as voltage gating seems awkward. Further experimental work is needed to clarify the issue.

Recent research has demonstrated a strong association of the Cx37 C1019T polymorphism, a protein normally expressed in endothelial cells but also found in monocytes and macrophages, with arterial stenosis and myocardial infarction in human [122-124, 130, 131]. The human Cx37 genotype was then also shown to predict survival after an acute coronary syndrome [159]. In a previous study, we have identified Cx37 as a potential “protector protein” that prevents excessive monocyte recruitment in atherosclerosis [47]. Cx37 HCs appeared to control the initiation of atherosclerotic plaque development in mice by modulating the autocrine ATP-dependent regulation of monocyte/macrophage adhesion. We have also shown in the afore-mentioned study that a human macrophage cell line transfected with Cx37-S319 or Cx37-P319 revealed differential adhesiveness to substrates. In the present

study, we found that Cx37-P319 cells released more ATP and were less adhesive than HeLa cells expressing a similar level of Cx37-S319. Moreover, the electrical measurements implied that Cx37-P319 HCs exhibit a larger unitary conductance than Cx37-S319 HCs. Based on these results, we conclude that the larger conductance of Cx37-P319 HCs is largely responsible for the increased ATP release and the subsequent impaired substrate adhesiveness of these cells. Assuming the properties of Cx37 HCs are similar in monocytes and transfected HeLa cells, this study offers a molecular mechanism whereby the Cx37-P319 variant protects against atherosclerosis.

2.6 ACKNOWLEDGEMENTS

We thank Esther Sutter, Bernard Foglia, Christos Chadjichristos, Marc Chanson, Sandrine Morel, Laurent Burnier, Daniel Lüthi and Hamdy Shaban for technical assistance and helpful discussions. This work was supported by grants from the Swiss National Science Foundation (PP00A-68883 and PP00A-116897 to BRK and 3100A0-108175 to RW), the Helmut Horten Foundation, and the Swiss University Conference Program 'Heart Remodeling in Health and Disease'.

2.7 FIGURE LEGENDS

Fig. 1. Transfection and selection of HeLa cells with Cx37 polymorphs. (A) Stringent sorting was performed on HeLa cell clones transfected with hCx37-1019T (S319; green), hCx37-1019C (P319; blue), or empty eGFP vector cDNA (EV; black). Only transfected cells with a fluorescent signal above background (i.e. untransfected cells; white) were selected. (B) Western blots for Cx37 in the HeLa transfectants. Clones with similar expression levels (*) of Cx37-S319 and Cx37-P319 were subsequently used for experiments. (C) Western blots comparing total (top left panel) and membrane (top right panel) Cx37 expression in the selected Cx37-S319 and Cx37-P319 clones. β-actin was used as a control for loading (bottom panels). Western blots are representative of 3 independent experiments. (D) Reconstituted confocal Z-axis images of Cx37 immunostaining (green) of the transfected HeLa cells. Cells were counterstained with Evans Blue (red).

Fig. 2. Currents carried by hCx37 hemichannels. (A) Electrical signals of a single cell expressing Cx37-S319. Dashed trace: voltage-ramp protocol representing the applied membrane potential, V_m, *versus* time. During the 10 s ramp the voltage changes from 50 to -100 mV. Grey trace: plot of membrane current, I_m, *versus* time, associated with the ramp protocol, recorded in control solution. Black trace: corresponding plot of I_m *versus* time recorded in low Ca^{2+} solution, revealing an extra current with an inward peak at negative V_m. (B) Superimposed plots of membrane currents, I_m, versus membrane potential, V_m, obtained by re-plotting the original current and voltage traces in Fig. 2A. The I_m signals depicted were gained in different solutions. Grey trace: control solution (background current). Black trace: Ca^{2+}-free solution (extra current). Red trace: low Ca^{2+} solution plus 2 mM heptanol.

Fig. 3. Properties of hCx37 hemichannels. (A) Comparison of averaged current/voltage relationships obtained from cells expressing the Cx37-S319 (grey trace) and Cx37-P319 form (black trace). In each experiment, the HC current, I_{hc}, was determined as I_m(low Ca^{2+} solution) − I_m(control solution). The plotted curves correspond to the averaged I_{hc} (N=9 for each group). (B) Comparison of averaged conductance/voltage relationships for HC made of Cx37-S319 (grey curve) and Cx37-P319 form (black trace). Conductances were calculated as $g_{hc}=I_{hc}/V_m$ in each group. Values of g_{hc} close to V_m=0 mV show a large scatter due to disperse numeric ratios and hence were ignored.

Fig. 4. Boltzmann characteristics of hCx37 hemichannels. The curves in black show the functions $g_{hc}=f(V_m)$ for both clones. The curves in red represent the best fit of data to the Boltzmann equation using the parameters $V_{m,0}$ (voltage at which g_{hc} is half maximally inactivated), $g_{hc,min}$ (minimal g_{hc} at large voltage) and z (constant expressing gating charge): (A) Cx37-P319 clone: $V_{m,0}$=-61.5/-3.5 mV, $g_{hc,min}$=0.03/0.08, z=2.3/3.1 (left-hand/right-hand shank of curve). (B) Cx37-S319 clone: $V_{m,0}$=-50.1/-4.8 mV, $g_{hc,min}$=0.11/0.09, z=2.3/3.6.

Fig. 5. Properties of single hCx37 gap junction channels. (A) and (B) Top: recordings from pairs of transfected cells with one operational channel. Current signal I_j elicited by a V_j = ±30 mV and V_j = ±50 mV for Cx37-P319 and Cx37-S319 channels, respectively. Continuous line: zero current level; dotted line: channel residual state; dashed line: channel main state. (A) and (B) Bottom: histogram of single channel conductances. The left-hand and the right-hand distribution represent the conductance of the residual state $\gamma_{j,residual}$, and the main state $\gamma_{j,main}$, respectively. Bin width: 10 pS. Smooth curves: best fit of data to the Gaussian function yielding the following mean values ($\gamma_{j,main}/\gamma_{j,residual}$) Cx37-P319 (A) 290±2.6/76.5±4.9 pS; Cx37-S319 (B) 195±2.7/51.2±2.7 pS.

Fig. 6. Differential Cx37 hemichannel-dependent release of ATP. Cells were incubated in a low Ca^{2+} solution to induce opening of hemichannels. The release of ATP into the extracellular medium was enhanced in cells transfected with hCx37 when compared to control cells transfected with the empty vector (EV). The enhancement of ATP release was significantly different in the Cx37 polymorphs. Cx37-P319 cells: 299±15.4%; Cx37-S319 cells: 207±22.9%. Data of 6 independent experiments are expressed as percentage of control cells. Error bar shows SEM and $^{*}P<0.001$.

Fig. 7. Differential Cx37 hemichannel-dependent adherence. (A) The number of HeLa cells that adhered to tissue-culture plates was reduced in cells transfected with either hCx37 cDNA (Cx37-S319, 62.9±10.7% and Cx37-P319, 18.7±4.6%) compared to cells transfected with empty vector cDNA. This reduced adhesion was significantly different between the two Cx37 polymorphs. Data of 5 independent experiments are expressed as percentage of control cells. (B) Similar differences in adhesion were obtained in Ca^{2+}-free medium, i.e. Cx37-S319, 65±5.8% and Cx37-P319, 45±6.4%, N=5. (C) The reduction of adhesiveness of hCx37-expressing HeLa cells was canceled by extracellular apyrase. Thus, the number of apyrase-treated HeLa cells that adhered to tissue culture plates was unaffected in cells transfected with empty vector cDNA (98.3±12.5%) and reversed in cells transfected with either hCx37 cDNA (Cx37-S319, 98.2±7.5% and Cx37-P319, 99.8±7.6%). Data of 6 independent experiments are expressed as percentage of control cells. Error bars show SEM and $^{*}P<0.005$.

2.8 FIGURES

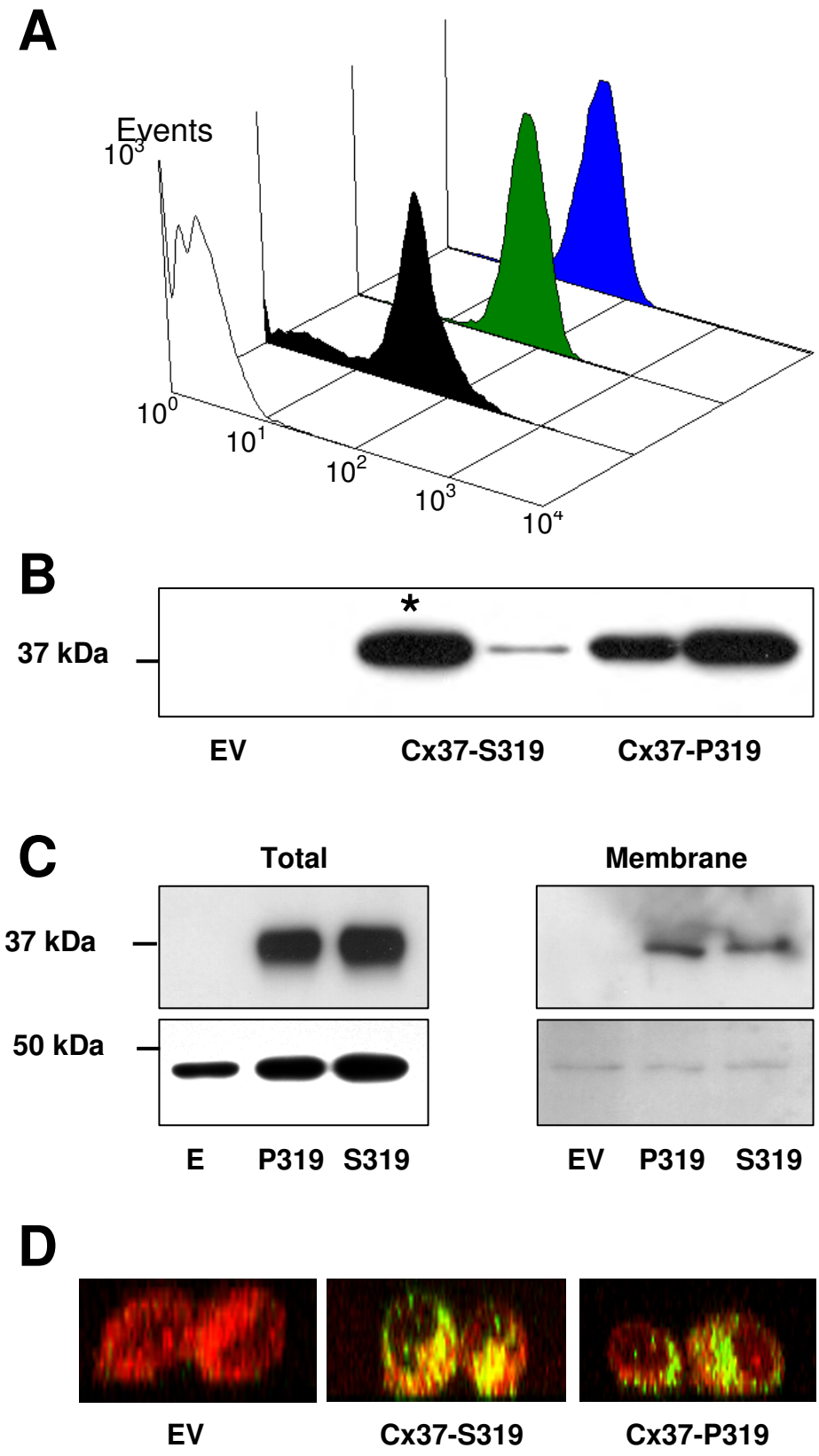

Figure 1

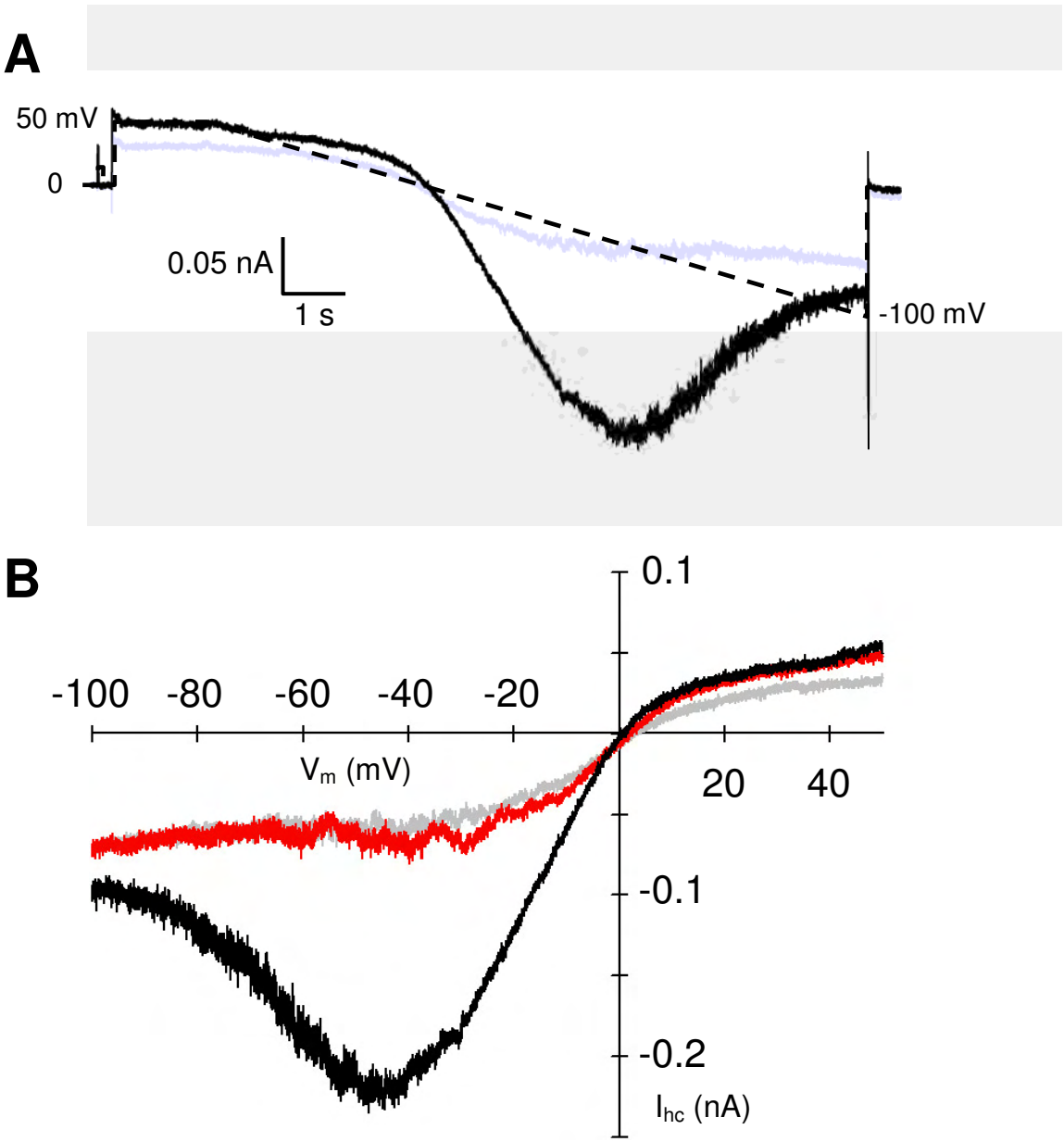

Figure 2

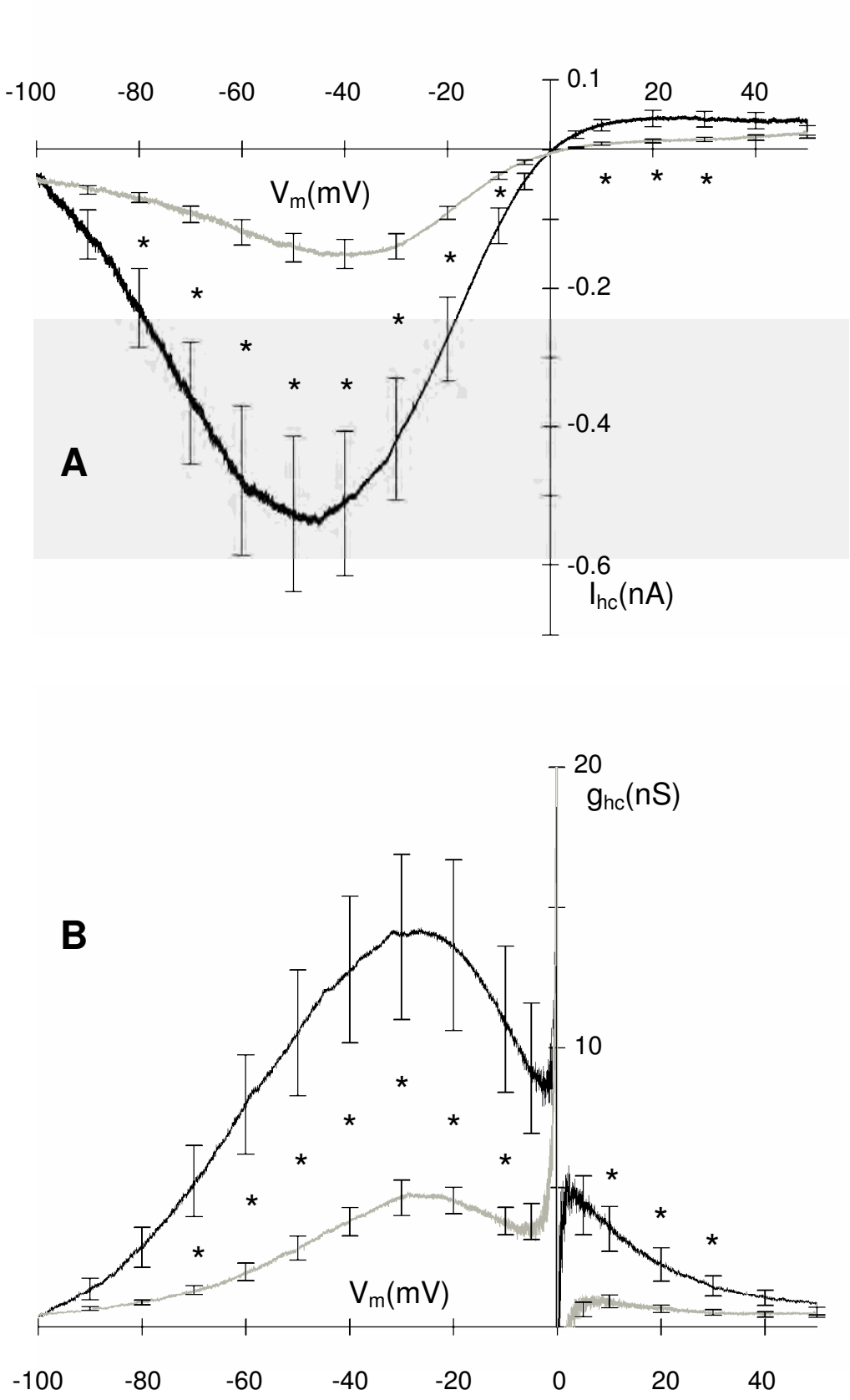
-100
-80
-60
-40
-20
0.1
20
40
V_m(mV)
-0.2
-0.4
-0.6
I_{hc}(nA)
A
20
g_{hc}(nS)
B
10
V_m(mV)
-100
-80
-60
-40
-20
0
20
40

Figure 3

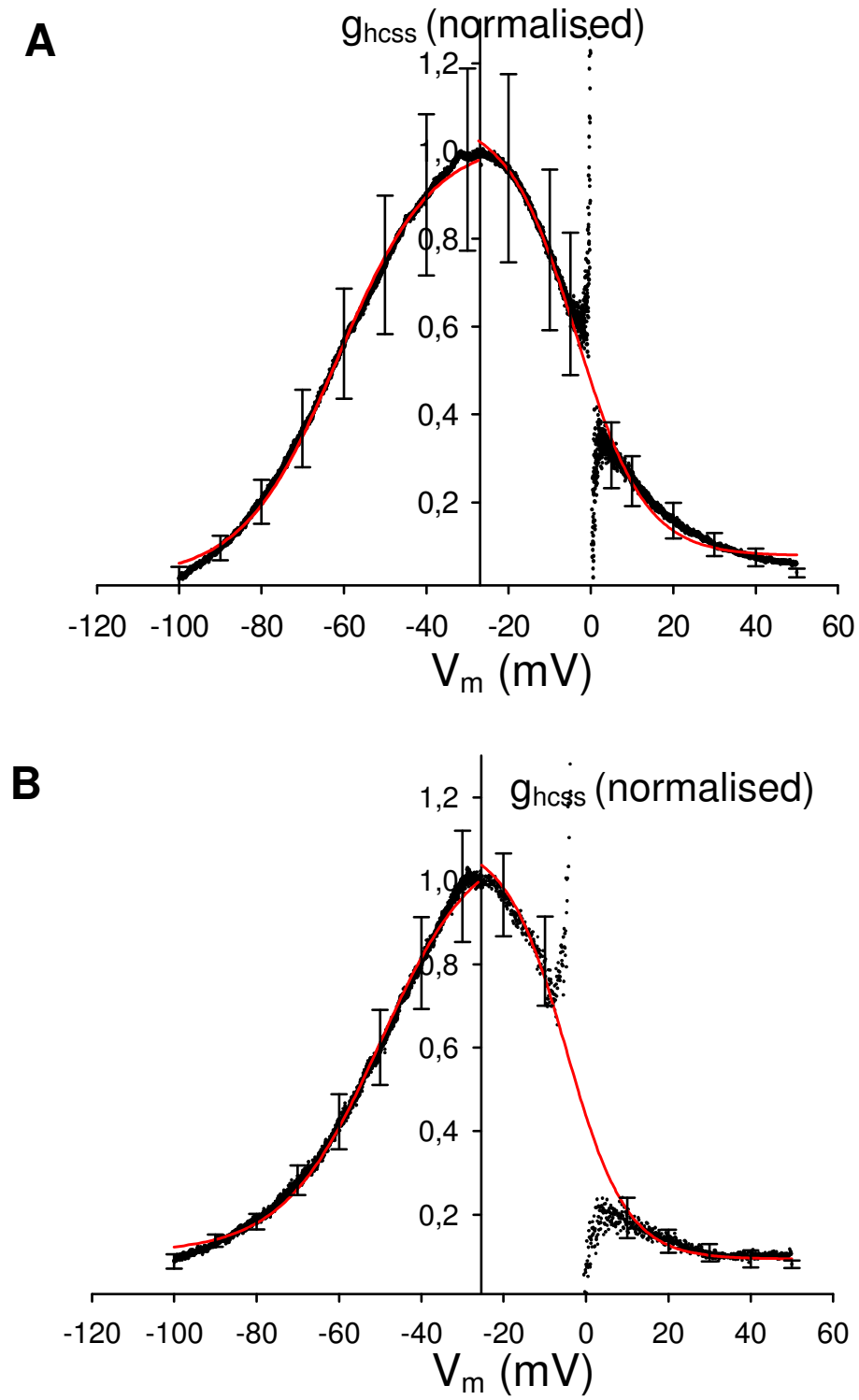
A
g_{hcss} (normalised)
1,2
1,0
0,8
0,6
0,4
0,2
-120 -100 -80 -60 -40 -20 0 20 40 60
V_m (mV)
B
g_{hcss} (normalised)
1,2
1,0
0,8
0,6
0,4
0,2
-120 -100 -80 -60 -40 -20 0 20 40 60
V_m (mV)

Figure 4

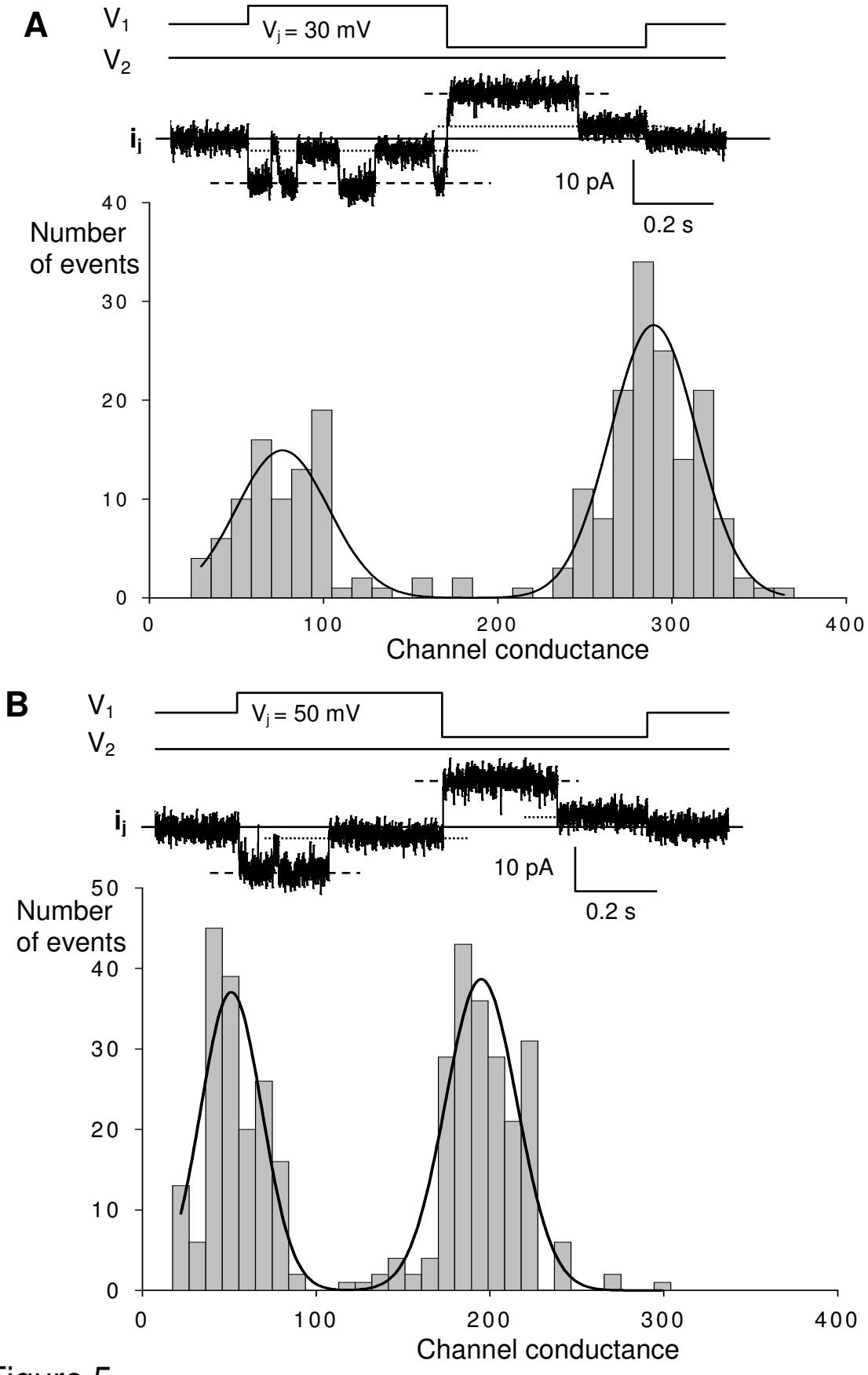
A
V1
V2
Vj = 30 mV
ij
10 pA
0.2 s
Number of events
40
30
20
10
0
0
100
200
300
400
Channel conductance
B
V1
V2
Vj = 50 mV
ij
10 pA
0.2 s
Number of events
50
40
30
20
10
0
0
100
200
300
400
Channel conductance

Figure 5

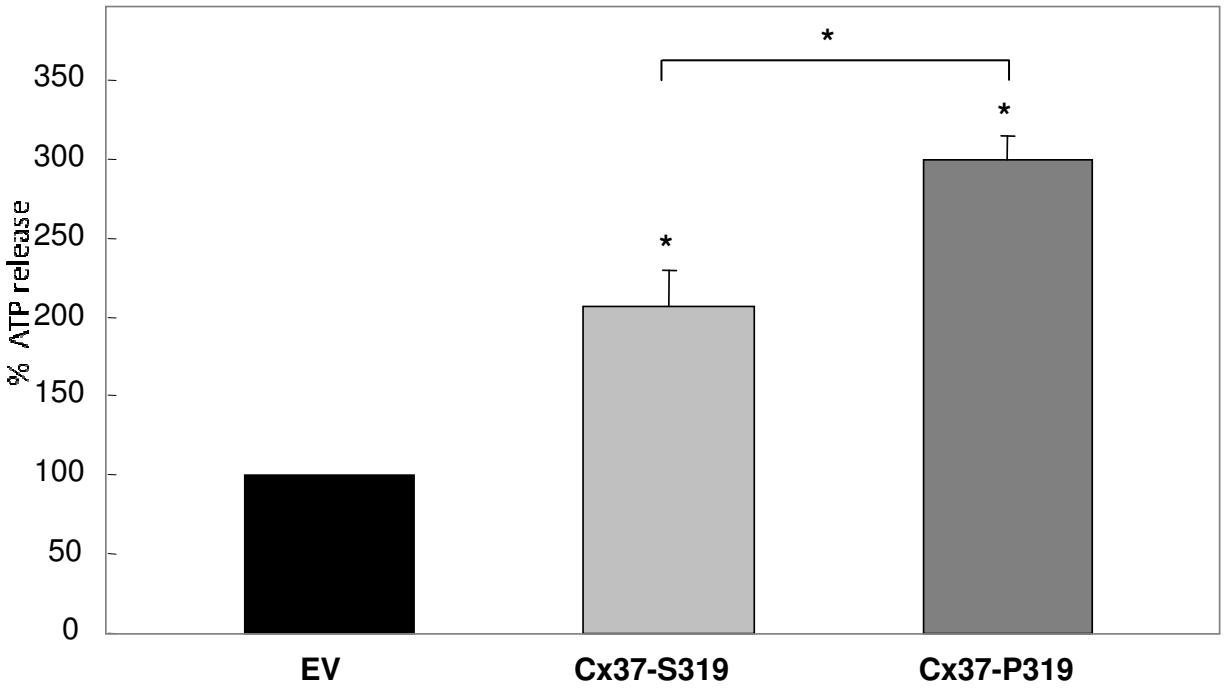

Figure 6

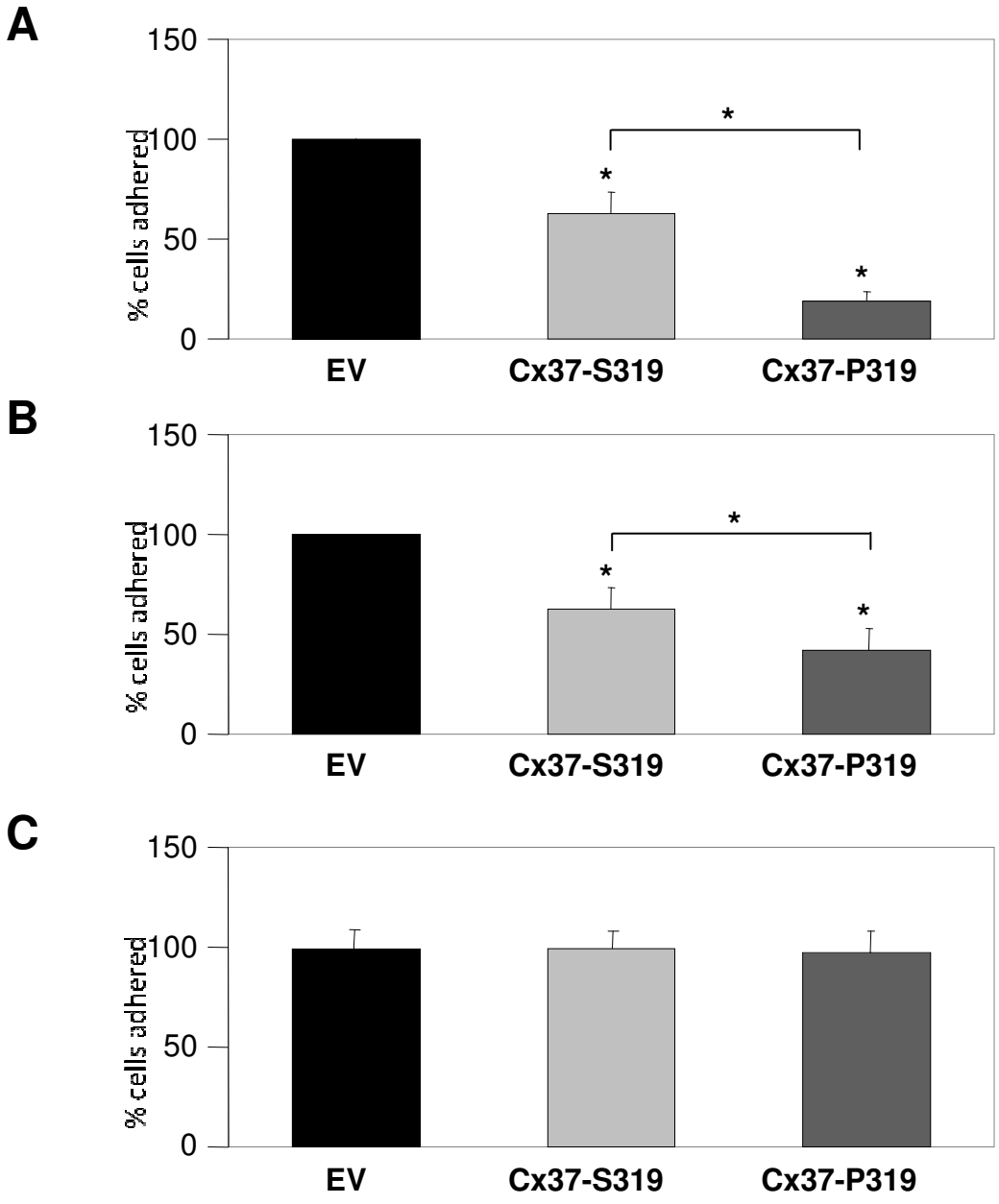
A
150
100
50
0
% cells adhered
*
*
*
EV
Cx37-S319
Cx37-P319
B
150
100
50
0
% cells adhered
*
*
*
EV
Cx37-S319
Cx37-P319
C
150
100
50
0
% cells adhered
EV
Cx37-S319
Cx37-P319

Figure 7

3 THE GAP JUNCTION PROTEIN Cx37 INTERACTS WITH eNOS IN ENDOTHELIAL CELLS

Submitted on the 15th of May, 2008; under revision.

The gap junction protein Cx37 interacts with eNOS in endothelial cells

Jean-Paul Derouette[1]*, Anna Pfenniger[1,2]*, Vandana Verma[2], Bernard Foglia[1], Wanda Coombs[3], Isabelle Roth[1], Paul Sorgen[4], Steve Taffet[3], Brenda R. Kwak[1] and Mario Delmar[2]

[1]Division of Cardiology, Department of Internal Medicine, Faculty of Medicine, University of Geneva, Switzerland; [2]Division of Cardiovascular Medicine, Department of Internal Medicine, University of Michigan, AnnArbor MI, USA; [3]Department of Immunology and Microbiology, SUNY Upstate Medical University, Syracuse, NY, USA; [4]Department of Biochemistry and Molecular Biology, University of Nebraska Medical Center, Omaha, NE, USA;

*Authors contributed equally to the study

Short title: Cx37 interacts with eNOS.

Word count: 6025, abstract word count: 243, 4 figures and 2 tables

Address for correspondence:

Mario Delmar MD PhD FAHA

Division of Cardiovascular Medicine

Department of Internal Medicine

University of Michigan Center for Arrhythmia Research

5025 Venture Dr

Ann Arbor MI 48109

Email: mdelmar@umich.edu

3.1 ABSTRACT

Cx37 is a gap junction protein essential for cell-cell communication in the vasculature. A C1019T Cx37 gene polymorphism, encoding for a P319S amino acid substitution in the regulatory C-terminus of Cx37 (Cx37CT), was found to correlate with arterial stenosis and myocardial infarction in humans. The aim of this study was to identify potential binding partners for Cx37CT and to determine whether the polymorphism modified this interaction. Using a high throughput phage display, we retrieved 2 consensus binding motifs for Cx37CT: WHK…[K,R]XP... and FHK…[K,R]XXP…, the first one being more frequent for Cx37CT-319P and the second more frequent for Cx37CT-319S. One of the peptides (WHRTPRLPPPVP) showed a 77.7% homology with amino acids 843-854 of endothelial nitric oxide synthase (eNOS). *In vitro* binding of this peptide to both forms of Cx37CT was confirmed by cross-linking and surface plasmon resonance. Electrophysiological analysis of Cx37 single channel activity in transfected N2a cells showed that eNOS-like peptides increased the frequency of occurrence of conductances higher than 300 pS. eNOS co-immunoprecipitated with Cx37 in human endothelial cells (ECs) transfected with human Cx37 polymorphs and in a mouse EC line (bEnd.3). Immunofluorescence microscopy showed a co-localization of these proteins at membranes in bEnd.3 cells and a dose-dependent increase in NO production was observed when they were treated with Cx37-antisense. Overall, our data show for the first time a functional interaction between eNOS and Cx37. This interaction may be relevant for the control of vascular physiology both in health and in disease.

(243 words)

Key words: Connexin37, GJA4, endothelial nitric oxide synthase, gene polymorphism.

3.2 INTRODUCTION

Connexins are integral membrane proteins that oligomerize to form intercellular channels called gap junctions. The gating, permeability and regulatory properties of a gap junction channel vary depending on the connexin isotype. The present study focuses on connexin37 (Cx37), an isotype expressed mostly in endothelial cells (ECs), monocytes and macrophages, but also found in vascular smooth muscle cells (SMCs) [139]. Studies on genetically-modified mouse models suggest an involvement of Cx37 on the pathogenesis of atherosclerosis [47]. Additional studies have shown atherosclerosis-related changes in Cx37 expression; in particular, Cx37 can no longer be detected in the endothelium overlaying advanced atheromas, whereas there is high expression in resident macrophage foam cells and expression in the – previously Cx37 deprived – medial SMCs [111]. Studies in humans indicate that a polymorphism at position 1019 of the *GJA4* gene, encoding for human Cx37, may be a prognostic marker for atherosclerosis [139]. This C1019T polymorphism codes for a proline-to-serine substitution (P319S) in the C-terminal domain of the protein. Two separate studies showed a correlation between the presence of the Cx37-319S isoform and an increased incidence of myocardial infarction in the sampled population [123, 124]. The Cx37-319S genotype was also shown to predict survival after an acute coronary syndrome [159]. In three additional studies, the alternative isoform (Cx37-319P) was found to segregate with an increased incidence of stenosis in the coronary [130, 131] or the carotid arteries [122]. Studies at the cellular level recently showed that Cx37 expression inhibited monocyte adhesion to the endothelium; this effect was more pronounced in monocytes expressing Cx37-319P than in those expressing Cx37-319S [47]. Overall, the data support the notion that Cx37 could play a protective role against the development of atherosclerosis, and leave open the possibility that variations in the sequence of the C-terminal domain of Cx37 could have functional effects relevant to pathophysiology.

Little is known about the functional role of the C-terminus of Cx37. Primary sequence analysis of this region identifies a number of potential consensus sites for phosphorylation, and/or for the binding of Cx37 to other molecules [160, 161]. As such, it is reasonable to speculate that, as in the case of other connexin isotypes [138, 137, 70], the C-terminal region is the major regulatory domain of Cx37 and perhaps, the P319S polymorphism alters Cx37 regulation. Yet, a non-biased search for potential molecular partners of Cx37 remains to be conducted.

In the present study, we have carried out a high-throughput phage display screening in search for peptidic sequences that bind to the C-terminal domain of Cx37. Our results show that Cx37-319P preferentially binds to peptides containing the motif WHK…[K,R]XP..., whereas Cx37-319S displayed a preference for FHK…[K,R]XXP... motifs. Moreover, we identified a particular peptidic sequence homologous to a region of endothelial nitric oxide synthase (eNOS), an enzyme of fundamental importance to vascular biology and disease [162, 163, 164]. Additional studies showed that this peptide (heretofore dubbed "eNOS-like") could affect the function of Cx37 channels. Moreover, these results led us to demonstrate that Cx37 associates with eNOS in the native environment of an endothelial cell, thereby functionally affecting the enzyme. Overall, our data indicate a possible cross-talk between these two molecules and suggest a functional role for this interaction in the production of nitric oxide (NO) in the vascular endothelium.

3.3 MATERIALS AND METHODS

3.3.1 Production and purification of recombinant Cx37CT

Recombinant Cx37CT was produced following methods previously described [165]. For details on the production of the Cx37CT-319P and Cx37CT-319S clones, see the Online Supplement.

3.3.2 Phage display

Phage display is a high-throughput method for identification of molecules binding to a ligand of interest. Here, we applied it to the detection of potential ligates of the CT domain of both isoforms of Cx37. The protocol was similar to that previously described [166] and can be found in the Online Supplement at http://atvb.ahajournals.org/cgi/reprint/ATVBAHA.109.200816v1

3.3.3 Motif analysis

The significance of particular motifs in the retrieved phage display sequences was assessed by comparing their actual frequency to their theoretical occurrence based on the experimental ratio of each amino acid. For more details, see online supplement.

3.3.4 Surface plasmon resonance

Surface plasmon resonance (SPR) is a spectroscopic method to determine the amplitude and kinetics of binding between two molecules in real time [167, 168]. Recombinant Cx37CT-319P and Cx37CT-319S were covalently bound to a carboxymethyl dextran matrix (Sensor Chip CM5, Biacore), and synthetic peptides were presented to assess binding. For details on the method, see online supplement.

3.3.5 Cross-linking experiments

Cross-linking reagents enable the formation of covalent bonds between molecules in close proximity. A total of 0.25mmol/L of recombinant Cx37CT and 0.5mmol/L of a peptide were incubated for 1 hour at room temperature with 1mM of the cross-linker reagent BS^3 at pH 7.4

[169, 170]. The reaction was subsequently blocked with 100mmol/L ethanolamine for 10 min. The samples were separated by SDS-PAGE (4-20%) and stained with Coomassie-Blue.

3.3.6 Cell culture

Three different cell lines were used: a) a communication-incompetent line of murine neuroblastoma cells (N2a; American Type Culture Collection; Manassas, VA), b) a mouse endothelial cell line (bEnd.3) which endogenously expresses all three endothelial connexins [140], and c) a human endothelial cell line (EA.hy926; ATCC) which has no detectable endogenous expression of Cx37. For details on the cell culture, see the online supplement.

3.3.7 cDNA preparation and transfection into cells

Communication-incompetent EA.hy926 and N2a cells were induced to express Cx37-319P and Cx37-319S. For details on transfection, selection and detection methods [47], refer to the Online Supplement.

3.3.8 Patch clamp recording and analysis

The effect of the eNOS-like peptide on the electrical properties of Cx37-319P and Cx37-319S has been studied in transfected N2a cells using the dual whole-cell patch-clamp technique. For details on methods, solutions used and recording procedures, see the Online Supplement.

3.3.9 Co-immunoprecipitation studies

The interaction of eNOS and Cx37 in of bEnd.3 cells or transfected EA.hy926 cells was assessed by the co-immunoprecipitation of eNOS with Cx37. For details on the reagents and the method, see the Online Supplement.

3.3.10 Immunofluorescence

bEnd.3 cells were immuno-labelled with Cx37 (ADI) and eNOS (BD Sciences) antibodies, as described previously[3]. For details, see the Online Supplement.

3.3.11 NO release

NO release assays were performed using 96-well plates (Falcon). Ten thousand bEnd.3 cells were plated per well and grown to confluence for 48 hours in the presence of 10, 25 or 50 μmol/L Cx37 anti-sense oligonucleotides (5'-GTCCCTTCGTGCCTTTATCTC-3'). Cx37 sense oligonucleotides (5'-TGCTAGACCAGGTCCAGGAAC-3') were used as controls. Total NO release to culture supernatant was measured during the final 16 hours using the Total Nitric Oxide Assay Kit (Assay Designs) according to the manufacturers' instructions. NO release was assayed in duplicate.

3.3.12 Statistics

Results are presented as mean ± SEM. Unpaired t-test was used to compare differences between two groups and ANOVA for comparison of multiple groups. Data were considered statistically significant at $P<0.05$.

3.4 RESULTS

3.4.1 Phage display

We analyzed the sequence of the insert retrieved from a total of 120 plaques. Of the estimated $2.5x10^9$ different sequences presented in the phage display, 44 were captured by the Cx37CT-319P protein, and 41 by Cx37CT-319S. Thirteen of these sequences were recovered by both baits. The corresponding peptide sequences, and the number of plaques analyzed that contained the same sequence, are presented in Table 1. When compared to the prebound library, basic residues were more frequently found in the captured peptides, whereas acidic residues showed an opposite trend (see online data supplement Table 1). In addition, most peptides presented amino acids [F,W]HK in positions 1-3 and included the motif [K,R]XP or [K,R]XXP as part of their sequence (Table 1). Motif [K,R]XP was more frequent in peptides captured by the Cx37CT-319P bait, whereas [K,R]XXP was more frequent in those peptides captured by Cx37CT-319S.

We calculated the probability of occurrence of these motifs by chance alone, taking into account the abundance of individual amino acids in the library prior to screening (see Methods). The results indicate that the actual occurrence of the specific sequences was significantly higher than their expected probability (see online data supplement: Tables 2 and 3). Overall, the data support the notion that Cx37CT-319P bound with enhanced selectivity to peptides containing the motif WHK…[K,R]XP…, whereas the sequence FHK…[K,R]XXP… was selected by the Cx37CT-319S protein. Moreover, sequence alignments against the NCBI protein database (BLAST) indicated homology between one of the selected peptides, and amino acids 843-854 of the endothelial nitric oxide synthase (eNOS; see Table 2) with the eNOS(843-854) sequence containing both the [K,R]XP as well as the [K,R]XXP motif. Given the biological importance of eNOS in cells where Cx37 is naturally present, we pursued further characterization of these peptides and the CT domain of Cx37.

3.4.2 In vitro binding detected by SPR and cross-linking

Phage display allows screening for many potential binding sequences, but it does not give information as to the characteristics of the binding reaction. We therefore used SPR to quantitatively characterize the binding of selected peptides to Cx37CT. Our studies focused on the peptide showing the highest homology to eNOS (dubbed: "eNOS-like") and a 12-mer peptide corresponding to sequence 843-854 of eNOS ("eNOS(843-854)"). Each Cx37CT isoform was bound to a separate carboxymethyl dextran matrix. Synthetic peptides were presented at concentrations varying between 1mmol/L and 62.5µmol/L (for eNOS-like) or between 0.5mmol/L and 62.5µmol/L (for eNOS(843-854)) and the time course and amplitude of binding was recorded. As shown in Figure 1, superfusion of the peptides elicited a concentration-dependent resonance shift indicative of binding to Cx37CTs. The binding of eNOS-like to Cx37CT-319P or to Cx37CT-319S was best described by a first-rate order model with average dissociation constants (K_D) of 66µmol/L and 65µmol/L, respectively. The binding of Cx37CT-319P to eNOS(843-854) yielded a K_D value of 142µmol/L, whereas the interaction of this same peptide to Cx37CT-319S was too weak to allow for proper quantitative analysis. Overall, our data show that these peptides are able to interact with a recombinant protein containing the Cx37CT sequence. Further confirmation of these intermolecular interactions was obtained by cross-linking experiments, as described below.

3.4.3 Cross-linking of Cx37CT to eNOS-like and eNOS(843-854) peptides

Whereas SPR analysis requires the physical constraint of the bait protein to the matrix of the sensor chip, the use of a cross-linker reagent allows for the study of intermolecular interactions when the purported molecular partners are free in solution. Figure 2 shows the

results obtained from the cross-linking of Cx37CT to either the eNOS-like (Figure 2A) or the eNOS(843-854) peptides (Figure 2B). After separation by SDS-PAGE, the samples were stained with Coomassie-Blue. A band around 11kDa representing Cx37CT could be seen in all samples. In the samples incubated with the cross-linking reagent (lanes 1, 2, 4 and 5), some supplementary bands were observed in the range between 22 and 36kDa, likely resulting from polymerization of Cx37CT. Lanes 2, 3, 5 and 6 show results obtained in the presence of the peptides. Bands of low molecular weight, corresponding to monomers or multimers of the peptides can be observed. Interestingly, in lanes 2 and 5, where the samples contain one isoform of Cx37CT, eNOS-like or eNOS(843-854) peptides and the cross-linker, a supplementary band can be seen above the Cx37CT band. The mobility of the band corresponded to the estimated molecular weight of a Cx37CT-peptide complex (approximately 12kDa). Notice that the density of this band was actually higher than that of the multimers of Cx37CT, suggesting a higher affinity for the peptide-protein interaction than for oligomerization of the free Cx37CT (see, e.g., Sorgen et al [170]). These results are consistent with those obtained by SPR and suggest that the eNOS-like and the eNOS(843-854) peptides bind to both Cx37CT isotypes.

3.4.4 Effect of peptide eNOS-like on the function of Cx37 channels

The ability of eNOS-like and eNOS(843-854) peptides to bind Cx37CT led us hypothesize that the peptides may also change the behavior of Cx37 channels. As the eNOS-like peptide showed a stronger affinity by SPR, we focused on the effect of this peptide in this study. Gap junction currents were recorded from N2a cells transfected with Cx37-319P or Cx37-319S. To reduce macroscopic currents, cell pairs were superfused with 2-4mmol/L octanol.

The control recordings and all-events histogram of unitary conductances obtained from Cx37-319P or Cx37-319S cell pairs (Figure 3A and 4B, respectively) show the

characteristic pattern that Cx37 channels transit between various conductive states up to 400 pS. Interestingly, the presence of the eNOS-like peptide alters the frequency of occurrence of high-conductance events (Figure 3C and 4D). A continuous line represents the best-fit of Gaussian functions describing the distribution of events. Quantitative analysis showed that for Cx37-319P, the frequency of events corresponding to channels of 300 pS or higher increased from 51% to 72% in the presence of the peptide (Figures 4A and 4C); for Cx37-319S, the same parameter changed from 9.6% in control, to 37% in the presence of the peptide (Figure 3B and 4D). Overall, the data indicate that peptide eNOS-like can modify the function of Cx37 channels, suggesting that, if interacting within the cellular environment, eNOS could modify Cx37 properties and, likely, its function within the cell.

3.4.5 Effect of Cx37 interaction on eNOS function

To study the possible interaction between eNOS and Cx37 polymorphic proteins in a cellular environment, we transfected the human EC line EA.hy926 with Cx37-319P or Cx37-319S and performed co-immunoprecipitation studies. Cx37-antibody immunoprecipitates obtained from EA.hy926/Cx37-319P or EA.hy926/Cx37-319S cell lysates contained a ~150-kDa protein that was immunoreactive to eNOS antibodies (Figure 4A, lanes 2 and 5). Control experiments using EA.hy926/empty vector transfectants showed the absence of an eNOS-immunoreactive protein in the precipitate (Figure 4A, lane 1). In addition, immunoprecipitation of Cx37 from HeLa/Cx37-319P or HeLa/Cx37-319S transfectants revealed no signal for eNOS, further illustrating the specificity of this antibody (Figure 4A, lanes 3 and 4).

As transfected proteins might lack a proper regulation and trafficking, therefore resulting in artifactual co-immunoprecipitation, we carried out experiments using the mouse endothelial cell line bEnd.3 which constitutively expresses Cx37. Similar to human cells,

Cx37 antibody immunoprecipitates from bEnd.3 cells contained a ~150-kDa protein that was immunoreactive to eNOS antibodies (Figure 4B, lane 2). No signal for eNOS was observed in control experiments where Cx37 antibody was omitted from the immunoprecipitation procedure (Figure 4B, lane 3). The subcellular localization of eNOS and Cx37 was next examined by immunofluorescence. As expected [140], a strong Cx37 signal was observed at cell-cell contacts in bEnd 3 cells. After incubation with eNOS antibodies, bEnd.3 cells showed a staining in the perinuclear region and at cell membranes. Cx37 and eNOS colocalization was mostly observed in regions of cell-cell contacts (Figure 4C). Previous studies have indicated that eNOS enzyme activity might be affected by interacting proteins [171], [172]. The colocalization and co-immunoprecipitation of eNOS and Cx37 in the endothelial cell line led us hypothesize that the interaction may also affect the activity of eNOS. In a next series of experiments, we exposed bEnd.3 cells to Cx37 anti-sense. As illustrated in Figure 4D, Cx37 expression was considerably decreased in response to 50 μM Cx37 anti-sense (bottom panel), while the same concentration of sense oligonucleotides did not affect the expression of the protein (top panel). Constitutive NO production from bEnd.3 cells was 25.8±1.9μmol/L in 16 hours (N=8) Interestingly, this NO production dose-dependently increased with increasing concentration of Cx37 anti-sense (Figure 4E). Overall, the data suggest that the interaction with Cx37 decreases the activity of the eNOS enzyme.

3.5 DISCUSSION

We have used phage display to identify peptides capable of binding to Cx37CT-319P and Cx37CT-319S. Our results identified two main consensus motifs, RXP and RXXP, in the peptidic sequences binding to Cx37CT. By comparing the obtained sequences to the protein database, we found one particular peptide with homology to a region of the enzyme eNOS. The binding of this peptide as well as of the corresponding sequence of eNOS to both

isoforms of Cx37CT was then assessed by various *in vitro* methods and in a cellular environment. In addition, the functional consequences of the interaction were evaluated. Before discussing these results and their implications, we will address a few technical aspects of our study.

3.5.1 Technical considerations

Phage display is a method that allows for high-throughput screening of binding sequences. Yet, it has limited sensitivity and as such, it is possible to miss sequences of interest. While the peptides found are capable of interacting with Cx37CT fragments, we likely failed to detect peptides of biological relevance that correspond to sequences of native Cx37 partners. It is also likely that some of the identified peptides lack biological relevance. In this study, we decided to focus our attention on one peptide (eNOS-like), as it opened the possibility that these two proteins, Cx37 and eNOS, may interact in intact cells.

Surface plasmon resonance is a powerful technique to measure the binding kinetics of a peptide to a protein. To detect a shift in resonance, the target (in our case each isoform of Cx37CT) was covalently bound to a matrix. The consequence of this step is that the configuration of Cx37CT might be modified and might not reflect the proper structural order of the protein when in solution (or *in vivo*). Moreover, SPR is limited in its ability to detect low affinity interactions, particularly when these involve molecules of low mass. Yet, those limitations notwithstanding, SPR allowed us to characterize the interaction of eNOS-like to Cx37 and determine, comparatively, the interactions to the two specific Cx37 polymorphs. Cross-linking experiments are an alternative method to SPR to assess binding *in vitro*. They allow for studying the interaction of peptidic molecules in a soluble conformation. In our study, this method confirmed the results obtained by SPR, which indicate that both synthetic peptides, eNOS-like and the corresponding sequence of eNOS, interact with both isoforms of

Cx37CT with a comparable affinity.

3.5.2 Binding motifs

Based on the occurrences of the two motifs identified, we constructed a consensus motif for sequences binding to each isoform of Cx37CT. For Cx37CT-319P, the consensus motif would be WHK…[K,R]XP… and for Cx37CT-319S, FHK…[K,R]XXP… . Our results showed that the Cx37CT consensus binding motifs are rather similar to those previously identified for Cx43[19]. This indicates that, though different in primary sequence, both CT domains may share higher order structures. The identification of the RXP-motif led to the discovery of a peptide (RXP-E) able to interfere with the regulation of Cx43. Whether peptides known to affect the function of Cx43 could also affect the function of Cx37 (or vice versa) remains to be determined.

3.5.3 Endothelial nitric oxide synthase and Cx37CT

We have shown by three different methods that a peptide similar to a part of eNOS binds to the C-terminal domain of Cx37. The homologous sequence extracted from amino acids 843-854 of eNOS bound to Cx37CT as well, even though with a lower affinity. These *in vitro* studies suggest a possible relation between those two proteins *in vivo*. The synthesis of NO by eNOS in endothelial cells is well known to play a vasoprotective role by different mechanisms. Thus, endothelium-derived NO controls vascular tone, inhibits leukocyte adhesion to the endothelium, inhibits platelet aggregation and decreases endothelial permeability [162], [163]. Endothelial production of NO also inhibits vascular smooth muscle cell migration and proliferation. Adequate levels of endothelial NO are thus important to preserve normal vascular physiology; diminished NO bioavailability can lead to endothelial

dysfunction, and increased susceptibility to atherosclerotic disease [163]. Interestingly, Cx37 can also be considered a vasoprotective and anti-atherosclerotic protein [139]. While the normal endothelium displays sizable Cx37 expression throughout the vascular tree, Cx37 expression is decreased in response to factors inducing endothelial dysfunction [47, 173, 174, 175, 176]. Moreover, Cx37-deficient mice show enhanced susceptibility to atherosclerosis [47]. The close association between Cx37 expression levels and eNOS activity led us to hypothesize that the two proteins might interact in ECs and affect each other's function.

In agreement with previous studies [161, 158], we have shown here that human Cx37 channels in N2a cells transit between multiple conductive states up to ~400 pS. As shown in Figure 3A and 4B, the frequency of occurrence of high-conductance events (>300 pS) was higher for Cx37-319P channels (51%) compared with Cx37-319S channels (9.6%). In analogy to Cx43 [177], this may reflect differences in posttranslational modification, such as phosphorylation, between the two polymorphic proteins. The Cx37CT contains indeed multiple consensus sequences for phosphorylation by various protein kinases and such sequences include the serine at position 319. We have also shown that the frequency of occurrence of high-conductance events was increased in the presence of the eNOS-like peptide (Figure 3C and 4D), suggesting that eNOS-Cx37 interaction could modify Cx37 channel properties. Consistent with our *in vitro* binding experiments (SPR and cross-linking), eNOS-like peptide induced similar modification of channel properties for either polymorphic protein. This suggests that the interaction of Cx37CT and eNOS does not involve the region modified by the P319S polymorphism.

Transfection of EA.hy926 cells allowed for studying the interaction of eNOS with both Cx37 polymorphic proteins in a cellular environment. Our studies revealed that eNOS coimmunoprecipitated with full Cx37-319P and well as Cx37-319S. As transfected models might result in aberrant protein regulation and intracellular localization, and hence in

artifactual co-immunoprecipitation results, another more physiological model was needed to confirm these results. Unfortunately, previous studies have shown that primary ECs, such as HUVECs, progressively decrease Cx37 expression upon repeated passaging with virtually no remaining protein at passage 3 to 4 [178]. In contrast, the mouse EC line bEnd.3 is known to constitutively express Cx37, which is localized at cell-cell contacts [140]. Like in human cells, eNOS coimmunoprecipitated with Cx37 in these ECs of mouse origin, suggesting that the physical interaction between the two proteins is preserved among different species. Moreover, our functional studies demonstrated that decreasing Cx37 expression enhanced NO release in bEnd.3 cells, suggesting that eNOS-Cx37 interaction could modify enzyme activity. Structural studies have revealed that eNOS is a multi-domain enzyme consisting of an N-terminal oxygenase domain (amino acids 1-492) that contains binding sites for heme, L-arginine, and tetrahydrobiopterin (BH_4), and a reductase domain (493-1205) containing binding sites for FMN, FAD, NADPH, and calmodulin (CaM) [171]. During NO synthesis, NADPH-derived electrons pass into the reductase domain flavins, are then transferred to the heme located in the oxygenase domain of the dimer partner that binds O_2 and catalyzes stepwise NO synthesis from L-arginine. CaM binding is known to activate NO synthesis by enabling the reductase domain to transfer electrons to the eNOS dimer. The “843-854” binding motif resides in the eNOS reductase domain, a part that also contains a caveolin-1 binding domain [179]. Although the possible modes of Cx37-based inhibition remain to be explored, one could imagine that, similar to caveolin-1, Cx37 binding to eNOS reductase compromises its ability to bind CaM, thereby inhibiting NO synthesis.

In summary, the data presented here demonstrate for the first time an interaction between Cx37 and eNOS in endothelial cells. However, this study could not detect a difference between the interactions of each isoform of Cx37CT with the peptides corresponding to

eNOS. This suggests that the interaction of Cx37CT and eNOS does not involve the region modified by the P319S polymorphism. It also indicates that the epidemiological correlation between the Cx37 polymorphism and atherosclerosis does likely not result from a modification in eNOS function. Nevertheless, this newly identified interaction may lead to new insights in vascular physiology and pathologies, such as hypertension.

3.6 ACKNOWLEDGEMENTS

This work was supported by grants from the Swiss National Science Foundation (PPOOA-116897 to BRK), the Swiss University Conference Program 'Heart Remodeling in Health and Disease' (to BRK), and the National Institutes of Health (GM057691 to MD and HL39707 to MD).

3.7 FIGURE LEGENDS

Figure 1: Surface Plasmon Resonance on Cx37CT and binding peptides

Cx37CT-319P or Cx37CT-319S were fixed on a carboxymethyl dextran matrix, which was superfused with a solution containing various concentrations of a synthetic peptide (either eNOS-like or eNOS(843-854)) and binding was assessed in real time. A representative set of association and dissociation curves is shown for each condition, with: Cx37CT-319P and eNOS-like in panel A, Cx37CT-319S and eNOS-like in panel B, Cx37CT-319P and eNOS(843-854) in panel C and Cx37CT-319S and eNOS(843-854) in panel D. Peptides were superfused at concentrations of 1mmol/L (red), 500µmol/L (blue), 250µmol/L (green), 125µmol/L (orange) and 62.5µmol/L (pink). The binding kinetics were best fitted by a first-rate order model, with a mean K_D of 66µmol/L for Cx37CT-319P and eNOS-like (panel A), 65µmol/L for Cx37CT-319S and eNOS-like (panel B), 142µmol/L for Cx37CT-319P and eNOS(843-854) (panel C) and the K_D was not quantifiable for Cx37CT-319S and eNOS(843-854) (panel D). These K_Ds were not statistically different. N=3 for each condition.

Figure 2: Cross-linking experiment on Cx37CT and peptides

The binding in solution of the peptides eNOS-like (lanes 2, 3, 5 and 6 of panel A) and eNOS(843-854) (lanes 2, 3, 5 and 6 of panel B) to Cx37CT-319P (lanes 1-3) or Cx37CT-319S (lanes 4-6) was assessed by the incubation with the cross-linking reagent BS^3 (lanes 1, 2, 4 and 5), separation by SDS-PAGE and Coomassie-Blue staining. Lanes 2 and 5 of each panel show an additional band at approximately 12 kDa, just above the band corresponding to the Cx37CT (estimated molecular weight 11 kDa), which is absent in the other lanes, where either the peptide (lanes 1 and 4) or the cross-linker (lanes 3 and 6) are missing. Bands are also seen at higher molecular weights in lanes 1, 2, 4 and 5 (*i.e.* where BS^3 is present). They are thought to represent multimers of Cx37CT.

Figure 3: Single-channel data from N2a cells transfected with Cx37-319P and Cx37-319S.

All events histograms of unitary conductance in control cells transfected with Cx37-319P (panel A: N=4; n=267) and Cx37-319S (panel B: N=12; n=253), and in the presence of eNOS-like peptide in the pipette solution for Cx37-319P expressing cells (panel C: N=5; n=447) and for Cx37-319S expressing cells (panel D: N=4; n=205). The presence of the eNOS-like peptide increased the number of channel openings greater than 300pS by 21% for Cx37-319P and by 27.4% for Cx37-319S. Histograms were fit by Gaussian functions.

Figure 4: Studies of human ECs transfected with Cx37-319P or Cx37-319S and of mouse ECs after inhibition of Cx37 expression.

Panel A: Lysates of EA.hy926 or HeLa transfectants were incubated with Cx37 antibodies and immunoprecipitates probed for eNOS. Note that the Cx37 antibodies pulled down a protein of ~150 kDa labeled with anti-eNOS in EA.hy926/Cx37 transfectants only. Panel B: Lysate of bEnd.3 cells were incubated with Cx37 antibodies and immunoprecipitate probed for eNOS. The Cx37 antibodies pulled down a protein of ~150 kDa labeled with anti-eNOS. L indicates total cell lysate, IP, immunoprecipitate, and C negative control. Panel C: bEnd.3 cells were immunostained for Cx37 and eNOS and examined for the localization of overlay of the two proteins. eNOS was found perinuclearly and around the periphery of the cells outlining the cell membranes (arrow). Cx37 was detected at sites of cell-cell contact (arrow). Merged images show that the two proteins show areas of colocalization in these mouse ECs. Bar represents 50µm. Panel D: Cx37 immunostaining (green) fluorescence microscopy images of confluent cultures of bEnd.3 cells incubated with 50µmol/L of Cx37-sense (top) or Cx37-antisense (bottom) oligonucleotides for 48 hours. Cells were counterstained with Evans Blue (in red). Panel E: The release of NO into the extracellular medium was measured in

Cx37 sense-treated bEnd.3 cells and compared to bEnd.3 cells incubated with 10, 25 or 50 50µmol/L Cx37 anti-sense for 48 hours. Overnight NO release increased with increasing dose of the anti-sense. N=6, error bars show SEM, and * $P<0.05$.

3.8 FIGURES

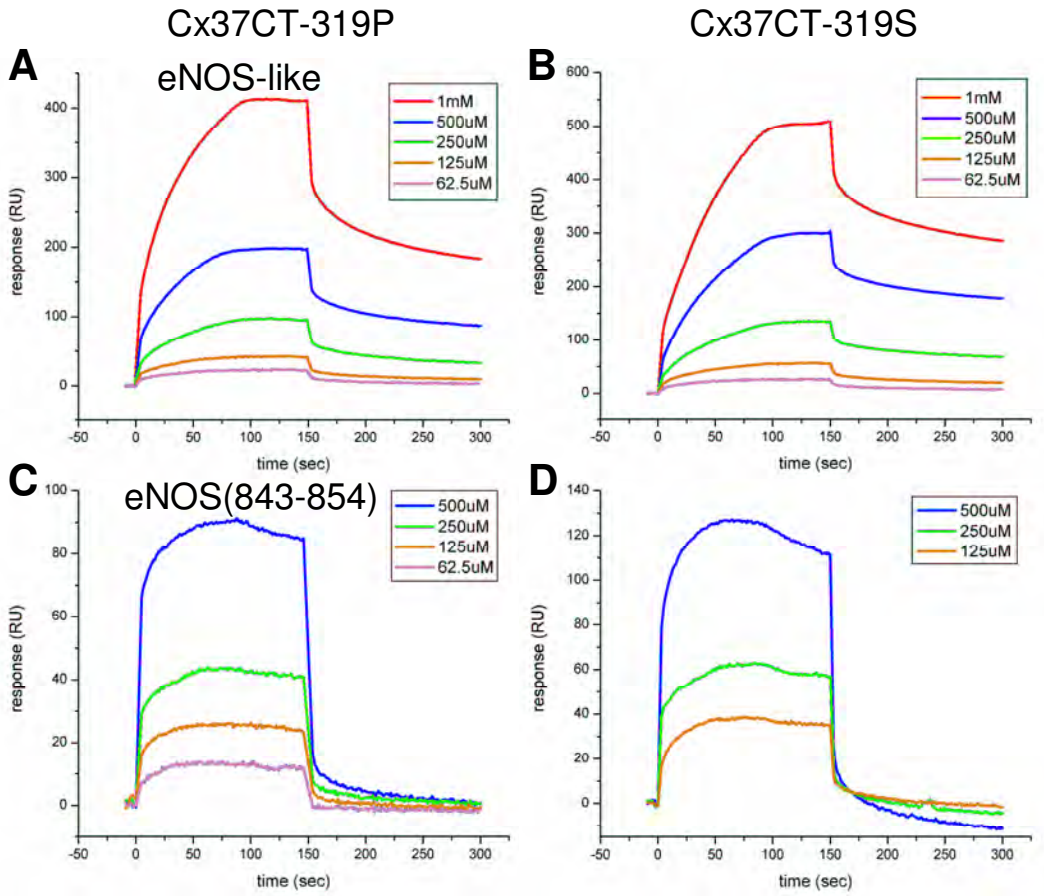

Figure 1

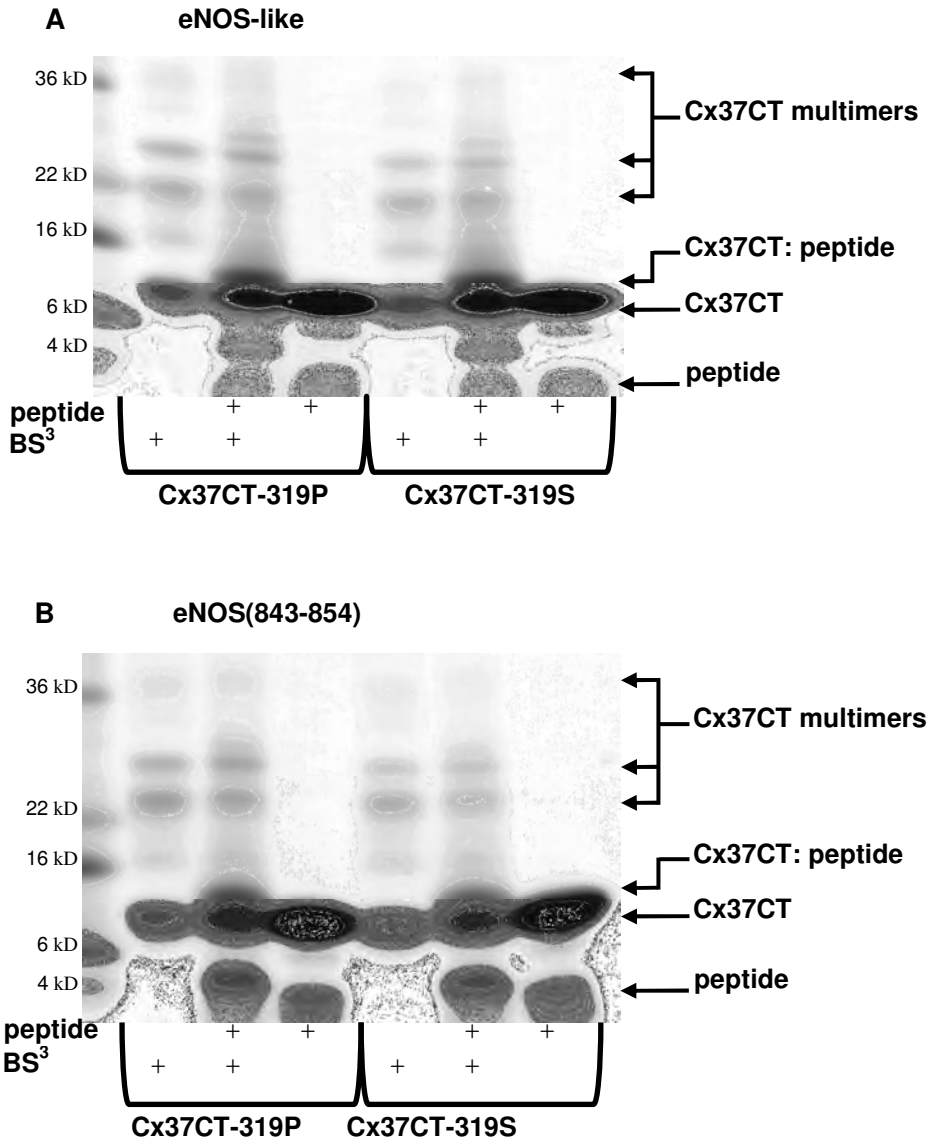
A
eNOS-like
36 kD
22 kD
16 kD
6 kD
4 kD
Cx37CT multimers
Cx37CT: peptide
Cx37CT
peptide
peptide
BS3
Cx37CT-319P
Cx37CT-319S
B
eNOS(843-854)
36 kD
22 kD
16 kD
6 kD
4 kD
Cx37CT multimers
Cx37CT: peptide
Cx37CT
peptide
peptide
BS3
Cx37CT-319P
Cx37CT-319S

Figure 2

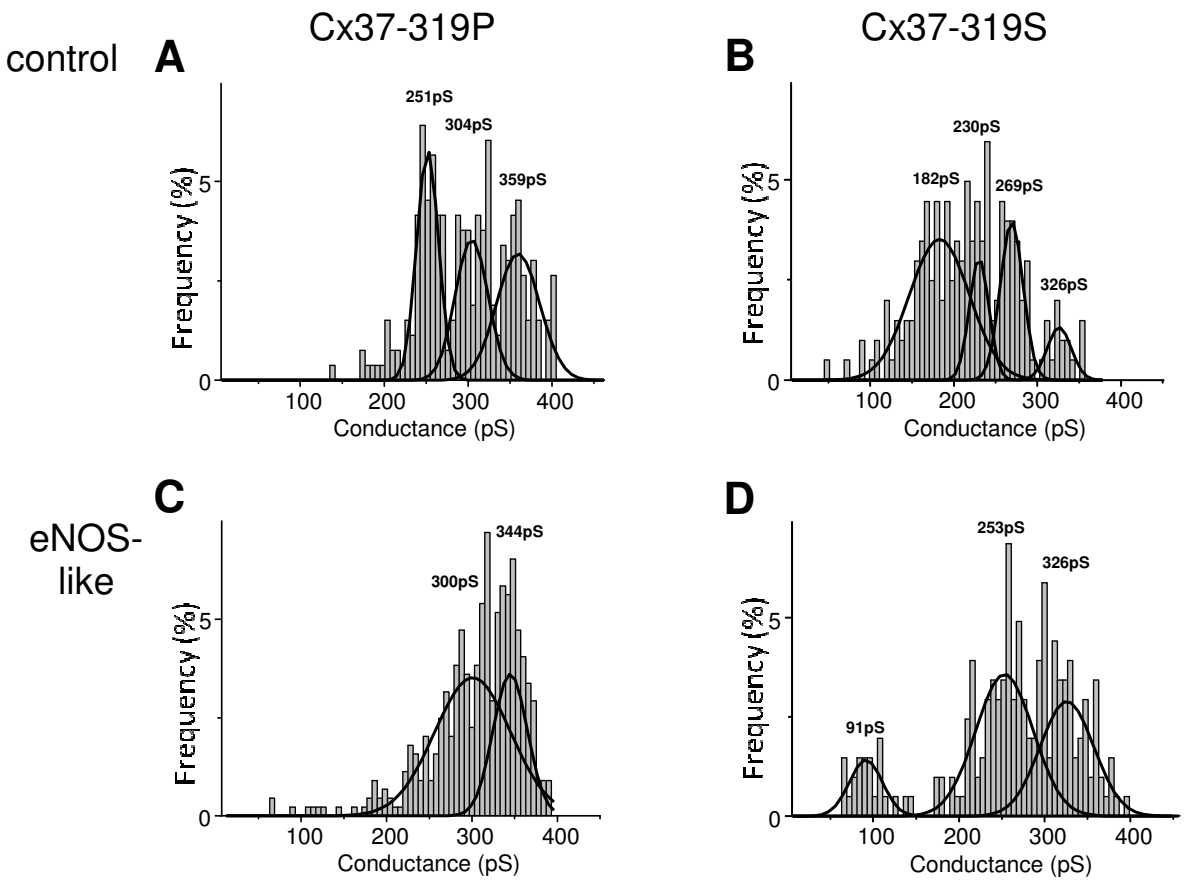
control
Cx37-319P
Cx37-319S
A
B
C
D
eNOS-like
251pS
304pS
359pS
230pS
182pS
269pS
326pS
344pS
300pS
253pS
326pS
91pS
Frequency (%)
Conductance (pS)
0
5
100
200
300
400

Figure 3

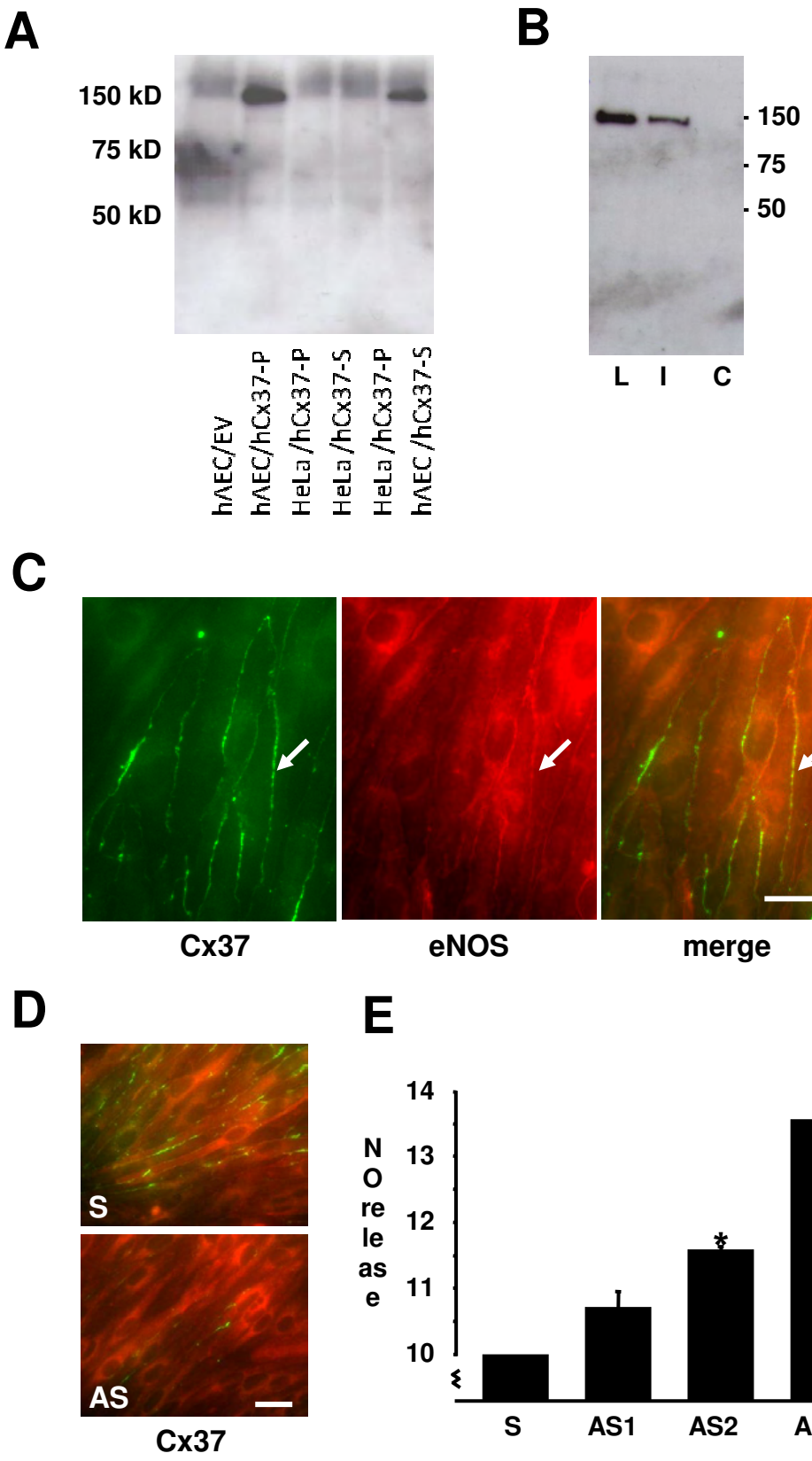
A
150 kD
75 kD
50 kD
hAEC/EV
hAEC/hCx37-P
HeLa/hCx37-P
HeLa/hCx37-S
HeLa/hCx37-P
hAEC/hCx37-S
B
150
75
50
L I C
C
Cx37
eNOS
merge
D
S
AS
Cx37
E
NO release
14
13
12
11
10
S
AS1
AS2
AS5

Figure 4

3.9 TABLES

3.9.1 Table 1: Phage display peptidic sequences

Peptidic sequence	Cx37CT-319P display	Cx37CT-319S display	Peptidic sequence	Cx37CT-319P display	Cx37CT-319S display
AHKDLVKWLSSI		1	SHWWNRYPQHRL	1	
FHKFHKRTPARS		1	TPFRKHKRPLRD	4	
FHKHKPTPIPTA	5	2	WHGKWKSLPPAT	1	
FHKHKSPALSPV	11	9	WHHPSKFTRYTP		1
FHKHNRVVPWTL		1	WHKAPRPTYLSY	1	
FHKHNYKSPPII	2	2	WHKAPRQAPLFV	1	11
FHKHPSHMWRLS		1	WHKAVPRWLASP	1	
FHKHQTRYFIPQ		3	WHKGNPLRSLRT	2	
FHKHRSLPMLYP		1	WHKHIPSIRFPS		1
FHKHRVPTQLLG	3	2	WHKHPRYYPLPP	1	2
FHKHSPRSPIFI		12	WHKHRVSPEIEW	1	1
FHKNSPTWKHHR		1	WHKLPSRYQPTS	1	
FHKPFFPKGSAR		4	WHKNTNWPWRTL	7	5
FHKPFKPTHRTL	13	2	WHKPFMRPVPPP		14
FHKPKTWTYLLS		3	WHKPFRTTVPSS	1	
FHKPQRTSPMFK		1	WHKPKPTSAPIL		1
FHKQRLPFLNYL		1	WHKPPRQVLQPS	1	
FHKRPLIAPPYK		1	WHKPQKYLLAPP		1
FHKRPPPPPFNA		1	WHKPRLPASPGA	10	
FHKRPQQPAPPT	1		WHKRTPMPPIPI	13	
FHKTPKSPAVWR	1		WHKSPKLYLAVP		1
FHKVKPKQELIF	1		WHKSPRIWSSPT	1	9
FHTKWRPSWTYP		1	WHKSPRLPPHKN	1	3
HHKYPWSRYMPL		1	WHKSPSRTPYAP		1
HWKHNRHDPSPP		1	WHKSWSPNPSKT	1	
ISDFDYMLSPMK	1		WHKTKPTVPPIP	1	
KFNQDHILHASF	1		WHKTRTVPVVAT	3	
KHLDRYNYWKAR	2		WHKTWNLRSPSL	1	
KHYMHDTWRTKY	1		WHKYDRPWPQKR		2
KIHRRKPFTSIA	3	3	WHKYPRGSVAPM	1	
KSHRPRLRRERP		7	WHNKLWQYRVSP	1	
LTPQPTLPPTND	1		WHRLPNLKPTAP		1
NRRHRRPHVQGT	4		WHRTPRLPPPVP	1	
QTPTWQPTQNFP	1		WHTKFLPRYLPS	1	1
RRHKTRSPIAHF	3		WHWQKFRAPLLN	1	
SHFSTWKWWQNR		2	WPSKQRRPQRTL	1	

3.9.2 Table 2: Alignment of eNOS-like peptide with eNOS(843-854)

peptide	sequence
eNOS-like	*N*-**W**H**R**T**PRLPP**PVP-*C*
eNOS(843-854)	*N*-**WV****R**D**PRLPPC**TL-*C*

3.10 SUPPLEMENTED DATA ONLINE

3.10.1 Expanded Methods

3.10.1.1 Production and purification of recombinant Cx37CT

Recombinant Cx37CT was produced following methods previously described[18]. Briefly, cDNA derived from human Cx37-319P was inserted into pGEX-6P-2 plasmids (Amersham) and expressed in BL-21 competent cells. The resultant GST-fusion protein was cleaved from the GST by PreScission Protease® (Amersham Biosciences). The recombinant product after cleavage from GST contained the sequence 233-333 of human Cx37. Protein concentration was measured using the Bio-Rad DC Protein Assay. Protein purity was assessed by SDS-PAGE and Coomassie staining.

The Cx37CT-319S clone was produced using the QuikChange Site-Directed Mutagenesis Kit® (Stratagene) on the Cx37CT-319P pGEX-6P-2 plasmid. The following primers were used forward, GAA TGG CCA AAA ATC CCC AAG TCG TC and reverse, GAC GAC TTG GGG ATT TTT GGC CAT TC.

3.10.1.2 Phage display

Phage display is a high-throughput method for identification of molecules binding to a ligand of interest. Here, we applied it to the detection of potential ligates of the CT domain of Cx37. The protocol was similar to that previously described[19]. Briefly, recombinant Cx37CT-319P, or recombinant Cx37CT-319S were used as baits. A well of a 24-well plate was coated with 15µg of the pertinent recombinant protein. The well was treated with blocking buffer (0.1mol/L $NaHCO_3$ (pH 8.6), 5mg/ml BSA, 0.02% NaN_3) for 1 hour. A phage library consisting of $2.7x10^9$ different M13KE bacteriophages displaying a random 12-mer peptide in their minor coat protein (Ph.D.-12™ Phage display peptide library kit; New England BioLabs

Inc.) was first pre-cleared in an uncoated well, and then presented to the bait protein. Low-affinity binders were first eluted using a 100µg/ml solution of free Cx37CT in TBS. The well was overlaid with a culture of *E. coli* ER2738, which was then amplified for 4.5 hours. The amplified phages were precipitated with PEG-NaCl. The extracted phages were subsequently used for a new round of panning. After four rounds, the phages were grown on a lawn of *E. coli* ER2738 for plaque purification. A total of 120 plaques, each one representing a single clone, were amplified for 4.5 hours. Phages were precipitated with PEG/NaCl and their ssDNAs were extracted and sequenced. The sequences were analyzed using the ExPasy translate tool as well as the NCBI protein-protein BLAST (Basic Local Alignment Search Tool).

3.10.1.3 Motif analysis

The significance of particular motifs in the retrieved phage display sequences was assessed by comparing their actual frequency to their theoretical occurrence based on the experimental ratio of each amino acid. If for example the frequency of K in the display sequences is 10.2%, the frequency of R is 8.9% and the frequency of P is 16.1%, then the probability of finding a [K,R]XP motif in a 12-mer would be even without a selection for this motif.

$$p([K,R]XP) = 10 \times (p(K) + p(R)) \times p(P) = 30.8\%$$

These probabilities were then compared to the obtained data.

3.10.1.4 Surface plasmon resonance

Surface plasmon resonance (SPR) is a spectroscopic method to determine the amplitude and kinetics of binding between two molecules in real time [20, 21]. Recombinant Cx37CT-319P and Cx37CT-319S were covalently bound to a carboxymethyl dextran matrix (Sensor Chip CM5, Biacore), and synthetic peptides were presented to assess binding. All experiments were

performed at pH 7.4. Dissociation constants (K_D) were calculated from the recorded association and dissociation phases of the peptide-protein interaction, using a 1:1 Langmuir association and dissociation kinetic model (Biacore software package). In both phases (association and dissociation), the first 8 seconds of recording were not included in the fit to avoid artifacts resulting from peptide distribution within the flow cells [21].

3.10.1.5 Cross-linking experiments

Cross-linking reagents enable the formation of covalent bonds between molecules in close proximity. A total of 0.25mmol/L of recombinant Cx37CT and 0.5mmol/L of a peptide were incubated for 1 hour at room temperature with 1mM of the cross-linker reagent BS^3 at pH 7.4 [22]. The reaction was subsequently blocked with 100mmol/L ethanolamine for 10 min. The samples were separated by SDS-PAGE (4-20%) and stained with Coomassie-Blue.

3.10.1.6 Cell culture

Three different cell lines were used: a) a communication-incompetent line of murine neuroblastoma cells (N2a; American Type Culture Collection; Manassas, VA), b) a mouse endothelial cell line (bEnd.3) which endogenously expresses all three endothelial connexins [26], and c) a human endothelial cell line (EA.hy926; ATCC) which has no detectable endogenous expression of Cx37. Cells were grown in DMEM (Gibco, Invitrogen, Grand Island, NY) and supplemented with 10% fetal bovine serum, 5mg/L L-glutamine, 5000U/L penicillin and 5mg/ml streptomycin (Mediatech, Herndon, VA).

3.10.1.7 cDNA preparation and transfection into cells

GJA4-1019T and *GJA4*-1019C cDNAs were subcloned into the pIRES2-eGFP mammalian expression vector (Clontech) using *Eco*RI and *Bam*HI restriction sites [2]. These vectors were separately transformed into DH5α competent cells (Invitrogen) and selected as positive kanamycin-resistant clones, according to the manufacturer's protocol. For transfection of EA.hy926 cells, 5-10µg of plasmid DNA were electroporated into 5×10^5 cells using a Gene Pulser II device (Bio-Rad) at 220V and 975µF capacitance. After 5 min on ice, cells were transferred to a six-well tissue-culture plate. Selection was initiated in 350µg/ml G418 (Invitrogen) after 24 hours of recovery time. After 14-21 days, cells were selected by expression of eGFP using flow cytometry (FACSVantage; Becton Dickinson); Cx37 expression was verified by immunostaining. Transiently transfected cells were used within one month after starting G418 selection. In the case of N2a cell transfection, cells were grown to 35-40% confluence and transiently transfected with the above-mentioned plasmids. Transfections were carried out using 0.5µg of plasmid DNA and Effectene (Qiagen, CA) according to the manufacturer's instructions. Transfection efficiency ranged between 70 and 80%.

3.10.1.8 Patch clamp recording and analysis

Electrophysiological recordings were performed 24-48 hours post-transfection. eGFP positive (green) pairs of cells were identified by illumination under monochromatic light (495nm) and emitted fluorescence filtered at 520nm. Electrophysiological recordings were then made using the dual whole-cell patch-clamp technique. Patch electrodes had resistances of 5MΩ and were filled with (in mmol/L) 130 CsCl, 0.5 $CaCl_2$, 10 HEPES, 10 EGTA, pH 7.2. In some recordings eNOS-like peptide (WHRTPRLPPPVP; MW1454) was added to the pipette solution at a concentration of 0.1mmol/L. The external solution was (in mmol/L) 160 NaCl,

10 CsCl, 10 $CaCl_2$, 0.6 $MgCl_2$, 10 HEPES, pH 7.4. All experiments were carried out at room temperature.

Single channel recordings were obtained from cell pairs treated with the uncoupler agent octanol (2-4mmol/L). Junctional current traces were acquired during repetitive pulses of 10s to Vj=30mV using pClamp software (version 10.0, Axon instruments, CA). The resting potential was -40mV. Signals were filtered at 200 Hz and sampled at 2 kHz. Single channels events lasting more than 20ms were considered for further analysis. Gaussian distribution best fits were constructed for all-events histograms using Origin software. (Version 7.0, Microcal, MA).

3.10.1.9 Co-immunoprecipitation studies

Confluent cultures of bEnd.3 cells or transfected EA.hy926 cells were rinsed in phosphate-buffered saline (PBS), pH 7.4, and lysed in 500µl RIPA buffer (50mmol/L Tris-HCl, pH 7.4, 0.25mmol/L sodium-deoxycholate, 150mmol/L NaCl, 2mmol/L EGTA, 0.1mmol/L Na_3VO_4, 10mmol/L NaF, 1mmol/L phenylmethylsulfonyl fluoride, 1% Triton X-100, Complete protease inhibitor (Roche Applied Science). Lysates were sonicated for 30s, maintained on ice for 30 min, and then triturated and spun at 12,000rpm for 20 min. For co-immunoprecipitation studies, 50µl of Sepharose G beads (Sigma-Aldrich Corporation, MO) was rinsed twice with 750µl of RIPA buffer and then spun at 12,000rpm for 1 min. A 250µl volume of supernatant was pre-cleared overnight at 4°C with 30µl of Sepharose G beads in gentle rotation (Sigma-Aldrich Corporation, MO) and spun at 12'000rpm for 1 min. Following the preclearing step, 7.5µg of Cx37 antibody were added (Cx37A11-A, ADI), and incubated with the supernatant using gentle rotation for 6 hours at 4°C. Thereafter, 50µl of protein G-agarose were added, and the sample was incubated overnight at 4°C. Negative controls included omission of antibodies from the procedure. The following day, the sample was spun at 12,000rpm for 1

min and the supernatant was discarded. The beads were rinsed 5 times in lysis buffer, incubated in 50µl of loading buffer, incubated at 95°C for 10 min, and then placed immediately on ice for 2 min. The sample was then and spun at 12'000rpm and the loading buffer removed from the beads for running on Western blots using 10% SDS-PAGE. Proteins were transferred to nitrocellulose membrane, and eNOS (BD Sciences) was detected with the appropriate antibodies.

3.10.1.10 Immunofluorescence

bEnd 3 cells were grown to confluence onto culture medium–coated coverslips, fixed in ice-cold methanol for 5 min at -20°C, and immunolabeled with Cx37 (ADI) and eNOS (BD Sciences) antibodies, as described previously[3]. Slides were mounted with Vectashield mounting medium (Vector laboratories, Burlingame, CA) and examined with a TMD300 microscope (Nikon AG, Küsnacht, Switzerland) equipped with a high-sensitivity CCD Visicam camera (Visitron systems GmbH, Puchheim, Germany) connected to a personal computer. Images were captured using the software Metafluor 4.01 (Universal Imaging Corp., Downington, PA) and processed using Adobe Photoshop.

3.10.1.11 NO release

NO release assays were performed using 96-well plates (Falcon). Ten thousand bEnd.3 cells were plated per well and grown to confluence for 48 hours in the presence of 10, 25 or 50 µmol/L Cx37 anti-sense oligonucleotides (5'-GTCCCTTCGTGCCTTTATCTC-3'). Cx37 sense oligonucleotides (5'-TGCTAGACCAGGTCCAGGAAC-3') were used as controls. Total NO release to culture supernatant was measured during the final 16 hours using the Total Nitric Oxide Assay Kit (Assay Designs) according to the manufacturers' instructions. NO release was assayed in duplicate.

3.10.1.12 Statistics

Results are presented as mean ± SEM. Unpaired t-test was used to compare differences between two groups and ANOVA for comparison of multiple groups. Data were considered statistically significant at $P<0.05$.

3.10.2 Supplementary tables on line

3.10.2.2 Table 1

Table 1: Frequency of acidic and basic residues in phage display sequences

	Cx37CT-319P display	Cx37CT-319S display	library
Asp	1.3%	0.6%	2.8%
Glu	0.6%	0.6%	3.1%
His	10.0%	12.8%	6.3%
Lys	10.2%	11.8%	2.8%
Arg	8.9%	8.1%	4.7%

3.10.2.3 Table 2

Table 2: Frequency of [K,R]XP motif in Cx37CT-319P and Cx37CT-319S displays versus theoretical occurrence

	Cx37CT-319P	Cx37CT-319S
Theoretical frequence	30.8%	33.6%
Experimental frequence	54.5%	46.3%
Ratio Exp/Th	1.77	1.38

3.10.2.4 Table 3

Table 3: Frequency of [K,R]XXP motif in Cx37CT-319P and Cx37CT-319S displays versus theoretical occurrence

	Cx37CT-319P	Cx37CT-319S
Theoretical frequence	27.7%	30.2%
Experimental frequence	40.9%	58.5%
Ratio Exp/Th	1.48	1.94

4 ENHANCED CALCIFICATION IN ADVANCED ATHEROSCLEROSIC LESIONS OF Cx37-DEFICIENT MICE

Submitted in ATH on the 11th of July 2008

Enhanced calcification in advanced atheroma of Cx37-deficient mice

Jean-Paul Derouette[1], Cindy Wong[1], Christos E. Chadjichristos[1], Esther Sutter[1], Anne C. Brisset[1,2], Isabelle Roth[1], Brenda R. Kwak[1]

[1]Division of Cardiology, Department of Internal Medicine, and [2]Department of Pediatrics, Faculty of Medicine, University of Geneva, CH-1211 Geneva, Switzerland

The manuscript contains 4'537 words and 4 figures, the abstract contains 266 words.
Supplementary online figures (2) and tables (4) are provided as well.

Address of correspondence:

Brenda R. Kwak, PhD
Foundation for Medical Research
Division of Cardiology
Geneva University Hospitals
64 avenue de la Roseraie
CH-1211 Geneva
Switzerland
Tel: (41 22) 382.72.37
Fax: (44 22) 382.72.45
E-mail : Brenda.KwakChanson@medecine.unige.ch

4.10 ABSTRACT

Recently, we showed that connexin37 (Cx37) protects against early atherosclerotic lesion development by regulating monocyte adhesion. The expression of this gap junction protein is altered in mouse and human atherosclerotic lesions; it is increased in macrophages newly recruited to the lesions and disappears from the endothelium of advanced plaques. To obtain more insight into the molecular role of Cx37 in advanced atherosclerosis, we used microarray analysis for gene expression profiling in aortas of $ApoE^{-/-}$ and $Cx37^{-/-}$ $ApoE^{-/-}$ mice before and after 18 weeks of cholesterol-rich diet. Out of >15'000 genes, 106 genes were significantly differentially expressed in young mice before diet (p-value of <0.05, fold change of >0.7 or <-0.7, and intensity value >2.2 times background). Ingenuity Pathway Analysis (IPA) revealed differences in genes involved in cell-to-cell signaling and interaction, nutrition/lipid metabolism, and cellular growth and differentiation. In addition, we identified 100 genes that were significantly perturbed after the cholesterol-rich diet. Similar to the analysis on 10 weeks-old mice, IPA revealed differences in genes involved in cell-to-cell signaling and interaction as well as to immuno-inflammatory disease. Furthermore, we found important changes in genes involved in calcium handling and matrix degradation, some of which were confirmed at protein level. Finally, the plaque morphology was altered in $Cx37^{-/-}$ $ApoE^{-/-}$ mice, with reduced extracellular matrix and enhanced calcification as most important differences. In conclusion, we suggest that Cx37 deficiency alters the global differential gene expression profiles in young mice towards a pro-inflammatory phenotype, which are then further influenced in advanced atherosclerosis. The results provide new insights into the significance of Cx37 in plaque calcification.

Keywords: Atherosclerosis; connexin; gap junction; tissue inflammation, plaque calcification

4.11 INTRODUCTION

Atherosclerosis is characterized by the presence of inflammatory, proliferative and lipid-rich lesions in the arterial intima leading to narrowing of the vessel lumen [180]. Risk factors for developing atherosclerosis include elevated serum low density lipoprotein (LDL) levels, low serum high density lipoprotein (HDL) levels, elevated serum triglyceride levels, obesity, hypertension, smoking, diabetes, and genetic factors. These factors are linked by their common ability to promote inflammatory reactions and injury to the endothelium [181].

After adhering to the injured endothelium, monocytes and T lymphocytes transmigrate through the endothelial barrier and infiltrate the arterial intima. Once in the intima, monocytes proliferate and mature under the influence of cytokines, chemokines and growth factors secreted by themselves and other atheroma-associated cells [182]. In addition, the induced expression of scavenger receptors allows macrophages to accumulate lipids within their cytoplasm and eventually progress to the typical foam cells. During the growing phase of the atherosclerotic lesion, medial smooth muscle cells (SMCs) migrate to the top of the intima where they proliferate and generate extracellular matrix (ECM). The SMCs and matrix molecules join together to form a fibrous cap that covers the original atherosclerotic lesion. As this cap matures some of the underneath foam cells die and lipids are released, thus forming the necrotic or lipid core of the advanced atherosclerotic plaque. In addition, the activated macrophages produce matrix metalloproteinases (MMPs) that degrade the ECM thus deteriorating the plaque's fibrous cap and increasing its chance to rupture [183]. Rupture of an atherosclerotic plaque is the primary cause of sudden cardiac death [125, 181-183].

With increasing age, calcium accumulates in the arteries. Calcification of aortic valve leaflets and atherosclerotic plaques have long been recognized as clinically important for cardiovascular mortality and morbidity in the elderly [184]. Moreover, the presence of calcium deposits in the vessel wall is an indication of clinically advanced atherosclerotic lesions [185].

Recent studies indicate that atherosclerotic calcification is an organized process, even if exact regulatory mechanisms remain unclear [186, 187]. Increasing evidence suggests that atherosclerotic calcification share features with skeletal bone formation and calcification, such as chondrocyte and osteoblast differentiation, mineralization, bone matrix deposition, and bone matrix resorption [188].

Studies on atherosclerosis-susceptible ApoE$^{-/-}$ mice have shown an involvement of the gap junction protein connexin37 (Cx37) in early atherosclerotic lesion development [47]. In fact, Cx37 was protective against atherosclerosis by regulating monocyte adhesion. Connexins are integral membrane proteins that oligomerize to form intercellular channels that allow the direct exchange of ions, small metabolites and second messengers between adjacent cells, this way synchronizing responses in multi-cellular organisms [61, 62, 71]. Gap junction communication has been shown to play a role in important physiological processes such as cell growth and development. Previous immunohistological studies have not only revealed important changes in Cx37 expression in early atherosclerotic lesions, but also revealed significant changes in the advanced atherosclerotic plaques. Indeed, Cx37 has disappeared from the endothelium overlaying advanced atheromas, whereas it is highly expressed in macrophage foam cells and expression in the – previously Cx37 deprived – medial SMCs [111]. This has prompted our interest towards a possible role of Cx37 in advanced atherosclerosis.

Here, we have carried out a broad microarray-based screening to identify genes that were intrinsic differentially expressed (at 10 weeks of age) or that showed distinct expression in aortas containing advanced atherosclerotic lesions (after 18 weeks of high-cholesterol diet) between Cx37$^{-/-}$ApoE$^{-/-}$ and ApoE$^{-/-}$ mice. In some relevant cases, immunohistochemistry was performed to confirm differential gene expression at the protein level and to assess plaque morphology. Our results suggest that Cx37 deficiency alters the global gene expression profiles in young mice towards a pro-inflammatory phenotype. With respect to

advanced atherosclerosis, the differences mostly included genes involved in calcium handling and matrix degradation.

4.12 MATERIALS AND METHODS

4.12.1 Animals

Male $Cx37^{-/-}ApoE^{-/-}$ [47] and female $Cx37^{+/-}ApoE^{-/-}$ mice, both on a C57BL/6J background, were interbred. Cx37 wild-type and knock-out alleles were detected by polymerase chain reaction genotyping, as previously described [108]. All mice were kept in conventional housing. The University of Geneva Animal Care and Use Committee as well as the local Veterinary office, in accordance with Swiss guidelines and regulations, approved all animal experiments.

As a model of *in vivo* advanced atherosclerosis, 10 weeks-old $Cx37^{-/-}ApoE^{-/-}$ and control $ApoE^{-/-}$ mice were fed a high-cholesterol diet (1.25% cholesterol without cholate; Research Diets Inc., New Brunswick, USA) for 18 weeks. The mice were then killed, their aortas were isolated and separated into 2 parts: the aortic roots were snap-frozen in OCT compound whereas the aortic arches and thoraco-abdominal aortas were rapidly frozen and later used mRNA extraction. Control groups included 10 weeks-old $Cx37^{-/-}ApoE^{-/-}$ and $ApoE^{-/-}$ mice.

4.12.2 RNA extraction, amplification and microarray analysis

RNA was isolated from aortas of $Cx37^{-/-}ApoE^{-/-}$ and $ApoE^{-/-}$ mice (RNeasy Mini kit, Qiagen, Cologne, Germany). RNA quality was assessed using the RNA 6000 Nanochip assay (Agilent Technologies, Meno Park, USA) and RNA concentration was determined using the ND-1000 spectrophotometer (Nanodrop Technologies, Wilmington, USA).

A single round of amplification was performed with 3 μg of total RNA using the MessageAmp aRNA Amplification Kit (Ambion, Austin, USA) following the manufacturers' protocol. Next, 5 μg of amplified RNA was mixed with 9 μg random primers (Invitrogen, Carlsbad, USA) in 19 μl of water, heated for 5 min at 70°C and then immediately transferred to ice. Reverse transcription was performed for 2 hours at 42°C in a final reaction volume of

40 µl containing 1x SuperScript II buffer (Invitrogen), 40 units RNasin (Promega, Madison, USA), 10mM DTT, 0.5mM dATP, dGTP, dTTP, 0.2mM dCTP, 0.1mM of either Cy3-dCTP or Cy5-dCTP (GE Healthcare, Uppsala, Sweden) and 400 units of SuperScript II reverse transcriptase (Invitrogen). The RNA strand was hydrolyzed by adding 2 µl 500mM EDTA and 4.5 µl 1M NaOH and heating at 65°C for 15 min; the solution was then neutralized by adding 2.5 µl 1M Tris (pH 6.8) and 4.5 µl 1M HCl. The labeled cDNA was purified using the Qiagen MiniElute PCR Purification Kit (Cologne, Germany), eluting in 50 µl of elution buffer (10 mM Tris-HCl, pH 8.5) according to the manufacturers' instructions. The Cy3 and Cy5 labeled targets were combined and mixed with 400 µl of TE, 20 µg Cot1 DNA (Invitrogen), 10 µg polyadenylic acid (Sigma, St. Louis, USA) and 10 µg yeast tRNA (Sigma). This mixture was concentrated to a final volume of 19.4 µl using a Microcon YM-30 filter (Millipore, Billerica, USA) according to the manufacturers' instructions. 20x SSC and 10% SDS were added to final concentrations of 3x and 0.4%, respectively, in a final volume of 24 µl. This mixture was heated for 2 min at 98°C, distributed immediately onto the cDNA microarray and, after covering with a glass coverslip (Erie Scientific, Portsmouth, USA), placed in a humid chamber (Telechem, Sunnyvale, USA) and allowed to hybridize at 64°C for 20 hours. Slides were then washed at room temperature twice for 5 min in 2x SSC, 0.1% SDS, twice for 1 min in 0.2x SSC, once for 1 min in 0.1x SSC and once for 5 min in 0.1x SSC, 0.1% Triton X-100. After drying, slides were scanned on a microarray scanner (Agilent Technologies) and the resulting TIFF images were analyzed using the GenePix Pro 6.0 software (Molecular Devices, Sunnyvale, USA). The mouse cDNA microarrays used in this study consisted of approximately 17'000 PCR products generated from cDNA clones and control DNAs spotted onto Nexterion AL slides (Schott, Mainz, Germany). A complete description of the slides and their content can be obtained from the Lausanne DNA Array Facility (http://www.unil.ch/dafl).

4.12.3 Statistical analysis of microarray results

The analysis was performed with open source R software packages (http://www.r-project.org/ and http://www.BioConductor.org/). Gene expression was quantified with the marray package using print tip group lowess normalization without background subtraction [189, 190]. The resulting measures of expression for each array are the log2 ratios (M values) and the average log2 intensities (A value) of Cy3 and Cy5 signals. Statistics of differential expression between the different groups of samples were calculated with a linear model fitted by the limma package [191].

4.12.4 Immunohistochemistry

Six µm cryosections were obtained from aortic roots. Advanced atherosclerotic lesions were histologically examined after hematoxylin-eosin (HE) staining as well as with specific staining to identify lipids (Sudan IV), collagen/elastin (aldehyde-fuchsine; AF) and calcifications (VonKossa). In addition, cryosections were fixed for 5 min in acetone and immunostained with antibodies recognizing CD68 (Serotec SA, Germany), S100A9 (Santa Cruz Biotechnology, California) or MMP-9 (R&D Systems, Minneapolis), as previously described [146] or according to the manufacturers' protocol. MMP9 or S100A9 positive cells were counted under a microscope by a blinded observer. Unpaired t-test was used to compare differences between groups. P values <0.05 were considered statistically significant.

4.13 RESULTS AND DISCUSSION

4.13.1 Microarray analysis

After normalization of microarray data and statistical analysis, 106 genes were found to be differentially regulated (p-value of <0.05, fold change (M) of >0.7 or <-0.7 and an intensity value >2.2 times background) out of which 70 were up-regulated and 36 down-regulated in $Cx37^{-/-}ApoE^{-/-}$ mice at 10 weeks of age (supplementary Table 1). To identify molecular and cellular pathways by which Cx37 disruption may predispose for enhanced atherosclerosis [47], we performed pathway analysis using Ingenuity Pathways Analysis (IPA). Supplementary Table 2 lists the 6 most important differentially expressed networks detected by IPA; totals of 18/35 (51%) until 14/35 (40%) of genes included in these networks were significantly up- or down-regulated. Interestingly, most networks contained genes involved in cell-to-cell signaling and interaction, nutrition/lipid metabolism and cellular growth and differentiation. Supplementary Figure 1 illustrates the underlying connections between the various genes within the most important network involved in cell-to-cell signaling/interaction and hematological/immune system development. Specific IPA analysis towards hematological system development and function revealed changes groups of genes involved in growth of leukocyte cell lines (FOS, GADD45B, GHR, MAPK1, MAPK3, TGFB1), development of mononuclear leukocytes and lymphocytes (EGR1,FOS,MAPK1, MAPK3, PLCG2, TGFB1), infiltration of macrophages (ADIPOQ, SPP1, SREBF1, TGFB1), differentiation of blood cells (ADIPOQ, EGR1, FOS, HOXB4, JUNB, MAPK1, PLCG2, SPP1, TGFB1), proliferation of leukocytes (ADIPOQ, CASP3, CDKN2C, EGR1, JUNB, MAPK3, PLCG2, SPP1, TGFB1) as well as cell death of endothelial cell lines (CASP3, MAPK1, MAPK3, SPP1, TGFB1). The initiation and the progression of atherosclerosis critically depend on the endothelial barrier and on the balance between pro-inflammatory and anti-inflammatory activities. The changes observed in the microarrays are in agreement with the phenotype observed in $Cx37^{-/-}ApoE^{-/-}$

mice. In addition, metabolic factors may affect the atherosclerotic process locally, by contributing to the lipid deposition in the artery, and systemically by the production of specific cytokines, i.e. adipokines, from adipose tissue [125]. In this respect, the up-regulation of adiponectin (ADIPOQ) and resistin (RETN) might also contribute to enhanced atherosclerotic plaque development in $Cx37^{-/-}ApoE^{-/-}$ mice. Whether the changes in endothelial, inflammatory and metabolic gene expression in 10 weeks-old mice are causally related to the Cx37 deficiency itself or already a consequence of enhanced atherosclerotic lesion development in these mice remains to be established.

After 18 weeks of cholesterol-rich diet, 100 genes were found to be differentially regulated ($p < 0.05$) out of which 45 were up-regulated and 55 down-regulated in $Cx37^{-/-}$ $ApoE^{-/-}$ mice (supplementary Table 3). IPA revealed the 5 important differentially expressed networks; up to 60% (21/35) of genes included in these networks were significantly up- or down-regulated (supplementary Table 4). Similar to the analysis on 10 weeks-old mice, the networks contained genes involved in cell-to-cell signaling and interaction as well as to immuno-inflammatory disease. In addition, we found important changes (17/35, 49%) in a network of genes related to connective tissue and skeletal/muscular development and function (supplementary Figure 2) as well as in a network involved in organ and embryonic development (12/35, 34%). Interestingly, the differences included a down-regulation of members from two related families of proteins, i.e. bone morphogenetic proteins (BMPs) and Wnt signaling proteins. As members of the TGF-β superfamily, BMPs are potent regulators of vascular development and vessel remodeling. These cytokines play key roles in atherosclerosis and restenosis by regulating endothelial cell, SMC, macrophage, T cell and vascular calcifying cell responses [192]. In the arterial vasculature, mechanical and inflammatory redox signals act as secretagogues for BMP production with downstream activation of endothelial NADPH oxidases. Recent data indicates that the paracrine signals provided by

BMP and reactive oxygen species augment aortic myofibroblast Msx2-Wnt signaling and matrix turnover as well as osteogenic differentiation of calcifying vascular cells [193]. However, other studies have suggested that another BMP family member (BMP-7) inhibits arterial calcification in the diabetic LDLR-deficient mouse model [194]. The mechanism by which it reduces calcification may be related to its ability to reduce serum phosphate levels and to promote a contractile phenotype in SMCs. Interestingly, Cx37 expression is induced in medial SMCs beneath advanced atherosclerotic lesions [111]. In addition, we have recently demonstrated that targeting Cx43 prevents growth factor-induced phenotypic change in porcine coronary artery SMCs [195]. Whether Cx37 might have an additional role in SMC differentiation remains to be investigated.

Advanced atherosclerosis is often associated with calcification, a process that results in less compliant vessels and more rupture-prone atherosclerotic lesions. We found an up-regulation of S100A9 in $Cx37^{-/-}ApoE^{-/-}$ mice after 18 weeks of cholesterol-rich diet. This calcium-binding cytosolic protein, which is expressed in myeloid cells, is associated with innate immunity and regulating processes leading to leukocyte adhesion and transmigration. In addition, S100A9 has been associated with dystrophic calcification in advanced human atherosclerosis and got recently identified as a biomarker for cardiovascular events [196, 197]. We have previously shown that Cx37 protect against atherosclerosis by inhibiting ATP-dependent monocyte adhesion [47]. The enhanced expression of S100A9 in $Cx37^{-/-}ApoE^{-/-}$ mice might further promote leukocyte adhesion and transmigration in these mice.

4.13.2 Histology and validation of microarray expression profiles at protein level

Advanced atherosclerotic lesions in aortic roots of $Cx37^{-/-}ApoE^{-/-}$ and $ApoE^{-/-}$ mice were histologically examined after HE stain as well as after specific staining to identify lipids and

ECM components. As expected [47], atherosclerotic lesions beneath the valves of $Cx37^{-/-}ApoE^{-/-}$ mice were larger than in control $ApoE^{-/-}$ mice (Figure 1A and 1B). In addition, Sudan IV staining revealed increased lipid deposition in atherosclerotic lesions of $Cx37^{-/-}ApoE^{-/-}$ mice (Figure 1C and 1D), which corresponded to an increased number of macrophages in these atherosclerotic plaques (Figure 1E and 1F). These results provide support for a general protective role of Cx37 in atherosclerosis, both in the initiation [47] as well as in advanced stages of the disease. Interestingly, specific ECM staining revealed reduced levels of collagen (in blue) and elastin (in purple) in the atherosclerotic lesions of $Cx37^{-/-}ApoE^{-/-}$ mice compared with $ApoE^{-/-}$ mice (Figure 1G and 1H). Matrix degradation in atherosclerotic lesions results from the secretion of MMPs by activated macrophages [183]. Most MMPs are secreted as inactive proteins which are activated when cleaved by extracellular proteinases. Interestingly, we observed in our microarrays up-regulation of MMP-13 gene expression in $Cx37^{-/-}ApoE^{-/-}$ mice after 18 weeks of cholesterol-rich diet (supplementary Table 3). Enhanced expression of this protein has been reported in aortas of $ApoE^{-/-}$ mice with advanced atherosclerosis [198]. In addition, MMP-13 deletion in $ApoE^{-/-}$ mice promotes collagen accumulation and organization in atherosclerotic lesions [199]. In human, MMP-13 gene polymorphisms have been associated with coronary artery disease or atherosclerosis in the abdominal aorta [200, 201]. MMP-13 can degrade triple helical fibrillar collagen at neutral pH, an initial step that permits further digestion by other MMPs, such as MMP-9 [202, 203]. It has been reported that ubibiquitous MMP-9 deletion in $ApoE^{-/-}$ mice reduced the atherosclerotic burden [204] and expression of active MMP-9 in macrophages induced acute plaque disruption in $ApoE^{-/-}$ mice [205]. MMP-9 immunostaining showed an increased expression in advanced lesions of $Cx37^{-/-}ApoE^{-/-}$ mice after 18 weeks of cholesterol-rich diet (Figure 2). Whether the changes in MMP expression are causally related to the Cx37 deficiency itself or are a consequence of enhanced atherosclerosis in these mice remains to be determined.

The microarray results revealed an up-regulation of S100A9 as well as down-regulation of BMPs and Wnt signaling proteins in $Cx37^{-/-}ApoE^{-/-}$ mice after 18 weeks of cholesterol-rich diet (supplementary Tables 3 and 4). Because these proteins are important regulators of arterial/atherosclerotic calcification, we performed VonKossa staining on aortic roots of $Cx37^{-/-}ApoE^{-/-}$ and $ApoE^{-/-}$ mice. We observed increased calcium carbonate (in black) throughout the atherosclerotic lesions of $Cx37^{-/-}ApoE^{-/-}$ mice (Figure 3B and 3D) as compared with $ApoE^{-/-}$ mice (Figure 3A and 3C). In addition, we observed increased expression of S100A9 in atherosclerotic lesions of $Cx37^{-/-}ApoE^{-/-}$ mice (Figure 4), thus confirming the up-regulation of S100A9 gene expression observed in microarrays. A recent report confined S100A9 expression to macrophages within atherosclerotic lesion, where it was strongly expressed in calcifying areas and the surrounding ECM [206]. Interestingly, vascular matrix vesicles contain high levels of calcium-binding proteins and phospholipids that regulate calcification. Therefore, the authors proposed that S100A9 associated with lipid structures in matrix vesicles may influence phospholipid-calcium binding properties to promote dystrophic calcification. Further studies are required to investigate a causal relation between Cx37, S100A9 and plaque calcification. In any case, our results show enhanced calcification in atherosclerotic lesions of $Cx37^{-/-}ApoE^{-/-}$ mice, opening the possibility that Cx37 protects against dystrophic calcification in atherosclerosis.

4.14 CONCLUSIONS

In this study, we have carried out a broad microarray-based screening to identify genes that were intrinsic differentially expressed (at 10 weeks of age) or that showed distinct expression in aortas containing advanced atherosclerotic lesions between $Cx37^{-/-}ApoE^{-/-}$ and $ApoE^{-/-}$ mice. Our results suggest that Cx37 deficiency alters the global gene expression profiles in young mice towards a pro-inflammatory phenotype. After 18 weeks of atherogenic diet, the

differences mostly included genes involved in macrophage recruitment, calcium handling and matrix degradation. These differences could account for the altered plaque morphology in $Cx37^{-/-}ApoE^{-/-}$ mice, with reduced ECM and enhanced calcification as most striking differences.

4.15 ACKNOWLEDGEMENTS

This work was supported by grants from the Swiss National Science Foundation (#PPOOA-116897/1 to BRK), the Swiss University Conference Program 'Heart Remodeling in Health and Disease' (to BRK) and the Novartis Consumer Health Foundation (to CW and BRK).

4.16 FIGURE LEGENDS

Figure 1. Effects of Cx37 deletion on advanced mouse atheroma

Photographs of aortic root cryosections of $ApoE^{-/-}$ (**A, C, E, G**) and $Cx37^{-/-}ApoE^{-/-}$ (**B, D, F, H**) mice after 18 weeks of cholesterol-rich diet. Panels **A** and **B** are hematoxylin-eosin staining, panels **C** and **D** are Sudan IV staining, and panels **G** and **H** are aldehyde-fuchsine staining. Panels **E** and **F** are pictures of cryoections incubated with primary antibodies against CD68. FITC-conjugated antibodies (green) were used as secondary antibody. Tissue is counterstained with Evans Blue (red). Bar represent 500 μm for panels **A-D** and **G-H,** and 200 μm for panels **E-F.** Photographs are representative of roots from 7 mice in both groups.

Figure 2. Cx37 deletion results in increased MMP-9 expression in mouse atheroma

Photographs of aortic root cryosections of $ApoE^{-/-}$ (**A**) and $Cx37^{-/-}ApoE^{-/-}$ (**B**) mice after 18 weeks of cholesterol-rich diet. Cryosections are incubated with primary antibodies against MMP-9. Alkaline-phosphatase-conjugated antibodies (red) were used as secondary antibody. Nuclei are counterstained with Mayer's Hemalum (purple). Bar represent 150 μm. Photographs are representative of roots from 5 mice in both groups. **C:** Quantification of MMP-9-positive cells in aortic roots in $ApoE^{-/-}$ and $Cx37^{-/-}ApoE^{-/-}$ mice. N=5 and $^{*}P<0.05$.

Figure 3. Cx37 deletion results in increased calcification in mouse atheroma

Photographs of aortic root cryosections of $ApoE^{-/-}$ (**A, C**) and $Cx37^{-/-}ApoE^{-/-}$ (**B, D**) mice after 18 weeks of cholesterol-rich diet. Cryosections are stained according to the VonKossa method to identify calcium carbonate (black). Bar represent 200 μm. Photographs are representative of roots from 7 mice in both groups.

Figure 4. Cx37 deletion results in increased S100A9 expression in mouse atheroma

Cryosections of $ApoE^{-/-}$ and $Cx37^{-/-}ApoE^{-/-}$ mice after 18 weeks of cholesterol-rich diet were stained for S100A9. Graph shows quantification of S100A9-positive cells in aortic roots in $ApoE^{-/-}$ and $Cx37^{-/-}ApoE^{-/-}$ mice. N=7 and $^{*}P<0.05$.

4.17 FIGURE

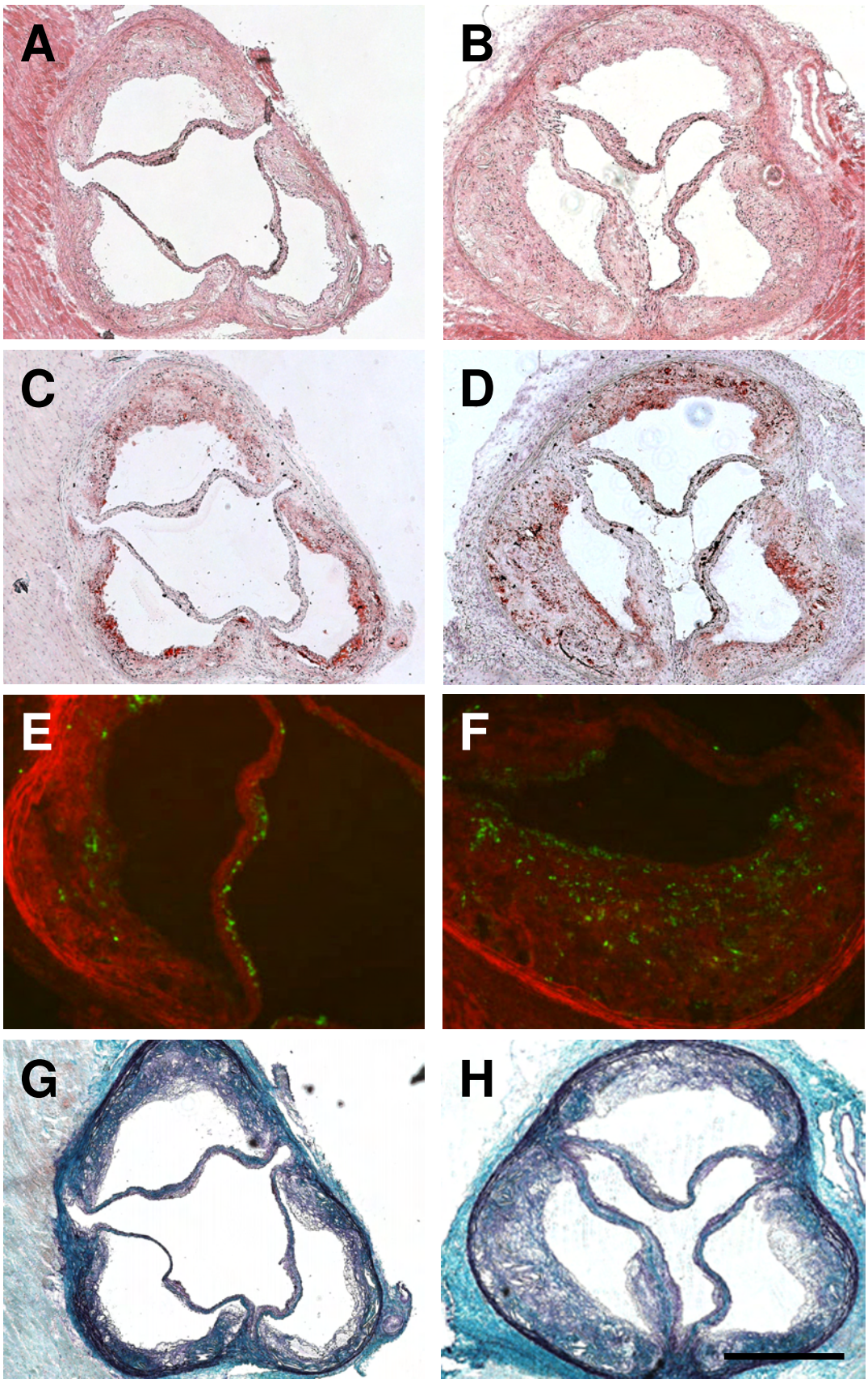

Figure 1

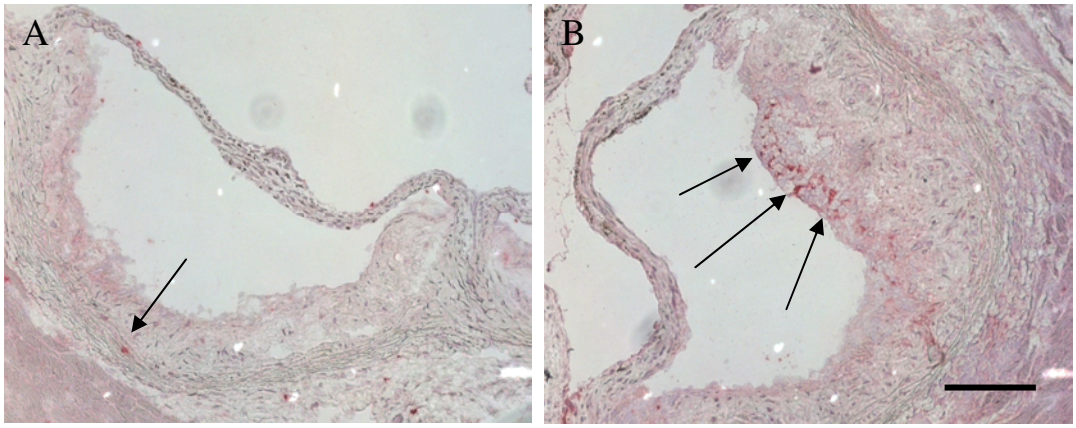

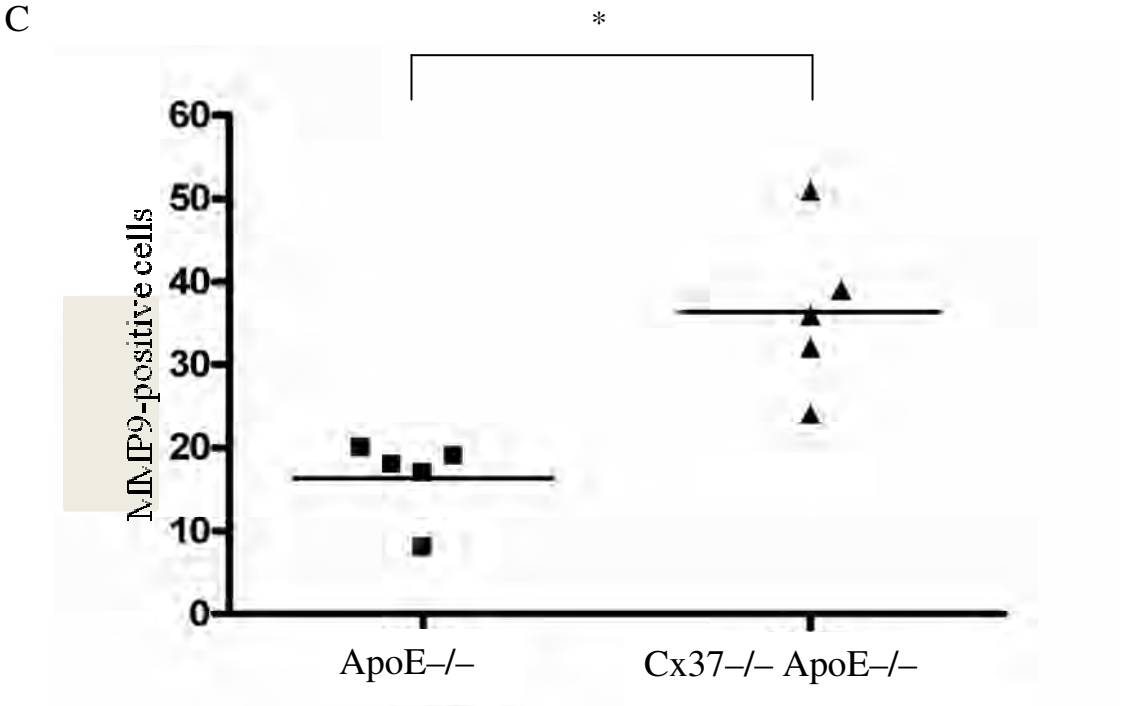

Figure 2

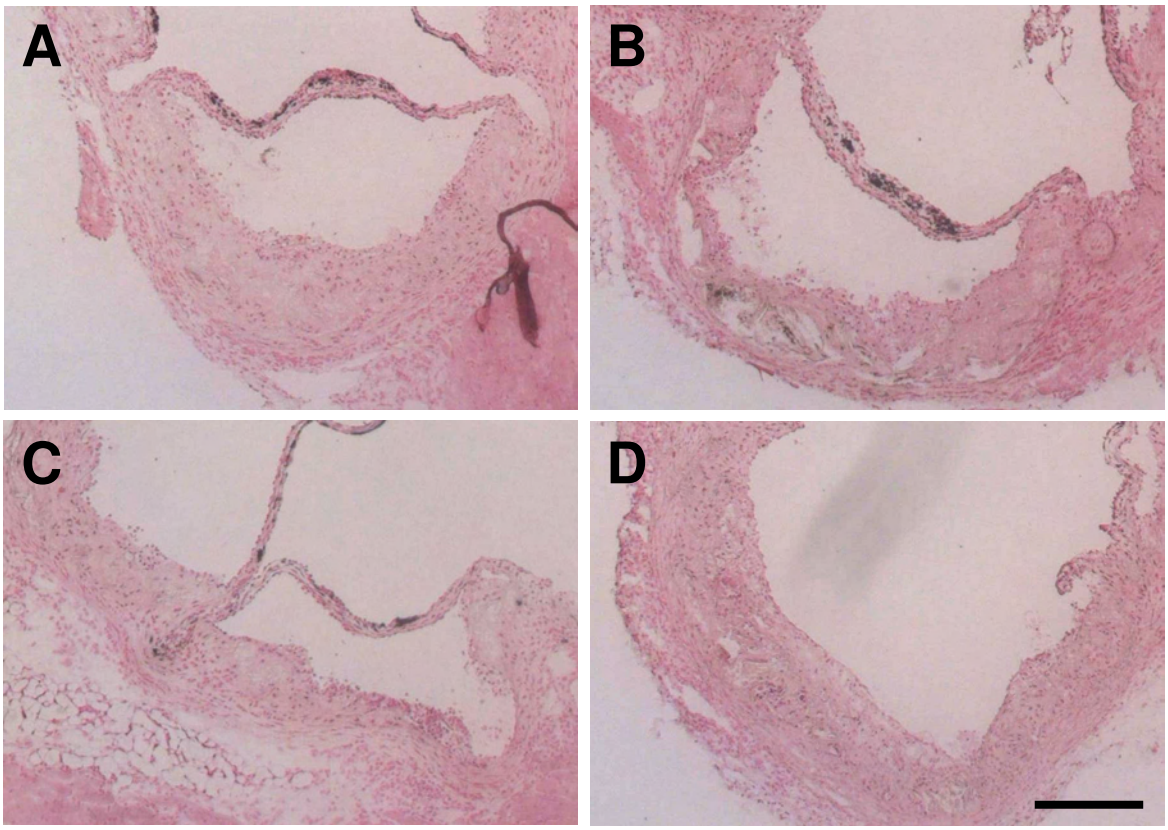

Figure 3

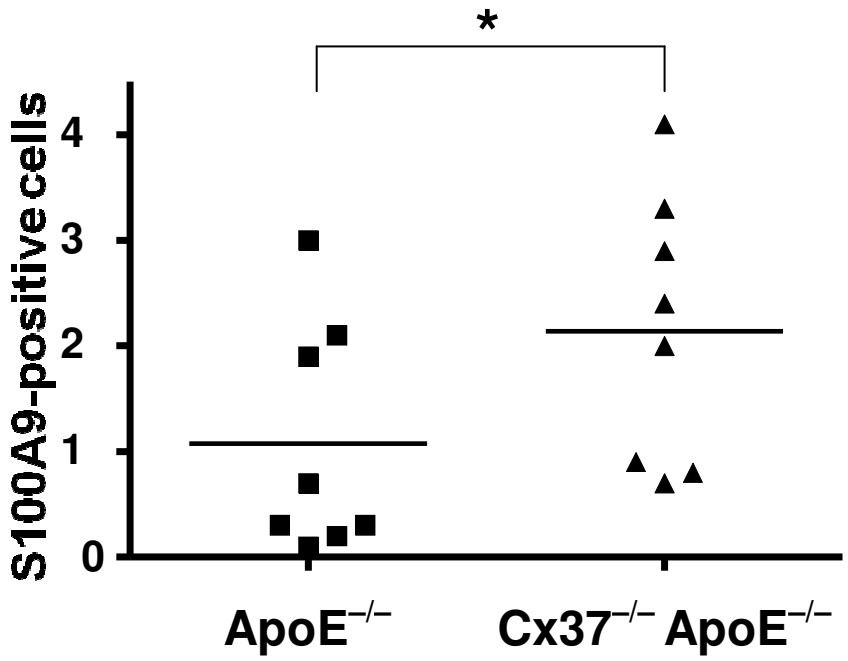

Figure 4

4.18 SUPPLEMENTARY DATA ON LINE

4.18.1 Supplementary Table 1:

Microarray data of 10 weeks-old $Cx37^{-/-}ApoE^{-/-}$ and $Cx37^{+/+}ApoE^{-/-}$ mice

Symbol	M-value (fold change)	P-value	RefSeq	Description
Gja4	-3.22575197	0.0000034	NM_008120.2	Gap junction membrane channel protein alpha 4
Tff3	-1.80417222	0.0003413	NM_011575.1	Trefoil factor 3, intestinal
Spp1	-1.79850679	0.0317000	NM_009263.1	Secreted phosphoprotein 1
Hspb1	-1.56069489	0.0002656	NM_013560.1	Heat shock protein 1
Hspa1b	-1.5544195	0.0083200	NM_010478.1	Heat shock protein 1B
Actn2	-1.43918036	0.0004690	NM_033268.3	Actinin alpha 2
Hsd17b4	-1.41389562	0.0435580	NM_008292.2	Hydroxysteroid (17-beta) dehydrogenase 4
Trim44	-1.40114065	0.0415230	NM_020267.2	Tripartite motif-containing 44
Gadd45b	-1.30913084	0.0016600	NM_008655.1	Growth arrest and DNA-damage-inducible 45 beta
Sf3a2	-0.98443345	0.0001950	NM_013651.3	Splicing factor 3a, subunit 2
Actl6a	-0.97507227	0.0018000	NM_019673.1	Actin-like 6A
Cdc42ep1	-0.97399173	0.0013920	NM_027219.1	CDC42 effector protein (Rho GTPase binding) 1
Mt2	-0.95748861	0.0175520	NM_008630.1	Metallothionein 2
Myd116	-0.92771153	0.0026000	NM_008654.1	Myeloid differentiation primary response gene 116
Mt1	-0.89714985	0.0221600	NM_013602.2	Metallothionein 1
Ucp2	-0.88384503	0.0041690	NM_011671.2	Uncoupling protein 2 (mitochondrial, proton carrier)
Por	-0.86530061	0.0007427	NM_008898.1	P450 (cytochrome) oxidoreductase
Stip1	-0.84447568	0.0054200	NM_016737.1	Stress-induced phosphoprotein 1
Hsp110	-0.84095008	0.0050130	NM_013559.1	Heat shock protein 110
Cenpi	-0.82126247	0.0330000	NM_145924.1	Centromere protein I
Odc1	-0.81672301	0.0112400	NM_016812.1	Ornithine decarboxylase, structural 1
Ccl9	-0.78816639	0.0059980	NM_011338.2	Chemokine (C-C motif) ligand 9
Plcg2	-0.78155489	0.0077000	NM_172285.1	Phospholipase C, gamma 2
Junb	-0.75805056	0.0101260	NM_008416.1	Jun-B oncogene
Itga7	-0.75789703	0.0006364	NM_008398.1	Integrin alpha 7
Tcfeb	-0.75512985	0.0026000	NM_011549.2	Transcription factor EB
Srm	-0.73922151	0.0184100	NM_009272.2	Spermidine synthase
Rps15	-0.73343783	0.0012330	NM_009091.1	Ribosomal protein S15
Dnajb1	-0.73033391	0.0243980	NM_018808.1	DnaJ (Hsp40) homolog, subfamily B, member 1
Vps72	-0.72891755	0.0048370		Vacuolar protein sorting 72 (yeast)
Ahsg	-0.72272462	0.0204600	NM_013465.1	Alpha-2-HS-glycoprotein
Ninj1	-0.7223561	0.0010352	NM_013610.1	Ninjurin 1
Camta1	-0.71646928	0.0085100		Calmodulin binding transcription activator 1
Hsp90ab1	-0.70896465	0.0017600	NM_008302.2	Heat shock protein 90kDa alpha (cytosolic), class B member 1
Mapk3	-0.70756315	0.0078400	NM_011952.2	Mitogen activated protein kinase 3

Tgfb1	-0.70502535	0.0006489	NM_011577.1	Transforming growth factor, beta 1

Ddc	1.2464024	0.042504	NM_016672.1	Dopa decarboxylase
Fos	1.2380776	0.0181481	NM_010234.2	FBJ osteosarcoma oncogene
Zc3h6	1.1495874	0.0078	NM_178404.2	Zinc finger CCCH type containing 6
Ctnna2	1.1236128	0.04032	NM_009819.1	Catenin (cadherin associated protein), alpha 2
Nkx3-1	1.0528021	0.042643	NM_010921.1	NK-3 transcription factor, locus 1 (Drosophila)
Egr1	1.0006906	0.00088	NM_007913.5	Early growth response 1
Sfrs5	0.9982048	0.005732	NM_009159.1	Splicing factor, arginine/serine-rich 5 (SRp40, HRS)
Defb2	0.9940429	0.0002592	NM_010030.1	Defensin beta 2
Msra	0.9546924	0.00209	NM_026322.3	Methionine sulfoxide reductase A
Malat1	0.9529243	0.02922		Metastasis associated lung adenocarcinoma transcript 1 (non-coding RNA)
Sfpq	0.9507010	0.0353	NM_023603.2	Splicing factor proline/glutamine rich (polypyrimidine tract binding protein associated)
Ghr	0.9229000	0.0371	NM_010284.1	Growth hormone receptor
Mapk1	0.9210545	0.00393	NM_011949.3	Mitogen activated protein kinase 1
Chmp2b	0.9171349	0.001174	NM_026879.1	Chromatin modifying protein 2B
Snx5	0.9089258	0.0218	NM_024225.2	Sorting nexin 5
Pcdh7	0.9028561	0.023271		Protocadherin 7
Sfrs2	0.8880145	0.010265	NM_011358.1	Splicing factor, arginine/serine-rich 2 (SC-35)
Eif2s3y	0.887645	0.000891	NM_012011.1	Eukaryotic translation initiation factor 2, subunit 3, structural gene Y-linked
Retn	0.8844326	0.049086	NM_022984.3	Resistin
Ddx3x	0.883026	0.03598	NM_010028.1	DEAD/H (Asp-Glu-Ala-Asp/His) box polypeptide 3, X-linked
Grpr	0.8672161	0.0006452	NM_008177.1	Gastrin releasing peptide receptor
Csde1	0.8558365	0.0471043	NM_144901.2	Cold shock domain containing E1, RNA binding
Lrp2	0.8546276	0.0009173		Low density lipoprotein receptor-related protein 2
Sh3bgrl	0.8430442	0.00898	NM_019989.2	SH3-binding domain glutamic acid-rich protein like
Zfp36l2	0.8399425	0.000782	NM_001001806.2	Zinc finger protein 36, C3H type-like 2
Tia1	0.838651	0.041988	NM_011585.3	Cytotoxic granule-associated RNA binding protein 1
Fbp2	0.8359137	0.0002872	NM_007994.1	Fructose bisphosphatase 2
Adipoq	0.8335196	0.0486562	NM_009605.4	Adiponectin, C1Q and collagen domain containing
Ppp1cb	0.8188264	0.0019	NM_172707.1	Protein phosphatase 1, catalytic subunit, beta isoform
Calm2	0.8166544	0.0004736	NM_007589.4	Calmodulin 2

Wnt9b	0.814540	0.0004766	NM_011719.2	Wingless-type MMTV integration site 9B
Srp54	0.8138811	0.00134	NM_028527.1	Signal recognition particle 54
Cd1d1	0.8107485	0.0358	NM_007639.1	CD1d1 antigen
Wwp1	0.8101727	0.0440373	NM_025476.3	WW domain containing E3 ubiquitin protein ligase 1
Ednrb	0.8094083	0.0470472	NM_007904.2	Endothelin receptor type B
Atp2a2	0.8074076	0.04195	NM_009722.1	ATPase, Ca++ transporting, cardiac muscle, slow twitch 2
Hisppd1	0.7943392	0.02284	NM_173760.3	Histidine acid phosphatase domain containing 1
Prpf38b	0.787150	0.01141	NM_025845.1	PRP38 pre-mRNA processing factor 38 (yeast) domain containing B
Fgf20	0.784814	0.0004673	NM_030610.1	Fibroblast growth factor 20
Ttc14	0.7726163	0.0429		Tetratricopeptide repeat domain 14
Upf3b	0.7702910	0.014457	NM_026573.1	UPF3 regulator of nonsense transcripts homolog B (yeast)
Mycl1	0.7655049	0.0038	NM_008506.2	V-myc myelocytomatosis viral oncogene homolog 1, lung carcinoma derived (avian)
Hoxd8	0.7578601	0.0003918		Homeo box D8
Exod1	0.7543676	0.02162	NM_027698.3	Exonuclease domain containing 1
Tmem49	0.7529592	0.0312		Transmembrane protein 49
Ptbp2	0.7437643	0.004875	NM_019550.1	Polypyrimidine tract binding protein 2; Polypyrimidine tract binding protein 2
Mbnl1	0.7393492	0.018663	NM_020007.2	Muscleblind-like 1 (Drosophila)
Hoxb4	0.7365732	0.000525	NM_010459.3	Homeo box B4
Map3k1	0.7361142	0.02014	NM_011945.2	Mitogen activated protein kinase kinase kinase 1
Mod1	0.7333521	0.011171	NM_008615.1	Malic enzyme, supernatant; Malic enzyme, supernatant
Elovl5	0.7327315	0.024605	NM_134255.2	ELOVL family member 5, elongation of long chain fatty acids (yeast)
Lin7c	0.7326349	0.00377	NM_011699.2	Lin-7 homolog C (C. elegans)
Avpr1a	0.731451	0.001484	NM_016847.2	Arginine vasopressin receptor 1A
Afp	0.7300725	0.00055	NM_007423.2	Alpha fetoprotein
Hoxd13	0.7230750	0.0005227	NM_008275.1	Homeo box D13
Casp3	0.7213905	0.01059	NM_009810.1	Caspase 3
Gas5	0.7190103	0.019172		Growth arrest specific 5
Za20d3	0.7185943	0.00269	NM_022985.3	Zinc finger, A20 domain containing 3
Nedd4	0.7147913	0.03498	NM_010890.3	Neural precursor cell expressed, developmentally down-regulted gene 4
Cdkn2c	0.7125735	0.027761	NM_007671.2	Cyclin-dependent kinase inhibitor 2C (p18, inhibits CDK4)
Rab3b	0.711225	0.0091	NM_023537.4	RAB3B, member RAS oncogene family
Cdh15	0.7083313	0.000812	NM_007662.1	Cadherin 15
Thrsp	0.7057617	0.005051	NM_009381.2	Thyroid hormone responsive SPOT14 homolog (Rattus)

Pnliprp1	0.7051344	0.0005676	NM_018874.1	Pancreatic lipase related protein 1
Ppp1r12a	0.7048449	0.0198		Protein phosphatase 1, regulatory (inhibitor) subunit 12A
Hcrt	0.7048274	0.0004797	NM_010410.1	Hypocretin
Myo1a	0.7035905	0.0004491		Myosin IA
Srebf1	0.7014550	0.00118	NM_011480.1	Sterol regulatory element binding factor 1
Gpkow	0.7003221	0.03982	NM_173747.2	G patch domain and KOW motifs

Microarrays were performed on RNA obtained from 10 weeks-old $Cx37^{-/-}ApoE^{-/-}$ and $Cx37^{+/+}ApoE^{-/-}$ mice. Data represent average of 3 arrays: $Cx37^{-/-}ApoE^{-/-}$ versus $Cx37^{+/+}ApoE^{-/-}$. Hundred and six genes were differentially expressed with a p-value of <0.05 and a fold change of >0.7 or <-0.7.

4.18.2 Supplementary Table 2:

Differentially expressed of networks of genes in 10 weeks-old $Cx37^{-/-}ApoE^{-/-}$ and $Cx37^{+/+}ApoE^{-/-}$ mice evaluated by Ingenuity Pathways Analysis

Molecules in Network	Score in %	Focus Molecules	Top Functions
Actin, ↓**ACTL6A,** ↓**ACTN2,** ↑**AFP,** ALP, ↑**AVPR1A,** ↑**CALM2,** ↑**CSDE1**, E2f, ↑**EDNRB**, G alphai, ↑**GRPR**, IL1, Interferon alpha, ↓**ITGA7,** LDL, Mapk, ↑**MAPK1,** ↓**MAPK3,** ↓**MT2A,** NMDA Receptor, PDGF BB, PI3K, Pka, Pkc(s), PLC, ↓**PLCG2,** PP2A, ↑**PPP1CB,** ↑PPP1R12A, Ras homolog, RNA polymerase II, ↓SRM, ↓**TGFB1,** ↓**VPS72**	51	18	Cell-To-Cell Signaling and Interaction, Hematological System Development and Function, Immune and Lymphatic System Development and Function
Akt, ↑**ATP2A2,** Calpain, ↑**CASP3,** Caspase, ↑**CDKN2C,** ↓**DNAJB1**, Fgf, ↓**GADD45B,** Hsp27, Hsp70, Hsp90, ↓**HSP90AB1,** ↓**HSPA1B,** ↓**HSPB1,** Ige, IL12, Jnk, ↓**JUNB,** ↑**LIN7C,** ↑**MAP3K1,** ↑**NEDD4,** NFkB, ↑**NKX3-1,** ↓**ODC1**, P38 MAPK, Pdgf, Pdgf Ab, Proteasome, ↑**PTBP2**, Ras, ↓**STIP1,** ↓**TFF3**, Tgf beta, Vegf	49	17	Cellular Compromise, Drug Metabolism, Endocrine System Development and Function
↑**ADIPOQ,** AMPK, Ap1, Ck2, Creb, Cyclin A, ↑**DEFB4** (includes EG:1673), ↑**EGR1**, ↑**ERK**, ERK1/2, ↑**FOS**, ↑**GAS5**, ↑**GHR,** ↑**HCRT**, Histone h3, ↑**HOXB4**, IKK, Insulin, MAP2K1/2, Mek, PEPCK, PLA2, ↑**RAB3B**, Raf, ↑**RETN**, RTK, ↓**SF3A2**, ↑**SFRS5,** ↓SPP1, ↑**SREBF1**, T3-TR-RXR, TCR, ↑**THRSP**, Thyroid hormone receptor, ↓**UCP2**	49	17	Nutritional Disease, Cell Morphology, Cell-To-Cell Signaling and Interaction

In bold: genes of the network that were significantly differentially expressed; arrows: genes up-regulated or down-regulated.

4.18.3 Supplementary figure 1

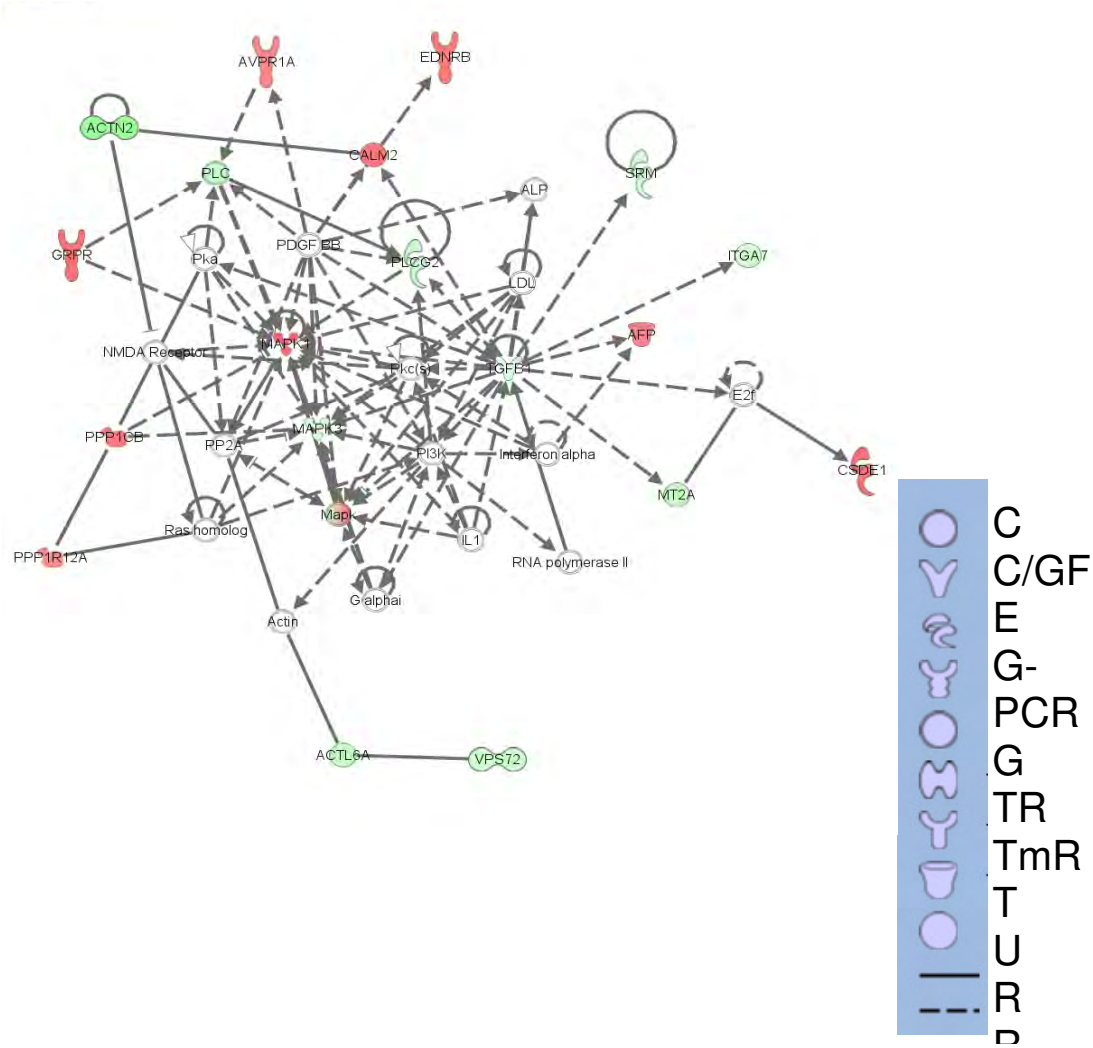

Supplementary Figure 1:
Illustration of the underlying connections between the various genes within the most important network involved in cell-to-cell signaling/interaction and hematological/immune system development revealed by Ingenuity Pathways Analysis (IPA). A total of 18/35 (51%) of genes included in this network were significantly up-regulated (in red) or down-regulated (in green). Blue bar explains the symbols used: C means complex, C/GF cytokine/growth factor, E enzyme, G-PCR G-protein coupled receptor, G group, TR transcription regulator, TmR transmembrane receptor, T transporter, U unknown and R relation.

4.18.4 Supplementary Table 3:

Microarray data of $Cx37^{-/-}ApoE^{-/-}$ and $Cx37^{+/+}ApoE^{-/-}$ mice after 18 weeks of cholesterol-rich diet

Symbol	M-value (fold change)	P-value	RefSeq	Description
Gja4	-2.45178444	0.000477	NM_008120.2	Gap junction membrane channel protein alpha 4
Bex1	-1.27448876	0.011474	NM_009052.2	Brain expressed gene 1
Nodal	-1.15821445	0.000168	NM_013611.3	Nodal
Zfyve9	-1.09197376	0.006240		Zinc finger, FYVE domain containing 9
Fblim1	-1.01983512	0.000074	NM_133754.2	Filamin binding LIM protein 1
Krt2-8	-0.97202678	0.021660	NM_001004194.1	Keratin complex 2, basic, gene 8
Dvl3	-0.9262656	0.006000	NM_007889.1	Dishevelled 3, dsh homolog (Drosophila)
Car6	-0.90971164	0.000081	NM_009802.1	Carbonic anhydrase 6
Dhh	-0.90952605	0.000347	NM_007857.2	Desert hedgehog
Hspb1	-0.89323505	0.009340	NM_013560.1	Heat shock protein 1
Hdac1	-0.88203613	0.017720		Histone deacetylase 1
Wnt2b	-0.86389979	0.000734	NM_009520.2	Wingless related MMTV integration site 2b
Armet	-0.86046636	0.003306	NM_029103.1	Arginine-rich, mutated in early stage tumors
Bhlhb8	-0.846911	0.000139	NM_010800.3	Basic helix-loop-helix domain containing, class B, 8
Bmp6	-0.84471303	0.001610	NM_007556.1	Bone morphogenetic protein 6
Hsp90ab1	-0.83744925	0.005236	NM_008302.2	Heat shock protein 90kDa alpha (cytosolic), class B member 1
Csnk2b	-0.8286864	0.001300	NM_009975.1	Casein kinase II, beta subunit
Actn1	-0.82447845	0.003494	NM_134156.1	Actinin, alpha 1
Egf	-0.8192537	0.000677	NM_010113.1	Epidermal growth factor
Wnt10a	-0.81892438	0.000467	NM_009518.1	Wingless related MMTV integration site 10a
Wnt6	-0.81502321	0.000616	NM_009526.2	Wingless-related MMTV integration site 6
Dpp3	-0.80025002	0.000116	NM_133803.1	Dipeptidylpeptidase 3
Reg3d	-0.79816028	0.004679	NM_013893.1	Regenerating islet-derived 3 delta
Smo	-0.79273623	0.000424	NM_176996.3	Smoothened homolog (Drosophila)
Glp1r	-0.79035626	0.000188	NM_021332.1	Glucagon-like peptide 1 receptor
Bmp4	-0.78778573	0.000232	NM_007554.1	Bone morphogenetic protein 4
Wnt8b	-0.78268912	0.004196	NM_011720.1	Wingless related MMTV integration site 8b
Furin	-0.77861696	0.000534	NM_011046.1	Furin (paired basic amino acid cleaving enzyme)
Id2	-0.77368773	0.000636	NM_010496.2	Inhibitor of DNA binding 2
Notch3	-0.7721882	0.000137	NM_008716.1	Notch gene homolog 3 (Drosophila)
Myh11	-0.76186378	0.031800	NM_013607.1	Myosin, heavy polypeptide 11, smooth muscle
Ptch1	-0.76143985	0.000803	NM_008957.1	Patched homolog 1
Bmp2	-0.76069929	0.000906	NM_007553.2	Bone morphogenetic protein 2
Tgfbr3	-0.75058757	0.003544	NM_011578.2	Transforming growth factor, beta receptor III
Serpini2	-0.74505193	0.009668	NM_026460.1	Serine (or cysteine) peptidase inhibitor, clade I, member 2
Palld	-0.74353388	0.005900		Palladin, cytoskeletal associated protein
Cdc25b	-0.74313789	0.000359	NM_023117.1	Cell division cycle 25 homolog B (S. cerevisiae)
Tgfbr1	-0.73247552	0.005900	NM_009370.2	Transforming growth factor, beta receptor I
Fgf9	-0.73191268	0.000951	NM_013518.1	Fibroblast growth factor 9
Pcsk4	-0.7317267	0.005620	NM_008793.1	Proprotein convertase subtilisin/kexin type 4

Dvl2	-0.72764987	0.003030	NM_007888.3	Dishevelled 2, dsh homolog (Drosophila)
Wnt5b	-0.72699758	0.003525	NM_009525.2	Wingless-related MMTV integration site 5B
Nkx2-2	-0.72395761	0.010300	NM_010919.1	NK2 transcription factor related, locus 2 (Drosophila)
Fkbp4	-0.72307062	0.004427	NM_010219.2	FK506 binding protein 4
Cdk2ap1	-0.72046386	0.002695	NM_013812.2	CDK2 (cyclin-dependent kinase 2)-associated protein 1
G6pc2	-0.715294	0.000862	NM_021331.1	Glucose-6-phosphatase, catalytic, 2
Tcea3	-0.71307264	0.003037	NM_011542.1	Transcription elongation factor A (SII), 3
Nkx6-1	-0.71230973	0.012190	NM_144955.1	NK6 transcription factor related, locus 1 (Drosophila)
Actb	-0.71212015	0.002044	NM_007393.1	Actin, beta, cytoplasmic
Rbp4	-0.71058677	0.007747	NM_011255.2	Retinol binding protein 4, plasma
Pdia4	-0.7092918	0.016162	NM_009787.2	Protein disulfide isomerase associated 4
Hsp110	-0.70712584	0.001243	NM_013559.1	Heat shock protein 110
Sars	-0.70585688	0.003444	NM_011319.1	Seryl-aminoacyl-tRNA synthetase
Ruvbl1	-0.70531182	0.000144	NM_019685.1	RuvB-like protein 1
Hspa8	-0.70339505	0.000176	NM_031165.3	Heat shock protein 8

Cap1	2.64982007	0.000063	NM_007598.2	CAP, adenylate cyclase-associated protein 1 (yeast)
Igh-6	1.3473453	0.04873	NM_198640.1	Immunoglobulin heavy chain 6 (heavy chain of IgM)
Camk2b	1.31646598	0.003229	NM_007595.2	Calcium/calmodulin-dependent protein kinase II, beta
Plac8	1.30249637	0.02751	NM_139198.1	Placenta-specific 8
Trim34	1.18464477	0.0055	NM_030684.1	Tripartite motif protein 34
Mmp13	1.17194791	0.001174	NM_008607.1	Matrix metallopeptidase 13
Stat2	1.086722	0.016045	NM_019963.1	Signal transducer and activator of transcription 2
Ly6e	1.07639676	0.022473	NM_008529.2	Lymphocyte antigen 6 complex, locus E
Egr1	1.04726278	0.002418	NM_007913.5	Early growth response 1
Clec4e	0.99039369	0.03681	NM_019948.1	C-type lectin domain family 4, member e
Nfkbiz	0.9849638	0.001126	NM_030612.1	Nuclear factor of kappa light polypeptide gene enhancer in B-cells inhibitor, zeta
Ddx58	0.9849203	0.027024	NM_172689.2	DEAD (Asp-Glu-Ala-Asp) box polypeptide 58
Cxcl2	0.97232284	0.019236	NM_009140.1	Chemokine (C-X-C motif) ligand 2
S100a9	0.96094164	0.000094	NM_009114.1	S100 calcium binding protein A9 (calgranulin B)
Mt2	0.94567516	0.0402	NM_008630.1	Metallothionein 2
Hivep3	0.89617976	0.00157	NM_010657.2	Human immunodeficiency virus type I enhancer binding protein 3
Tlr1	0.87462444	0.000077	NM_030682.1	Toll-like receptor 1
Selpl	0.87171847	0.004687	NM_009151.2	Selectin, platelet (p-selectin) ligand
Cxcl5	0.86771048	0.004125	NM_009141.1	Chemokine (C-X-C motif) ligand 5
Zcchc11	0.85011582	0.000344	NM_175472.3	Zinc finger, CCHC domain containing 11
Ifitm3	0.85011576	0.03206	NM_025378.1	Interferon induced transmembrane protein 3
Prmt1	0.84215949	0.002825	NM_019830.1	Protein arginine N-methyltransferase 1
Lcp2	0.82616712	0.026168	NM_010696.2	Lymphocyte cytosolic protein 2
Axud1	0.82212261	0.01041	NM_153287.2	AXIN1 up-regulated 1
Arg1	0.80777081	0.02093	NM_007482.2	Arginase 1, liver
Ms4a6d	0.80357857	0.017771	NM_026835.1	Membrane-spanning 4-domains, subfamily A, member 6D
Isgf3g	0.79185325	0.0163		Interferon dependent positive acting transcription factor 3 gamma
Nr1d2	0.78545027	0.006766	NM_011584.2	Nuclear receptor subfamily 1, group D, member 2
Cd86	0.77588908	0.00553	NM_019388.2	CD86 antigen
Fbxo3	0.76991189	0.000087	NM_212433.1	F-box only protein 3

Tlr7	0.7651594	0.00421	NM_133211.2	Toll-like receptor 7
Sp100	0.75939375	0.004007	NM_001013817.1	Nuclear antigen Sp100
Wdfy1	0.75505416	0.002992	NM_027057.1	WD repeat and FYVE domain containing 1
Nfxl1	0.75195627	0.007815	NM_177007.2	Nuclear transcription factor, X-box binding-like 1
Tbc1d8	0.74571942	0.012564	NM_018775.2	TBC1 domain family, member 8
Morc3	0.73270758	0.007946		Microrchidia 3
Vnn1	0.72944405	0.00597	NM_011704.1	Vanin 1
Mt1	0.72441918	0.0323	NM_013602.2	Metallothionein 1
Pde4b	0.72120246	0.01998		Phosphodiesterase 4B, cAMP specific
Trim14	0.71849805	0.00092	NM_029077.1	Tripartite motif-containing 14
Rgs2	0.71365523	0.002521	NM_009061.2	Regulator of G-protein signaling 2
Apobec1	0.71356276	0.000602	NM_031159.2	Apolipoprotein B editing complex 1
Il6	0.71095616	0.00751	NM_031168.1	Interleukin 6
Lcn2	0.7104538	0.000657	NM_008491.1	Lipocalin 2
Luzp5	0.70657438	0.000338	NM_133762.3	Leucine zipper protein 5

Microarrays were performed on RNA obtained from $Cx37^{-/-}ApoE^{-/-}$ and $Cx37^{+/+}ApoE^{-/-}$ mice after 18 weeks of cholesterol-rich diet. Data represent average of 3 arrays: $Cx37^{-/-}ApoE^{-/-}$ versus $Cx37^{+/+}ApoE^{-/-}$. Hundred genes were differentially expressed with a p-value of <0.05 and a fold change of >0.7 or <-0.7.

4.18.5 Supplementary Table 4:

Differentially expressed of networks of genes in $Cx37^{-/-}ApoE^{-/-}$ and $Cx37^{+/+}ApoE^{-/-}$ mice after 18 weeks of cholesterol-rich diet evaluated by Ingenuity Pathways Analysis

Molecules in Network	Score in %	Focus Molecules	Top Functions
AMPK, ↑**ARG1**, ↓**BEX1 (includes EG:55859),** ↑**CD86,** ↑**CLEC4E,** ↑**CXCL5,** Cyclin E, ↑**DDX58,** ↑**EGR1,** ↓**G6PC2**, Hsp70**,** ↓**HSPB1,** ↑**IFITM3**, Ifn alpha, IFN Beta, ↑**IL6**, IL12, Interferon alpha, ↑ **IRF9,** ↑**LCP2**, MHC Class I, NF-κB, NFkB**,** ↑**NFKBIZ**, P38 MAPK, PI3K, ↑**PLAC8**, Ras, ↓**RBP4,** ↑**SP100,** ↑**STAT2,** ↑**TLR1,** ↑**TLR7**, VAV, ↓**WNT10A**	60	21	Dermatological Diseases and Conditions, Inflammatory Disease, Immunological Disease
ALP, Ap1, BMP, ↓**BMP2**, ↓**BMP4**, ↓**BMP6**, Creb, ↑**CXCL2**, Cyclin D, ERK, ERK1/2, ↑**FBXO3**, ↓**FGF9,** ↓**FURIN**, ↓**ID2**, IL1**, LCN2**, LDL, Mmp, ↑**MMP13,** ↓**MYH11**, ↓**NODAL**, Notch, ↓**NOTCH3,** p70 S6k, ↓**PCSK4**, Pdgf, PDGF BB, Smad, Smad1/5/8, STAT, Tgf beta, ↓**TGFBR1,** ↓**TGFBR3,** ↓**ZFYVE9**	49	17	Cellular Development, Connective Tissue Development and Function, Skeletal and Muscular System Development and Function
↓**ACTB**, Actin, ↓**ACTN1**, ADCY, Alpha Actinin, ↑**CAMK2B**, ↑**CAP1,** ↓**CDC25B,** ↓**CDK2AP1**, Ck2, ↓**CSNK2B**, Cyclin A, ↓**DPP3**, E2f**,** ↓**EGF**, F Actin, G-Actin, ↓**GLP1R,** ↓**HDAC1**, Histone h3, Hsp90, ↓**HSPA8**, Insulin, MAP2K1/2, Mapk, ↑**MT2A,** ↓**PALLD**, Pkc(s), PLC gamma, Proteasome, Rb, ↑**RGS2**, RNA polymerase II, ↓**RUVBL1,** ↑**S100A9**	49	17	Cell-To-Cell Signaling and Interaction, Cellular Assembly and Organization, Hair and Skin Development and Function

In bold: genes of the network that were significantly differentially expressed; arrows: genes up-regulated or down-regulated.

4.18.6 Supplementary Figure 2:

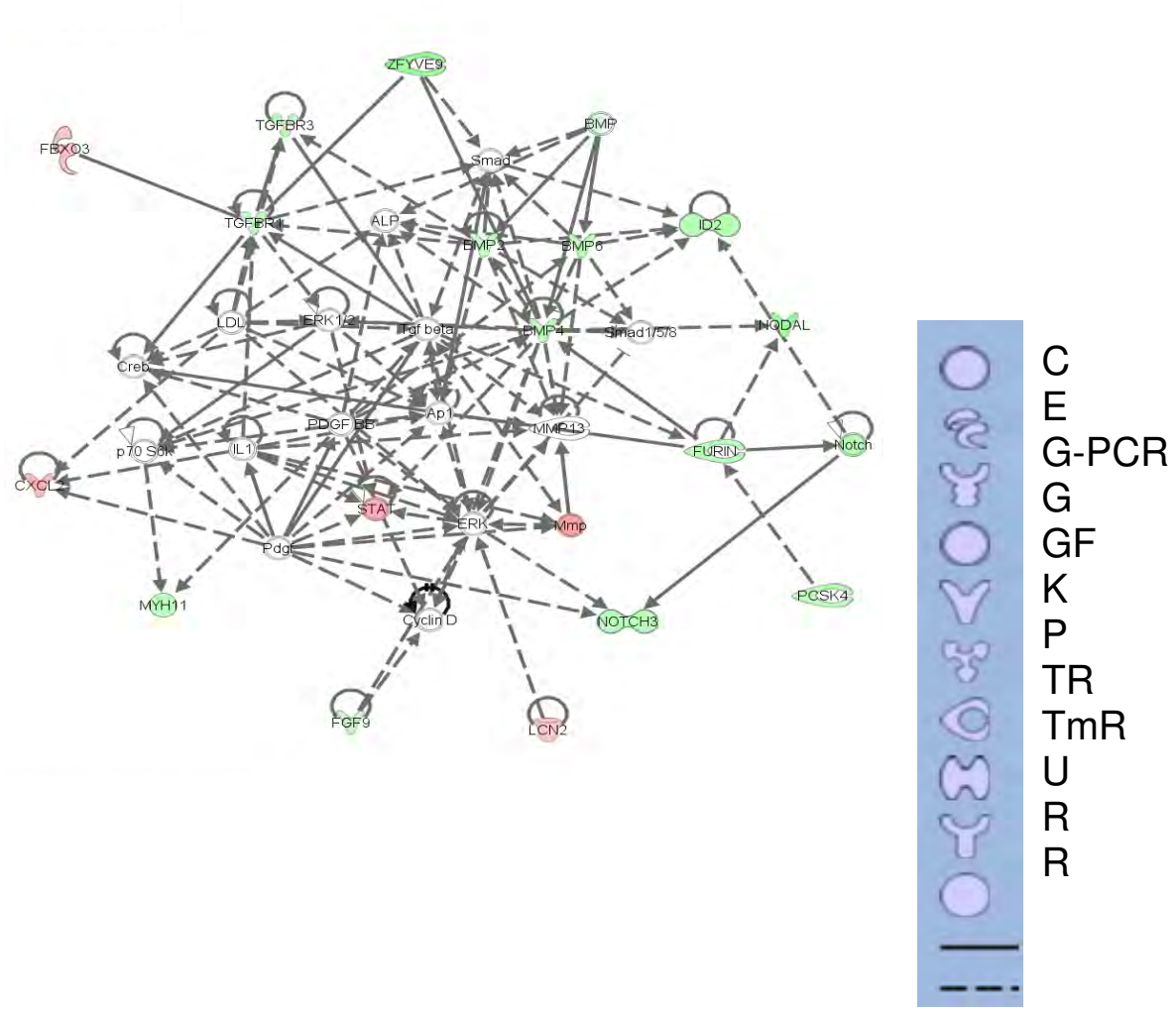

Supplementary Figure 2:
Illustration of the underlying connections in a network of genes related to connective tissue and skeletal/muscular development and function revealed by Ingenuity Pathways Analysis (IPA). A total of 17/35 (49%) of genes included in this network were significantly up-regulated (in red) or down-regulated (in green). Blue bar explains the symbols used: C means complex, E enzyme, G-PCR G-protein coupled receptor, G group, GF growth factor, K kinase, P peptidase, TR transcription regulator, TmR transmembrane receptor, U unknown and R relation.

5 GENERAL DISCUSSION AND PERSPECTIVES

It is commonly accepted at present that a critical balance between positive and negative regulatory factors influences all stages of atherosclerotic disease. We have previously shown that Cx37 hemichannels (HC) control the initiation of atherosclerotic plaque development by regulating ATP-dependent monocyte adhesion [47]. Furthermore, a C1019T polymorphism in the human Cx37 gene has been associated with increased risk for CAD and MI [122-124, 130, 131, 139, 159]. However, little was known about the specific properties of Cx37-P319 or Cx37-S319 gap junction- and hemi- channels. The work described in this thesis has revealed that (1) channels made of Cx37-S319 or Cx37-P319 show important differences in their biophysical properties, (2) Cx37-S319-CT or Cx37-P319-CT display a differential binding preference for RXP and RXXP consensus motifs, possibly leading to differential interaction of Cx37-P319 or Cx37-S319 with other proteins, and (3) the presence of Cx37 differentially affect the expression of other genes in a mouse model of advanced atherosclerosis.

5.10 HUMAN POLYMORPHIC Cx37 AND PERMEABILITY

To investigate the biophysical properties of polymorphic Cx37 HC in details, we have transfected hCx37-1019C, hCx37-1019T or empty pIRES-eGFP vector cDNA into communication-deficient HeLa cells. To confirm that the transfected proteins indeed formed functional gap junction channels (GJC), we then performed preliminary dye coupling assays with 4% Lucifer Yellow (LY-lithium salt, Sigma) and 4% Neurobiotin (NB, Vector Laboratories) in 150 mM LiCl in the clones EV and Cx37-S319 used in Chapter 1. We let the tracers diffuse for 3 minutes and cells were then fixed for 10 minutes in 4% paraformaldehyde in PBS as described by Elfgang et al. [207]. As shown in **Figure 16A**, we observed no transfer of LY to neighboring cells in pIRES-eGFP transfected HeLa cells (EV, N=8) and in HeLa cells expressing Cx37-S319 (N=12). In contrast, NB diffused to 3.2±1.3 Cx37-S319 cells (N=12).

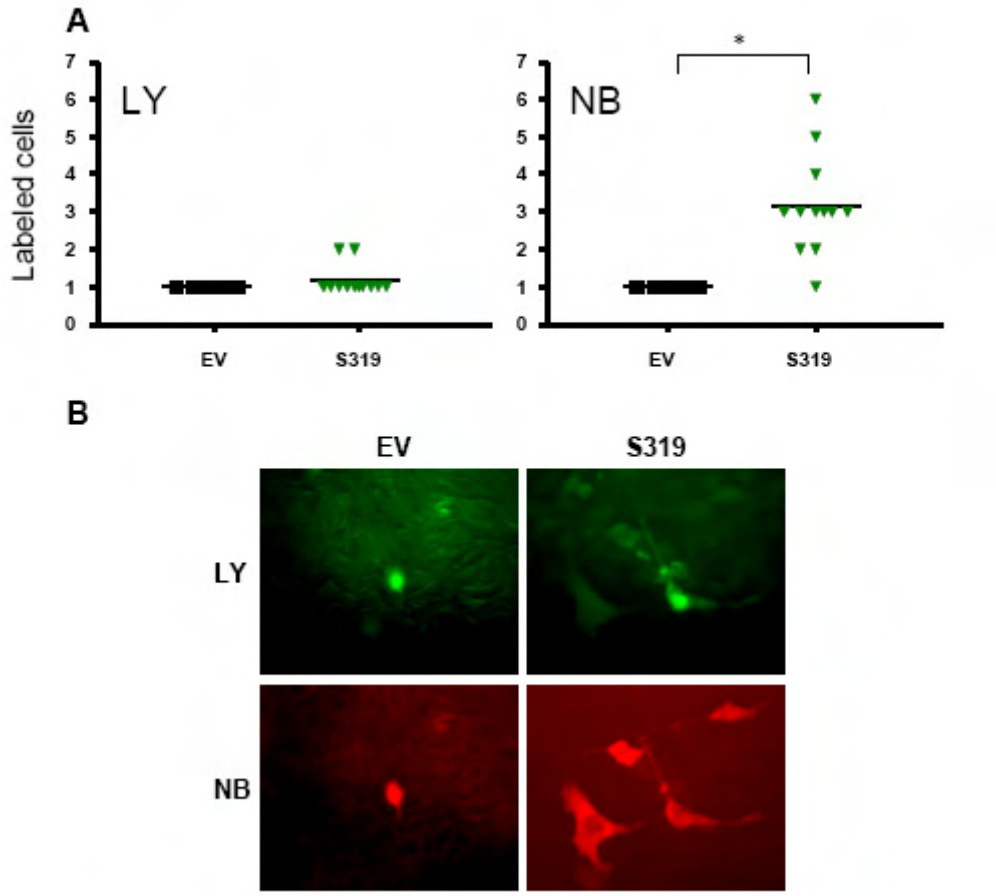

Figure 16: Functional GJC in cells transfected with Cx37-S319.

Elfgang et al. [207] found with murine Cx37 transfected in HeLa cells the same quantity of first neighbouring cells (60%) positive for the two tracers NB and LY (N=100). This may seem in contradiction with our data, in which clear differences were obtained in the diffusional properties of LY and NB through human Cx37 channels. Possible explanations for these differences include: 1) species-specific differences (murine vs. human) in permeabilities of Cx37. Species-specific differences in permeability have been described for Cx43 transfected in osteoblastic cells by Steinberg et al.[208]; 2) methodological differences in data analysis, i.e. counting total number of cells vs. first neighboring cells; and 3) experimental differences, i.e. each tracer separately injected vs. the two tracers injected together with the

same microelectrode. Finally, differences in Cx37 expression level may influence the amount of tracer passing to neighbouring cells during a given period. As described in Chapter 1, we have selected transfected clones with a moderate-to-low expression of Cx37, which may have limited transfer the transfer of the relatively large tracer LY during the 3 minutes microinjection. Interestingly, our data is supported by the *in vivo* data on mouse artery of Krüger et al.[209] who estimated the contribution of Cx40 and Cx37 to total gap junctional dye diffusionability. They found that when LY or NB were injected into aortic endothelium of wild-type mice, dye spread to multiple adjacent cells (9±3 cells; N=7). In contrast, when LY was injected into endothelium of *Cx40*-deficient mice, it remained in the cell of injection (N=5), but NB revealed extensive coupling between endothelial cells in the abdominal aorta of both wild-type and *Cx40*-deficient mice (>30 cells; N=8). Interestingly, Seul et al.[210] demonstrated a significant reduction of LY transfer when HUVECs were transfected with an adenovirus containing Cx37 (from 25±10 to 4±2 cells, N=18), whereas a significant increase of NB transfer was observed under these conditions (from 50±20 to 70±25 cells, N=18). Although in agreement with our results, these data should be interpreted with caution, because HUVECs are known to change Cx expression pattern with passage and start to express Cx43 [175 178], which is permeable to LY dye. In addition, Wang et al.[211] showed significant differential NB dye transfer in HeLa cells expressing Cx37 (from 38±6 to 10±3 cells, N=12) when they were infected with adenovirus containing Cx43 with a cytoplasmic loop deletion, suggesting an inhibitory effect mediated by the formation of heteromeric connexons between $Cx43del_{130–136}$ and wild-type Cx37. At last, microinjection experiments of Kyle et al.[212] on human Cx37 in HeLa cells with LY-LiCl and NB were in agreement with our results; they found no LY transfer but NB transfer to 8.8±0.6 cells (N=46). Unfortunately, they did not specify the type of polymorphic Cx37 transfected in their experiments. All together, most available data is in support of our observations on the permeability of NB and impermeability

of LY through human Cx37 channels when the dyes are dissolved in LiCl. These observations raised new questions:

1. Apart from the differences in size and charge between LY and NB (respectively MW: 457, charge: -2 and 328, +1) which is inducing selective permeability [213-215], are the differences in efficiency of dye transfer due to the medium used to dissolve the tracer?
2. The impermeability of Cx37 channels towards LY can not be due to conductance. As shown in Chapter 1 and 2, human Cx37 GJC exhibit unitary conductances ranging between 200 to 380pS, whereas it has been shown that Cx43 GJC exhibit unitary conductances ranging between 30 and 90pS. How LY could pass Cx43 GJC with a high resistance and not through Cx37 GJC with a low resistance?

To resolve these issues, we then performed dye transfer experiments on cell pairs (expressing similar total and membrane levels of Cx37 as shown in Figure 1 of Chapter 1) while monitoring conductance (**Table 1**). Thus, high resistance seals were made on both cells of a pair. Then, the membrane patch under the electrode tip was broken to achieve the whole cell configuration in one cell. The electrode solution (F1 solution) was consisting of Aspartic acid (120 mM), HEPES (5mM), Mg-ATP (3mM), CaCl2 (1mM), NaCl (10mM), KOH (120mM), EGTA (10mM), with an adjusted pH with KOH to 7.25 and an osmolarity between 280-285mOsm. We added to F1 solution 4% LY dissolved in potassium salt (Sigma). Surprisingly, we observed dye transfer within HeLa cell pairs transfected with Cx37-S319 (N=11) (**Figure 17**, left picture) and no dye transfer within HeLa cell pairs transfected with Cx37-P319 (N=10). As described in Chapter 1, the unitary conductance measured in Cx37-P319 cell pairs (~300 pS) is 1.5x larger than in Cx37-S319 cell pairs (~200 pS). The fact that LY is passing through the 200 pS Cx37-S319 channels and not through the 300 pS Cx37-P319 channels seems to contradict our original hypothesis (no.2). It is however in agreement

with an elegant study systematically comparing the single channel permeabilities of Cx26, Cx37, Cx40 and Cx43 in pairs of oocytes with similar macroscopic conductances [216]. In this study, the authors demonstrated that GJC with smaller unitary conductances do not necessarily possess smaller permeabilities and by interference may not have smaller pore diameters. They also showed that Cx37 is the least permeable of all connexins to three anionic Alexa probes with increasing molecular weight. Moreover, the permeability to Alexa594 (MW: 760, charge: -2) appeared reduced to the limits of the detection in their highly-coupled oocyte system. To investigate whether the lack of LY diffusion in our moderate-to-low expressing Cx37-P319 cell pairs was due to an absolute or relative impermeability of the dye, experiments should be repeated using other clones that highly express Cx37-P319. Interestingly, we measured macroscopic conductances at the end of the experiments and revealed 0.54±0.10 nS for Cx37-P319 (N=10) and 0.66±0.11 nS for Cx37-S319 (N=11) cell pairs. Given the equal surface expression of Cx37-P319 and Cx37-S319 cells and the differences in unitary conductances, this implies that the open probability of Cx37-S319 cell pairs must be ~1.5x larger than in Cx37-P319 cell pairs. Whether the difference in open probability observed between our Cx37-P319 and Cx37-S319 cell pairs is sufficient to explain the differential transfer of LY remains to be established.

Next, we repeated our experiments using LY-LiCl and observed no LY transfer for either Cx37-S319 (N=5) or Cx37-P319 (N=4) in transfected HeLa cell pairs, this way confirming our microinjection experiments. As expected when a smaller current-carrying ion is used (Li vs K), macroscopic conductances were increased and revealed 1.13±0.37 nS for Cx37-P319 (N=5) and 1.55±0.62 nS for Cx37-S319 (N=4) cell pairs. Thus, these experiments are in agreement our original hypothesis (no.1). Discrepancies observed in LY passing through the different types of GJC may not only due to ion selectivity of the channel [207] or due to size selectivity of the channel [216] but it might also be due to a gating mechanism

influenced by the pipette medium in which the tracer used. In other words, Li might act as an inhibitor of Cx37-S319 channels.

The sequence in Cx37 around the serine at position 319 implies that this residue may potentially be phosphorylated by various kinases. Interestingly, many studies have reported shifts in frequency histograms of unitary conductances for various Cx in response to serine phosphorylating/dephosphorylating treatments [87, 173, 177, 217-220]. Consequently, phosphorylation of serine319 might explain the differences in unitary conductances we observed for Cx37-S319 and Cx37-P319 channels (Chapter 1). A detailed NetPhos search resulted in the highest prediction strengths for cyclin dependent protein kinase 5 (cdk5) and glycogen synthase kinase 3 (GSK3). Li^+ and SB415286 have been described as inhibitors of GSK3 [221], a kinase that is endogenously active in most cells. Thus, we hypothesized that lithium might inhibit GSK3, which then results in reduced phosphorylation of the serine319 residue and modulation of the gating kinetics of Cx37 .We have then performed additional experiments on cell pairs using the whole double patch clamp technique with one pipette loaded with the F1 solution and LY-KCl and cells were incubated for one hour with 50 µM SB415286 (SB, Sigma). No transfer of LY was observed in Cx37-S319 or Cx37-P319 cell pairs (**Figure 17,** right panel). Macroscopic conductance was measured at the end of the experiments and not changed (0.7±0.16 nS, N=9) in Cx37-S319 cell pairs but increased in Cx37-P319 cell pairs (0.96±0.26 nS, N=6).

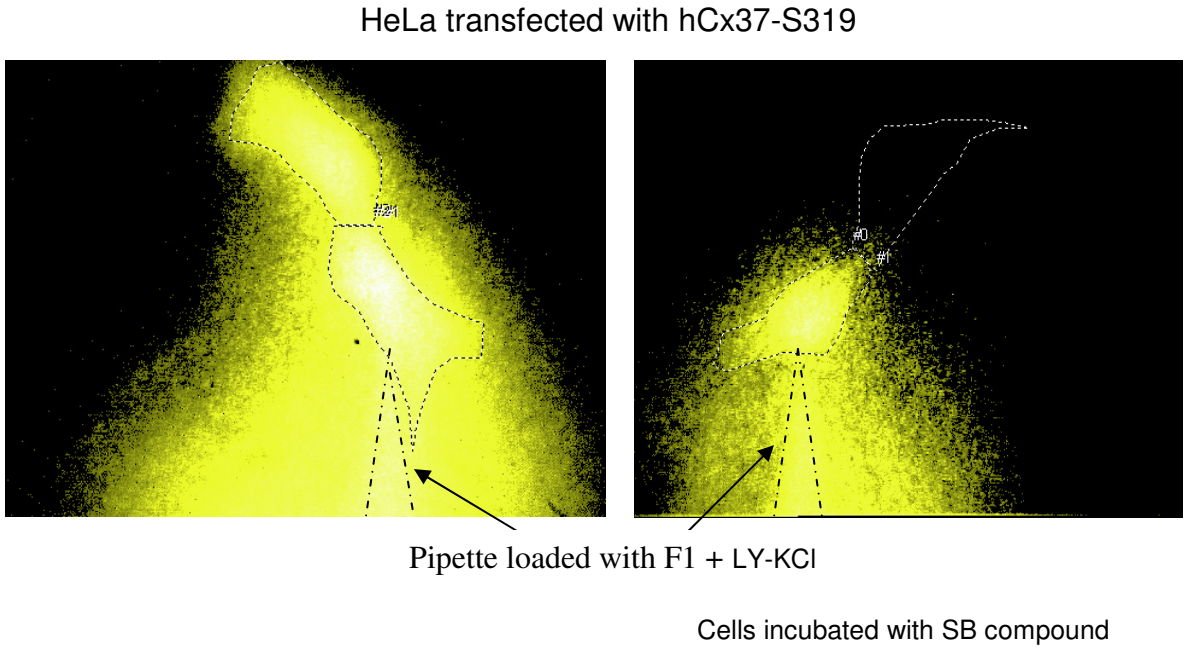

Figure 17

Figure 17: Images captured during whole double patch clamp performed on a cell pair (highlighted by the white dashed lines) in Cx37-S319 transfected HeLa cells. Right image, LY was passing through GJIC when LY-KCl pipette solution is used. Left image, LY was not passing through GJIC when LY-KCl + SB415286 pipette solution is used.

These preliminary experiments have led us to the following working hypothesis (**Figure 18, A and B**): Cx37-S319 is constitutively phosphorylated by GSK3, conditions that allow the passage of through GJ channels. When GSK3 is inhibited (phosphorylated) by Li^+ or SB415286, Cx37-S319 becomes progressively dephosphorylated resulting in a change in gating kinetics and reduced permeability for LY.

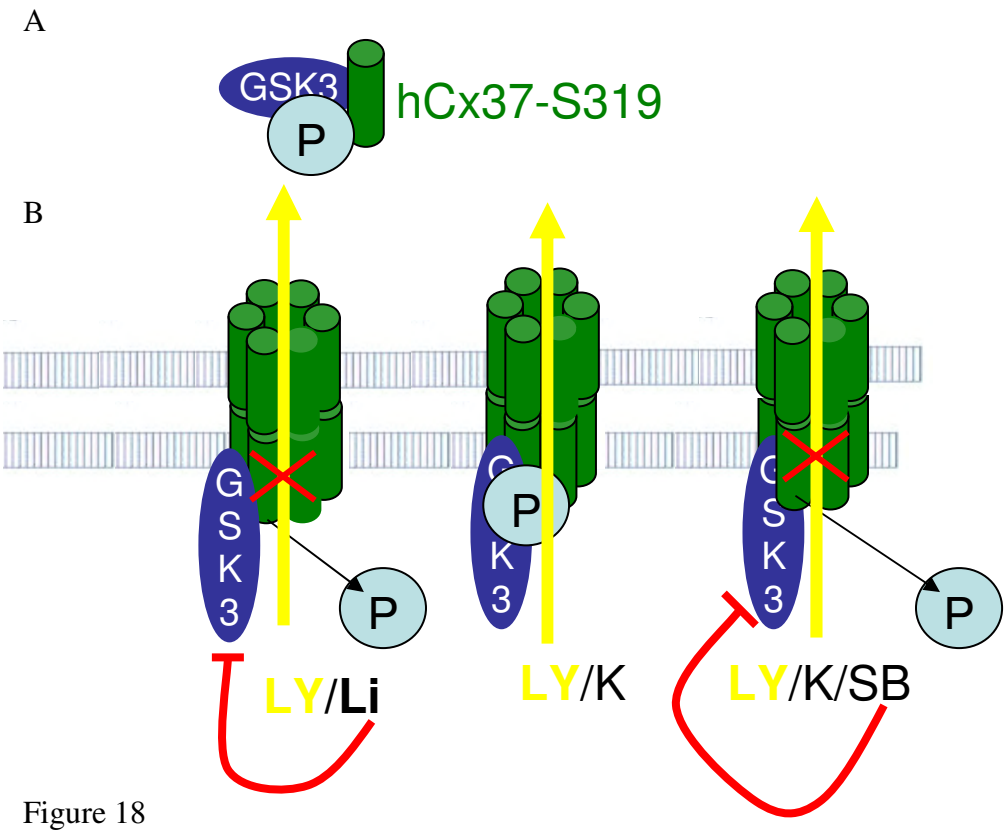

Figure 18

Figure 18: GSK3 hypothesis: Cx37-S319 is constitutively phosphorylated by GSK3 (A), thus allowing LY passage through GJIC; and when GSK3 is phosphorylated by its inhibitors as Li^+ or SB415286, Cx37-S319 is not phosphorylated anymore resulting in a change in full channel gating, which blocks the passage of LY (B).

Although this hypothesis is in agreement with the observed changes in LY transfer, the increased macroscopic conductance observed in Cx37-P319 cell pairs treated with SB415286 cannot be explained this way. Interestingly, the C-terminal tail of both Cx37-S319 and Cx37-P319 contain additional phosphorylation consensus sequences for GSK3. Beyond doubt, additional experiments might lead to a further refinement of the proposed hypothesis.

HeLa cell	F1 sol +	Mean conducatnce (nS)	SEM	N	LY through GJIC
CxP319	LY-KCl	0.54	0.103	10	no
CxS319	LY-KCl	0.66	0.107	11	yes
CxP319	LY-LiCl	1.13	0.367	5	no
CxS319	LY-LiCl	1.55	0.623	4	No
CxP319	LY-KCl + SB	0.96	0.264	6	No
CxS319	LY-KCl + SB	0.7	0.164	9	No

Table 3: Table resuming LY transfer using double patch technique in whole cell configuration on HeLa cell pairs transfected either with Cx37-S319 or with Cx37-P319 represented in first column. The second column indicates what was added to the F1 pipette solution. The third column represents the mean of conductance and its SEM calculated (fourth column) obtained at the end of each dye transfer (before-last column), after 5 minutes, a pulse protocol was done to avoid being in presence of cytoplasmic bridges and to assure us that dye transfer was due to GJIC (last column).

5.11 BIOPHYSICCAL PROPERTIES OF HUMAN POLYMORPHIC Cx37 HEMICHANNELS

Measuring electrical HC properties of Cx37-P319 or Cx37-S319 by patch clamp in low-calcium solution, we observed an induced voltage-sensitive current relaxing with time. As described in Chapter 1, the analysis resulted in a bell-shaped function $g_{SS}=f(V_m)$ (g_{SS}: normalized conductance at steady state, V_m: membrane potential) with a peak around -30mV, suggesting the involvement of two V_m-sensitive gating mechanisms, one operational at large negative voltage, the other at small negative and positive voltage. Our findings may at first sight seem partially in contrast with the work of Puljung et al. [157], who showed that hCx37 HCs closed at negative potentials and open in a time-dependent fashion at positive potentials; and that in absence of polyvalent cations, the channels were open at relatively negative potentials. But in fact the two studies are complementary. Puljung et al. [157] concentrated their

study on Ca^{2+} levels effects and polyvalent cations effects on the kinetics of the Cx37-P319. We concentrated our study on the differences between the two polymorphic HC using a similar low Ca^{2+} concentration (with 1 mM Mg^{2+}). In the presence of Ca^{2+}, we also found no current from negative potentials (-100 mV) up to +50 mV. In absence of Ca^{2+}, we could also open hemi-channels, thus measure current, at relatively negative potentials (-80 till -10mV). In both studies, we demonstrate voltage-dependence and Ca^{2+}-dependent HC properties. Moreover, the difference in single channel conductance for Cx37-P319 (370 pS towards 300 pS measured) between our studies may be explained by the difference in CsCl concentration used in the pipette solution and possibly also by the different cell types used (oocytes vs HeLa cells). We obtained approximately the same single channel conductance (~300 pS) than Ramanan et al. [222, 223] for Cx37-P319. The single channel conductance of Cx37-S319 was also not measured in this study.

In addition, we also observed a voltage-dependent two gating process suggesting that HCs have their own gating mechanism that is independent from a full GJC. At the top of the Boltzmann curves, we observed a step between the two Boltzmann fitted curves (**Figure 19A,** right panel), indicating that maximum conductance for each half curve has not been reached. It seems thus that the internal and external parts of the HCs possess their own gating, which are also different between Cx37-P319 and Cx37-S319 HC. This is a surprising and new concept knowing that the external part plays no role in the gating process in a full GJC. A hypothesis could be that the C-terminal loop acting at the cytoplasmic site would act as a gate and the tunnel part (transmembrane part and extracellular part) could act as a diaphragm. Based on these suppositions, the following possible scenario could eventually match if we play the Boltzmann curve through time as through voltage (**Figure 19A**, left panel with four bars numbered time 1 to time 4), corresponding to the four images in **Figure 19B.** Image 1: C-terminal tails are turned-in, obstructing the HC, thus impeaching conductance; image 2:

maximum conductance peak, all C-terminal tails are not blocking the entrance of the HC; image 3: the tunnel formed by the 6 connexin start to close as a diaphragm thus reducing the conductance to 0 as illustrated in image 4.

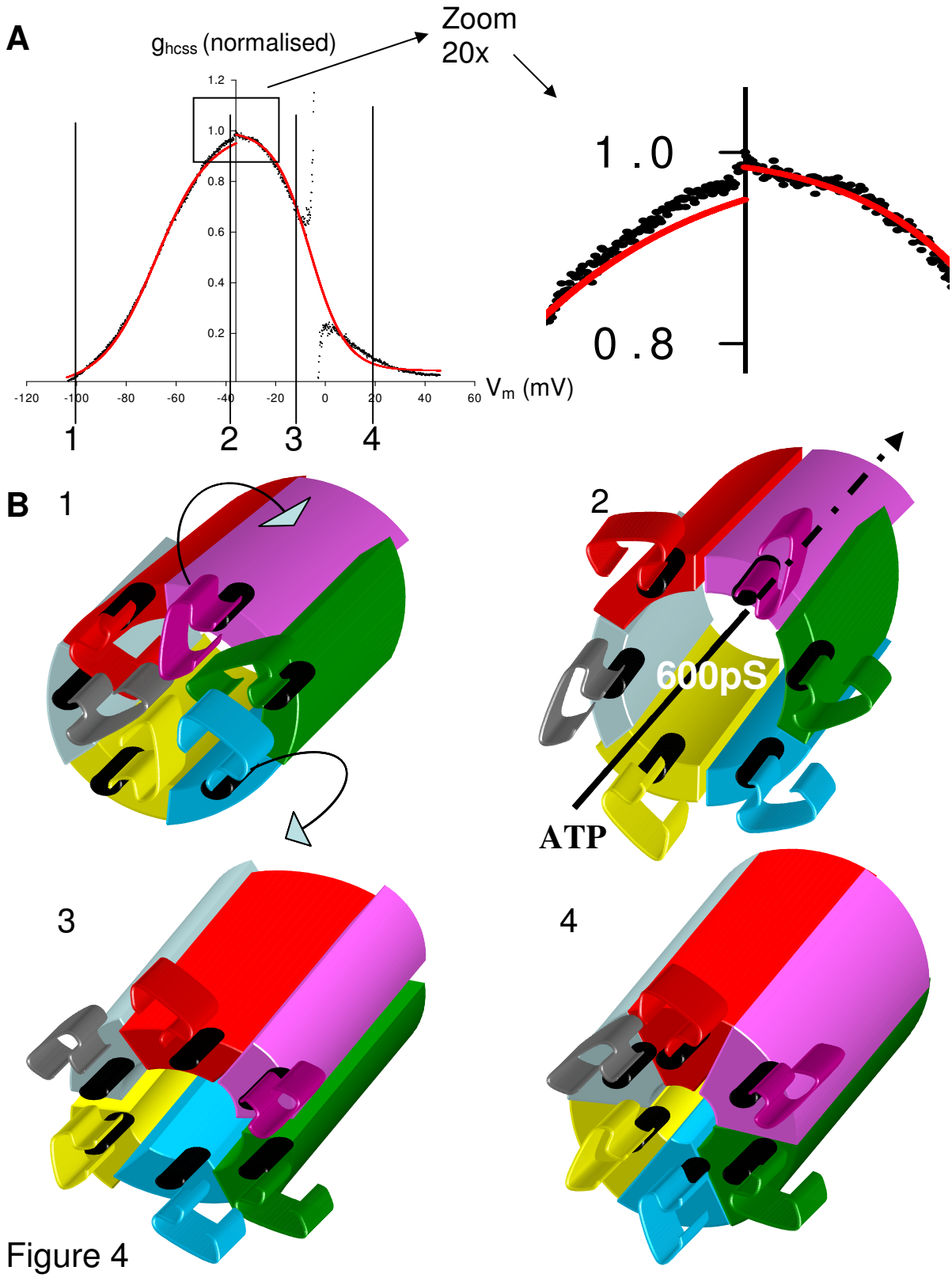

Figure 4

Figure 19: A) left panel is a reproduction of the Boltzmann curve from figure 4 chapter 1 (P319). Right panel represents a zoom (20 times) of the hedge of the peak conductance of the Boltzmann curve. B) Images representing an HC state at the four bars in the normalized conductance versus voltage, Boltzmann curve. The 3-dimension tunnel represents the transmembrane domain form by the Cx37 connexon, the hook represents the C-terminal tail of the connexin 37 (thus 6 hooks in a connexon). Image 1: the C-terminus tails are obstructing the entrance of the HC. Image 2: no obstruction of the C-terminus tails, maximum of conductance. Image 3: the tunnel starts to close a diaphragm till no ion could go through, therefore, no more conductance.

This last hypothesis gives a major role to functional HCs. As discussed in the review of Spray et al.[224], we need an open mind/view to explore the HC expectations as an independent function of full channels. The same protein might serve two different applications; full channels for cell-to-cell communication and HC for autocrine regulation.

5.12 FUNCTIONAL PROPERTIES OF HUMAN POLYMORPHIC Cx37 HEMICHANNELS

As also described in Chapter 1, we observed that the main unitary channel conductance in Cx37-P319 cell pairs (~300pS) was 1.5x increased compared to the one in Cx37-S319 cell pairs (~200pS). In addition we found that Cx37-P319 expressing HeLa cells were less adhesive and secreted more ATP than the Cx37-S319 cells. We hypothesized that the differences observed in the biophysical properties between polymorphic HC may be responsible for the inequality in ATP release between Cx37-S319 or Cx37-P319, which results in differential cell adhesion [47]. Over the last several years, evidence has shown that hemichannels do exhibit short-lasting openings resulting in controlled release of cytosolic compounds such as ATP. The primary evidence for efflux of ATP through hemichannels has been that exogenous expression of either Cx26, Cx32, or Cx43 by Cx-deficient cell lines, including C6, N2A, and HeLa cells, leads to a marked increase in ATP release and uptake of fluorescent indicators (<1 kDa) [150]. The notion that hemichannels can mediate ATP release has

been further supported thereafter [61, 225-228] and extended to efflux of other transmitters, including glutamate [229]. Nevertheless, the evidence linking ATP efflux to hemichannels is indirect. Moreover, alternative ATP release pathways do exist, including volume-sensitive channels [230] and P2 receptors-gated channels [231] as well as exocytosis of vesicular ATP [232]. Thus, the possibility exists that Cx expression modulates other release pathways and that exogenous expression of Cx indirectly enhances ATP release. Recently, Wang and colleagues from Gent University have shown ATP release in reponse to increase of intracellular calcium concentration that was independent of P2 receptors (presentation at the French GJ Conference in Poitiers, July 2008; entitled: Mechanism of high intracellular calcium induced suppression of Cx43 hemichannel responses). Little information is available on the relation between Cx37 HC and ATP release. Haussig et al. [233] did an interesting study relating NO and ATP release in HUVECs. Unfortunately, their results could not be attributed to a specific Cx HC because HUVECs express multiple connexins. Liu et al. [164] evaluated the pathways contributing to ATP release from mouse astrocytes during hypo-osmotic stress. They examined the expression of mRNAs for proteins constituting possible ATP-releasing pathways that have been suggested over the past several years such as connexins (Cx32, Cx37, Cx43), pannexin 1 (Px1), the P2X7 receptor, MRP1 and MDR1, but not CFTR by RT-PCR and propose that the maxi-anion (HC) channel constitutes a major pathway for swelling-induced ATP release from cultured mouse astrocytes as well. Again, it is not a direct answer towards Cx37 and ATP release but a contribution of it existence. Finally, the fact that no ligand-gated P2X channels were found in HeLa cells and that activation of P2Y purinergic receptor inhibits the activity of the Na+/K+-ATPase in HeLa cells [234] further supports our hypothesis ATP release and autocrine mechanism via Cx37 HC.

Within the similarity of the data obtained between the Cx43 HC autocrine regulation and what we observed in Chapter 1 with Cx37 HC, we can hypothesize that Cx37 and Cx43 C-terminal tails, may share more similar mechanisms of regulation.

5.13 HUMAN Cx37 CHANNEL AND PROTEIN INTERACTIONS (eNOS)

Most connexins (Cx31, Cx32, Cx37, Cx40, Cx43, Cx46, Cx50 and Cx56) have been shown to be phospho-proteins. Many connexins not only contain protein kinase consensus sequences, but have also been shown to be phosphorylated in the C-terminal region.

In this context, it is interesting to compare the similarities and differences described by Shibayama et al. [166] with their patch-clamp studies revealing that the peptide RXP-E partially prevented octanol-induced and acidification-induced uncoupling in Cx43-expressing cells with our studies with the eNOS-like peptide (containing RXP motifs) on Cx37 channels. RXP-E increased mean open time of Cx43 channels. As described in Chapter 2, we observed a shift in unitary conductance frequency histograms of Cx37. The shift in unitary conductance observed after the exposure to eNOS-like peptides might be induced by phosphorylation. Indeed, such frequency shifts have been observed before for Cx43 in response to cGMP and phorbol ester-dependent phosphorylation of serine residues [21, 22] for Cx45 and Cx26 in response to phorbol ester [23] and for Cx40 in response to protein kinase C (PKC) and PKA [24, 25]. Interestingly, Haussig et al. [42] demonstrated a failure in functional endothelial intercellular communication by sub-chronic nicotine exposure. HUVECs grown under nicotine exposure significantly reduced NO formation after ATP stimulation, thereby relating ATP and NO. Furthermore, they related the difference in NO-signal-propagation to GJIC by abolishing it with the gap junction blocker Na-propionate (inhibits Cx37 as well as Cx43). It would be interesting to investigate how our studies on ATP release through Cx37 HC (Chapter 1) and eNOS binding to Cx37 regulates the function of the enzyme (Chapter 2) relate to the

observations of Haussig et al. [42]. With respect to the possible pathophysiological relevance, every molecule that induces endothelial dysfunction may contribute to a decrease in Cx37-mediated endothelial GJIC and more NO release. This may open new horizons for physiology and possible pharmacological therapeutic approaches.

5.14 HIGH THROUGH PUT DATA AND Cx37 KO IN ADVANCED ATHEROSCLEROSIS

Micro-array assays are a powerful molecular technology that allows the simultaneous study of the expression of thousands of genes (i.e. their RNA products), giving an accurate picture of gene expression in the cell or the sample at the time of the study. A major unresolved problem in the post-genomic area is to assemble the large amounts of data generated into a meaningful biological context [235]. Many have developed comprehensive software tools for deriving biological insights from analysis of high through put (HTP) data. However, one of the limitations of these tools is the inability to handle multiple datasets simultaneously in an intuitive and up-to-date way. For example, in the tool that we used (IPA 6.0 program), Cx37 was not considered as a gene linked to atherosclerosis. There is a need for more flexible, interactive and comprehensive HTP data analysis software tools in the public domain that are accessible to the academic community and could provide a suite of utilities to analyze HTP data in biological contexts, such as corrected pathways. To facilitate the simultaneous analysis and comparison of multiple HTP experiments in the context of biological pathways and association networks, and allows pattern extraction of a selected gene list with biological themes, the programs should be more interactive and should propose more alternatives when suggestions are added. Nevertheless, to carry out the analysis of micro-arrays obtained in Chapter 3, we took advantage of the existing Ingenuity's Pathway Analysis

software which greatly helped us to reveal the gene pathways in an unbiased manner, some of which we confirmed then at a protein level.

In conclusion, the studies on the role of Cx37, and its human polymorphism, in atherosclerosis have revealed important insight mechanisms in mouse and in human through the different stages of the disease. Apart from the gain of knowledge on the pathogenesis of atherosclerosis related to Cx37, indeed, obtaining detailed mechanisms on how the Cx37 gene polymorphism affects the development of atherosclerosis opened our mind for different horizons in other diseases. This may lead to the use of this genetic variation in clinical risk assessment, and possibly the use of targeting molecules (i.e. molecules that would improve endothelium healing by up-regulating Cx37) before or during intervention in the case of cardiology but also for other therapeutics involved in other diseases.

6 ACKNOWLEDGEMENTS

I would like first to thank my former supervisors, whose scientific knowledge, insights and personalities have been a guideline and a source of inspiration for the work described in this PhD thesis. I am particularly grateful to Prof. Robert Weingart, at the Physiology Institute in Bern, for his trust and for giving me the opportunity to improve my skills in electrophysiology, in patch clamp techniques and to acquire the reflection needed to transpose knowledge into different disciplines, therefore supporting and encouraging me "to take my own rode". I am particularly grateful to Prof. Brenda Kwak, whom six years ago gave me the opportunity to start in the field of connexin for a Master degree and let me continue with this very interesting PhD project on the Cx37 human polymorphism. Her scientific knowledge and its application have been a guideline, inspiration and example for the work described in this PhD thesis. A special sentence I will remember from you Brenda: "…for you it is not the same! It is better like this…"

Thanks to Dr. Marc Chanson for his input all along these six years and for his time (the many scientific brainstormings we had) and for giving his trust and full time access to his patch clamp setup for the micro-injections.

A big thank you for the people of the lab I have crossed: Dr. Christos Chadjichristos, for his encouragements, help and motivation through hard times, for his scientific lessons (on the bench) and for giving me the opportunity to participate to his work; Isabelle Roth, whom gave a precious help (transmitting me her knowledge in WB and in animal surgery) all along these six years and with whom everything became possible; Thomas Desplantez for his patience, his patch clamp lessons and the scientific interactions we had in Bern; Esther Sutter for teaching me her knowledge and tricks in what she knows best: immunology staining; Hamdy Shaban for helping to prove my final hypothesis; Flore Mulhaupt for her three month time where she thought me the cell culturing art; Bernard Foglia for his many punctual helps on the bench; Sandrine Morel for taking on the work on Cx37 and Li+, for her precious help

during this last thesis year, for her scientific input and for supporting me in her office; Anne Brisset for the scientific discussions we had while I was writing my written thesis exam; and Laurent Burnier for helping me with his inputs for the world program he just understood (joke) because he went through just a few month ago.

Also a big thank you to François Mach, for his time, his trust and his will in giving me the opportunity to share these six years in the unity of cardiology, internal medicine, in his big and efficient cardiology scientific research group. I will remember his talks (specially the one in Toulouse, France, that was an example) and his humanity and generosity. Thank you to Vincent Braunersreuters, for his friendship.

A big thank to André Kleber for his trust, his financial help and for giving me, each time an abstract was accepted, the opportunity to present it via his travel grants.

A big thank you to Werner Schlegel and Dominic Belin whom were kind to support me during crisis time and for their scientific input and discussions we had.

The work described in this thesis benefit from fruitful collaborations with Thomas Desplantez (Bern), Robert Weingart (Bern), Hamdy Shaban (Bern), Mario Delmar (USA), Anna Pfeniger (Geneva and USA), Christophe Montésuit (Geneva), François Mach (Geneva), Grazziano Pelli, Dominic Wohlwend (Geneva FACS man), Tecla Dudez and Ludivic Wisniewski (Geneva). I warmly thank them.

Finally, I am indebted to Eloïse for her support and understanding and to Yann for the new sunlight he has brought home these last 8 month.

This PhD thesis work has been financially supported by the “Fondation pour la Recherche Médicale” and his President, Prof. Werner Schlegel and by the Swiss Cardiovascular Research and Training Network and his President, Prof André Kleber.

7 REFERENCES

1. Glass CK, Witztum JL. Atherosclerosis. the road ahead. *Cell.* Feb 23 2001;104(4):503-516.

2. Libby P. Changing concepts of atherogenesis. *J Intern Med.* Mar 2000;247(3):349-358.

3. Zhao SZ, Xu XY, Hughes AD, et al. Blood flow and vessel mechanics in a physiologically realistic model of a human carotid arterial bifurcation. *J Biomech.* Aug 2000;33(8):975-984.

4. Collins T. *Robbins Pathologic basis of disease.* 6th edition ed. ed; 1999.

5. Murray CJ, Lopez AD. Alternative projections of mortality and disability by cause 1990-2020: Global Burden of Disease Study. *Lancet.* May 24 1997;349(9064):1498-1504.

6. Moreno PR, Falk E, Palacios IF, et al. Macrophage infiltration in acute coronary syndromes. Implications for plaque rupture. *Circulation.* Aug 1994;90(2):775-778.

7. Wick G, Schett G, Amberger A, et al. Is atherosclerosis an immunologically mediated disease? *Immunol Today.* Jan 1995;16(1):27-33.

8. Ross R. Atherosclerosis--an inflammatory disease. *N Engl J Med.* Jan 14 1999;340(2):115-126.

9. Schroeder AP, Falk E. Vulnerable and dangerous coronary plaques. *Atherosclerosis.* Dec 1995;118 Suppl:S141-149.

10. Cottet J, Lenoir M. [Two thousand years of historical study on the words atheroma, atheromatosis, atherosclerosis, arteriosclerosis]. *Bull Acad Natl Med.* Dec 1992;176(9):1385-1390; discussion 1390-1381.

11. Mazzone A, Venneri L, Berti S. Aortic valve stenosis and coronary artery disease: pathophysiological and clinical links. *J Cardiovasc Med (Hagerstown).* Dec 2007;8(12):983-989.

12. Naghavi M, Libby P, Falk E, et al. From vulnerable plaque to vulnerable patient: a call for new definitions and risk assessment strategies: Part I. *Circulation.* Oct 7 2003;108(14):1664-1672.

13. Mazzini MJ, Schulze PC. Proatherogenic pathways leading to vascular calcification. *Eur J Radiol.* Mar 2006;57(3):384-389.

14. Yutani C. [Pathology of coronary arterial calcification]. *Clin Calcium.* Mar 2007;17(3):332-337.

15. Newman AB, Naydeck BL, Sutton-Tyrrell K, et al. Relationship between coronary artery calcification and other measures of subclinical cardiovascular disease in older adults. *Arterioscler Thromb Vasc Biol.* Oct 1 2002;22(10):1674-1679.

16. Falk E. [Plaque vulnerability and disruption]. *Rev Clin Esp.* Dec 1996;196(4 Monografico):6-12.

17. Libby P. Inflammation in atherosclerosis. *Nature.* Dec 19-26 2002;420(6917):868-874.
18. Sarig S, Utian WH, Sheean LA, et al. Distribution of unesterified cholesterol-containing particles in human atherosclerotic lesions. *Am J Pathol.* Jan 1995;146(1):139-147.
19. Lundberg B. Chemical composition and physical state of lipid deposits in atherosclerosis. *Atherosclerosis.* Jul 1985;56(1):93-110.
20. Friedman M. The coronary thrombus: its origin and fate. *Hum Pathol.* Mar 1971;2(1):81-128.
21. Loree HM, Kamm RD, Stringfellow RG, et al. Effects of fibrous cap thickness on peak circumferential stress in model atherosclerotic vessels. *Circ Res.* Oct 1992;71(4):850-858.
22. Richardson PD, Davies MJ, Born GV. Influence of plaque configuration and stress distribution on fissuring of coronary atherosclerotic plaques. *Lancet.* Oct 21 1989;2(8669):941-944.
23. Davies MJ, Richardson PD, Woolf N, et al. Risk of thrombosis in human atherosclerotic plaques: role of extracellular lipid, macrophage, and smooth muscle cell content. *Br Heart J.* May 1993;69(5):377-381.
24. Burleigh MC, Briggs AD, Lendon CL, et al. Collagen types I and III, collagen content, GAGs and mechanical strength of human atherosclerotic plaque caps: span-wise variations. *Atherosclerosis.* Sep 1992;96(1):71-81.
25. Geng YJ, Libby P. Evidence for apoptosis in advanced human atheroma. Colocalization with interleukin-1 beta-converting enzyme. *Am J Pathol.* Aug 1995;147(2):251-266.
26. Falk E. Plaque rupture with severe pre-existing stenosis precipitating coronary thrombosis. Characteristics of coronary atherosclerotic plaques underlying fatal occlusive thrombi. *Br Heart J.* Aug 1983;50(2):127-134.
27. van der Wal AC, Becker AE, van der Loos CM, et al. Site of intimal rupture or erosion of thrombosed coronary atherosclerotic plaques is characterized by an inflammatory process irrespective of the dominant plaque morphology. *Circulation.* Jan 1994;89(1):36-44.
28. Newby AC. Matrix metalloproteinases regulate migration, proliferation, and death of vascular smooth muscle cells by degrading matrix and non-matrix substrates. *Cardiovasc Res.* Feb 15 2006;69(3):614-624.
29. Libby P. Molecular bases of the acute coronary syndromes. *Circulation.* Jun 1 1995;91(11):2844-2850.
30. Hansson GK, Libby P. The immune response in atherosclerosis: a double-edged sword. *Nat Rev Immunol.* Jul 2006;6(7):508-519.
31. Mach F. Inflammation is a crucial feature of atherosclerosis and a potential target to reduce cardiovascular events. *Handb Exp Pharmacol.* 2005(170):697-722.
32. Gabbiani G. Control of smooth muscle cell activation. *Arterioscler Thromb Vasc Biol.* May 2004;24(5):804-805.

33. Ku DN, Giddens DP, Zarins CK, et al. Pulsatile flow and atherosclerosis in the human carotid bifurcation. Positive correlation between plaque location and low oscillating shear stress. *Arteriosclerosis.* May-Jun 1985;5(3):293-302.
34. Davies PF. Endothelial mechanisms of flow-mediated athero-protection and susceptibility. *Circ Res.* Jul 6 2007;101(1):10-12.
35. McGill HC, Jr., McMahan CA, Herderick EE, et al. Origin of atherosclerosis in childhood and adolescence. *Am J Clin Nutr.* Nov 2000;72(5 Suppl):1307S-1315S.
36. Mehta JL. The role of LOX-1, a novel lectin-like receptor for oxidized low density lipoprotein, in atherosclerosis. *Can J Cardiol.* Aug 2004;20 Suppl B:32B-36B.
37. Ohashi R, Mu H, Yao Q, et al. Cellular and molecular mechanisms of atherosclerosis with mouse models. *Trends Cardiovasc Med.* Jul 2004;14(5):187-190.
38. Kurosawa T, Kusanagi M, Yamasaki Y, et al. New mutant rabbit strain with hypercholesterolemia and atherosclerotic lesions produced by serial inbreeding. *Lab Anim Sci.* Aug 1995;45(4):385-392.
39. Bochaton-Piallat ML, Gabbiani G. Modulation of smooth muscle cell proliferation and migration: role of smooth muscle cell heterogeneity. *Handb Exp Pharmacol.* 2005(170):645-663.
40. Moghadasian M. Experimental atherosclerosis, A historical overview. *Life Sciences.* 2002;70:855-865.
41. Tangirala RK, Rubin EM, Palinski W. Quantitation of atherosclerosis in murine models: correlation between lesions in the aortic origin and in the entire aorta, and differences in the extent of lesions between sexes in LDL receptor-deficient and apolipoprotein E-deficient mice. *J Lipid Res.* Nov 1995;36(11):2320-2328.
42. Nakashima Y, Plump AS, Raines EW, et al. ApoE-deficient mice develop lesions of all phases of atherosclerosis throughout the arterial tree. *Arterioscler Thromb.* Jan 1994;14(1):133-140.
43. Reddick RL, Zhang SH, Maeda N. Atherosclerosis in mice lacking apo E. Evaluation of lesional development and progression. *Arterioscler Thromb.* Jan 1994;14(1):141-147.
44. Ishibashi S, Goldstein JL, Brown MS, et al. Massive xanthomatosis and atherosclerosis in cholesterol-fed low density lipoprotein receptor-negative mice. *J Clin Invest.* May 1994;93(5):1885-1893.
45. Rosenfeld ME, Polinsky P, Virmani R, et al. Advanced atherosclerotic lesions in the innominate artery of the ApoE knockout mouse. *Arterioscler Thromb Vasc Biol.* Dec 2000;20(12):2587-2592.
46. Johnson JL, Jackson CL. Atherosclerotic plaque rupture in the apolipoprotein E knockout mouse. *Atherosclerosis.* Feb 1 2001;154(2):399-406.

47. Wong CW, Christen T, Roth I, et al. Connexin37 protects against atherosclerosis by regulating monocyte adhesion. *Nat Med.* Aug 2006;12(8):950-954.
48. Cruciani V, Mikalsen SO. The vertebrate connexin family. *Cell Mol Life Sci.* May 2006;63(10):1125-1140.
49. Simon AM, Goodenough DA. Diverse functions of vertebrate gap junctions. *Trends Cell Biol.* Dec 1998;8(12):477-483.
50. Saitou N, Nei M. The neighbor-joining method: a new method for reconstructing phylogenetic trees. *Mol Biol Evol.* Jul 1987;4(4):406-425.
51. Bruzzone R. Learning the language of cell-cell communication through connexin channels. *Genome Biol.* 2001;2(11):REPORTS4027.
52. Sohl G, Willecke K. Gap junctions and the connexin protein family. *Cardiovasc Res.* May 1 2004;62(2):228-232.
53. Milks LC, Kumar NM, Houghten R, et al. Topology of the 32-kd liver gap junction protein determined by site-directed antibody localizations. *Embo J.* Oct 1988;7(10):2967-2975.
54. Yeager M, Gilula NB. Membrane topology and quaternary structure of cardiac gap junction ion channels. *J Mol Biol.* Feb 20 1992;223(4):929-948.
55. Kumar NM, Gilula NB. The gap junction communication channel. *Cell.* Feb 9 1996;84(3):381-388.
56. Unger VM, Kumar NM, Gilula NB, et al. Three-dimensional structure of a recombinant gap junction membrane channel. *Science.* Feb 19 1999;283(5405):1176-1180.
57. Ahmad S, Diez JA, George CH, et al. Synthesis and assembly of connexins in vitro into homomeric and heteromeric functional gap junction hemichannels. *Biochem J.* Apr 15 1999;339 (Pt 2):247-253.
58. Ahmad S, Evans WH. Post-translational integration and oligomerization of connexin 26 in plasma membranes and evidence of formation of membrane pores: implications for the assembly of gap junctions. *Biochem J.* Aug 1 2002;365(Pt 3):693-699.
59. Brink PR, Ricotta J, Christ GJ. Biophysical characteristics of gap junctions in vascular wall cells: implications for vascular biology and disease. *Braz J Med Biol Res.* Apr 2000;33(4):415-422.
60. White TW, Paul DL. Genetic diseases and gene knockouts reveal diverse connexin functions. *Annu Rev Physiol.* 1999;61:283-310.
61. Saez JC, Berthoud VM, Branes MC, et al. Plasma membrane channels formed by connexins: their regulation and functions. *Physiol Rev.* Oct 2003;83(4):1359-1400.
62. Chanson M, Derouette JP, Roth I, et al. Gap junctional communication in tissue inflammation and repair. *Biochim Biophys Acta.* Jun 10 2005;1711(2):197-207.

63. Kleber AG. Crosstalk between theoretical and experimental studies for the understanding of cardiac electrical impulse propagation. *J Electrocardiol.* Nov-Dec 2007;40(6 Suppl):S136-141.
64. Niggli E, Kleber A, Weingart R. Founder of cardiac cellular electrophysiology: honouring Silvio Weidmann, 7 April 1921- 11 July 2005. *J Physiol.* Feb 1 2006;570(Pt 3):431-432.
65. Meier C, Dermietzel R. Electrical synapses--gap junctions in the brain. *Results Probl Cell Differ.* 2006;43:99-128.
66. Wagner C. Function of connexins in the renal circulation. *Kidney Int.* Mar 2008;73(5):547-555.
67. Zhang YW, Kaneda M, Morita I. The gap junction-independent tumor-suppressing effect of connexin 43. *J Biol Chem.* Nov 7 2003;278(45):44852-44856.
68. Yamasaki H, Omori Y, Zaidan-Dagli ML, et al. Genetic and epigenetic changes of intercellular communication genes during multistage carcinogenesis. *Cancer Detect Prev.* 1999;23(4):273-279.
69. Yano T, Fujimoto E, Hagiwara H, et al. Connexin 32 as an anti-invasive and anti-metastatic gene in renal cell carcinoma. *Biol Pharm Bull.* Oct 2006;29(10):1991-1994.
70. Giepmans BN. Gap junctions and connexin-interacting proteins. *Cardiovasc Res.* May 1 2004;62(2):233-245.
71. Herve JC, Bourmeyster N, Sarrouilhe D, et al. Gap junctional complexes: from partners to functions. *Prog Biophys Mol Biol.* May-Jun 2007;94(1-2):29-65.
72. Harris AL. Emerging issues of connexin channels: biophysics fills the gap. *Q Rev Biophys.* Aug 2001;34(3):325-472.
73. Peracchia C, Sotkis A, Wang XG, et al. Calmodulin directly gates gap junction channels. *J Biol Chem.* Aug 25 2000;275(34):26220-26224.
74. Zhang X, Qi Y. Role of intramolecular interaction in connexin50: mediating the Ca2+-dependent binding of calmodulin to gap junction. *Arch Biochem Biophys.* Aug 15 2005;440(2):111-117.
75. Nusrat A, Chen JA, Foley CS, et al. The coiled-coil domain of occludin can act to organize structural and functional elements of the epithelial tight junction. *J Biol Chem.* Sep 22 2000;275(38):29816-29822.
76. Gonzalez-Mariscal L, Betanzos A, Nava P, et al. Tight junction proteins. *Prog Biophys Mol Biol.* Jan 2003;81(1):1-44.
77. Wu JC, Tsai RY, Chung TH. Role of catenins in the development of gap junctions in rat cardiomyocytes. *J Cell Biochem.* Mar 1 2003;88(4):823-835.
78. Giepmans BN, Feiken E, Gebbink MF, et al. Association of connexin43 with a receptor protein tyrosine phosphatase. *Cell Commun Adhes.* Jul-Dec 2003;10(4-6):201-205.

79. Yu XS, Yin X, Lafer EM, et al. Developmental regulation of the direct interaction between the intracellular loop of connexin 45.6 and the C terminus of major intrinsic protein (aquaporin-0). *J Biol Chem.* Jun 10 2005;280(23):22081-22090.

80. Herve JC, Plaisance I, Loncarek J, et al. Is the junctional uncoupling elicited in rat ventricular myocytes by some dephosphorylation treatments due to changes in the phosphorylation status of Cx43? *Eur Biophys J.* May 2004;33(3):201-210.

81. Solan JL, Lampe PD. Connexin phosphorylation as a regulatory event linked to gap junction channel assembly. *Biochim Biophys Acta.* Jun 10 2005;1711(2):154-163.

82. Yamane Y, Shiga H, Asou H, et al. Dynamics of astrocyte adhesion as analyzed by a combination of atomic force microscopy and immuno-cytochemistry: the involvement of actin filaments and connexin 43 in the early stage of adhesion. *Arch Histol Cytol.* Oct 1999;62(4):355-361.

83. Lin D, Zhou J, Zelenka PS, et al. Protein kinase Cgamma regulation of gap junction activity through caveolin-1-containing lipid rafts. *Invest Ophthalmol Vis Sci.* Dec 2003;44(12):5259-5268.

84. Leithe E, Rivedal E. Ubiquitination and down-regulation of gap junction protein connexin-43 in response to 12-O-tetradecanoylphorbol 13-acetate treatment. *J Biol Chem.* Nov 26 2004;279(48):50089-50096.

85. Morley GE, Ek-Vitorin JF, Taffet SM, et al. Structure of connexin43 and its regulation by pHi. *J Cardiovasc Electrophysiol.* Aug 1997;8(8):939-951.

86. Firek L, Weingart R. Modification of gap junction conductance by divalent cations and protons in neonatal rat heart cells. *J Mol Cell Cardiol.* Aug 1995;27(8):1633-1643.

87. Kwak BR, Jongsma HJ. Regulation of cardiac gap junction channel permeability and conductance by several phosphorylating conditions. *Mol Cell Biochem.* Apr 12-26 1996;157(1-2):93-99.

88. Beauchamp P, Choby C, Desplantez T, et al. Electrical propagation in synthetic ventricular myocyte strands from germline connexin43 knockout mice. *Circ Res.* Jul 23 2004;95(2):170-178.

89. Heyman NS, Burt JM. Hindered diffusion through an aqueous pore describes invariant dye selectivity of Cx43 junctions. *Biophys J.* Feb 1 2008;94(3):840-854.

90. Dudez T, Borot F, Huang S, et al. CFTR in a lipid raft-TNFR1 complex modulates gap junctional intercellular communication and IL-8 secretion. *Biochim Biophys Acta.* May 2008;1783(5):779-788.

91. Rackauskas M, Kreuzberg MM, Pranevicius M, et al. Gating properties of heterotypic gap junction channels formed of connexins 40, 43, and 45. *Biophys J.* Mar 15 2007;92(6):1952-1965.

92. Martinez AD, Saez JC. Arachidonic acid-induced dye uncoupling in rat cortical astrocytes is mediated by arachidonic acid byproducts. *Brain Res.* Jan 23 1999;816(2):411-423.
93. Willecke K, Kirchhoff S, Plum A, et al. Biological functions of connexin genes revealed by human genetic defects, dominant negative approaches and targeted deletions in the mouse. *Novartis Found Symp.* 1999;219:76-88; discussion 88-96.
94. Severs NJ, Rothery S, Dupont E, et al. Immunocytochemical analysis of connexin expression in the healthy and diseased cardiovascular system. *Microsc Res Tech.* Feb 1 2001;52(3):301-322.
95. Wong CW, Christen T, Kwak BR. Connexins in leukocytes: shuttling messages? *Cardiovasc Res.* May 1 2004;62(2):357-367.
96. van Kempen MJ, Jongsma HJ. Distribution of connexin37, connexin40 and connexin43 in the aorta and coronary artery of several mammals. *Histochem Cell Biol.* Dec 1999;112(6):479-486.
97. Blackburn JP, Connat JL, Severs NJ, et al. Connexin43 gap junction levels during development of the thoracic aorta are temporally correlated with elastic laminae deposition and increased blood pressure. *Cell Biol Int.* Feb 1997;21(2):87-97.
98. Hong T, Hill CE. Restricted expression of the gap junctional protein connexin 43 in the arterial system of the rat. *J Anat.* May 1998;192 (Pt 4):583-593.
99. Gabriels JE, Paul DL. Connexin43 is highly localized to sites of disturbed flow in rat aortic endothelium but connexin37 and connexin40 are more uniformly distributed. *Circ Res.* Sep 21 1998;83(6):636-643.
100. Yeh HI, Dupont E, Coppen S, et al. Gap junction localization and connexin expression in cytochemically identified endothelial cells of arterial tissue. *J Histochem Cytochem.* Apr 1997;45(4):539-550.
101. Little TL, Beyer EC, Duling BR. Connexin 43 and connexin 40 gap junctional proteins are present in arteriolar smooth muscle and endothelium in vivo. *Am J Physiol.* Feb 1995;268(2 Pt 2):H729-739.
102. Chadjichristos CE, Derouette JP, Kwak BR. Connexins in atherosclerosis. *Adv Cardiol.* 2006;42:255-267.
103. Haefliger JA, Nicod P, Meda P. Contribution of connexins to the function of the vascular wall. *Cardiovasc Res.* May 1 2004;62(2):345-356.
104. Figueroa XF, Isakson BE, Duling BR. Connexins: gaps in our knowledge of vascular function. *Physiology (Bethesda).* Oct 2004;19:277-284.
105. de Wit C, Roos F, Bolz SS, et al. Impaired conduction of vasodilation along arterioles in connexin40-deficient mice. *Circ Res.* Mar 31 2000;86(6):649-655.
106. Liao Y, Day KH, Damon DN, et al. Endothelial cell-specific knockout of connexin 43 causes hypotension and bradycardia in mice. *Proc Natl Acad Sci U S A.* Aug 14 2001;98(17):9989-9994.

107. Theis M, de Wit C, Schlaeger TM, et al. Endothelium-specific replacement of the connexin43 coding region by a lacZ reporter gene. *Genesis.* Jan 2001;29(1):1-13.
108. Simon AM, Goodenough DA, Li E, et al. Female infertility in mice lacking connexin 37. *Nature.* Feb 6 1997;385(6616):525-529.
109. van Veen TA, van Rijen HV, Jongsma HJ. Physiology of cardiovascular gap junctions. *Adv Cardiol.* 2006;42:18-40.
110. Simon AM, McWhorter AR. Vascular abnormalities in mice lacking the endothelial gap junction proteins connexin37 and connexin40. *Dev Biol.* Nov 15 2002;251(2):206-220.
111. Kwak BR, Mulhaupt F, Veillard N, et al. Altered pattern of vascular connexin expression in atherosclerotic plaques. *Arterioscler Thromb Vasc Biol.* Feb 1 2002;22(2):225-230.
112. Kwak BR, Veillard N, Pelli G, et al. Reduced connexin43 expression inhibits atherosclerotic lesion formation in low-density lipoprotein receptor-deficient mice. *Circulation.* Feb 25 2003;107(7):1033-1039.
113. Davies PF, Barbee KA, Volin MV, et al. Spatial relationships in early signaling events of flow-mediated endothelial mechanotransduction. *Annu Rev Physiol.* 1997;59:527-549.
114. Kwak BR, Silacci P, Stergiopulos N, et al. Shear stress and cyclic circumferential stretch, but not pressure, alter connexin43 expression in endothelial cells. *Cell Commun Adhes.* Jul-Dec 2005;12(5-6):261-270.
115. Watts SW, Webb RC. Vascular gap junctional communication is increased in mineralocorticoid-salt hypertension. *Hypertension.* Nov 1996;28(5):888-893.
116. Haefliger JA, Castillo E, Waeber G, et al. Hypertension increases connexin43 in a tissue-specific manner. *Circulation.* Feb 18 1997;95(4):1007-1014.
117. Meyer R, Malewicz B, Baumann WJ, et al. Increased gap junction assembly between cultured cells upon cholesterol supplementation. *J Cell Sci.* Jun 1990;96 (Pt 2):231-238.
118. Bastiaanse EM, Jongsma HJ, van der Laarse A, et al. Heptanol-induced decrease in cardiac gap junctional conductance is mediated by a decrease in the fluidity of membranous cholesterol-rich domains. *J Membr Biol.* Nov 1993;136(2):135-145.
119. Reaume AG, de Sousa PA, Kulkarni S, et al. Cardiac malformation in neonatal mice lacking connexin43. *Science.* Mar 24 1995;267(5205):1831-1834.
120. Guerrero PA, Schuessler RB, Davis LM, et al. Slow ventricular conduction in mice heterozygous for a connexin43 null mutation. *J Clin Invest.* Apr 15 1997;99(8):1991-1998.

121. Wong CW, Burger F, Pelli G, et al. Dual benefit of reduced Cx43 on atherosclerosis in LDL receptor-deficient mice. *Cell Commun Adhes.* Jul-Dec 2003;10(4-6):395-400.
122. Boerma M, Forsberg L, Van Zeijl L, et al. A genetic polymorphism in connexin 37 as a prognostic marker for atherosclerotic plaque development. *J Intern Med.* Aug 1999;246(2):211-218.
123. Yamada Y, Izawa H, Ichihara S, et al. Prediction of the risk of myocardial infarction from polymorphisms in candidate genes. *N Engl J Med.* Dec 12 2002;347(24):1916-1923.
124. Listi F, Candore G, Lio D, et al. Association between C1019T polymorphism of connexin37 and acute myocardial infarction: a study in patients from Sicily. *Int J Cardiol.* Jul 10 2005;102(2):269-271.
125. Hansson GK. Inflammation, atherosclerosis, and coronary artery disease. *N Engl J Med.* Apr 21 2005;352(16):1685-1695.
126. Libby P. Atherosclerosis: disease biology affecting the coronary vasculature. *Am J Cardiol.* Dec 18 2006;98(12A):3Q-9Q.
127. Lusis AJ, Fogelman AM, Fonarow GC. Genetic basis of atherosclerosis: part II: clinical implications. *Circulation.* Oct 5 2004;110(14):2066-2071.
128. Topol EJ. The genetics of heart attack. *Heart.* Jun 2006;92(6):855-861.
129. Miller DT, Ridker PM, Libby P, et al. Atherosclerosis: the path from genomics to therapeutics. *J Am Coll Cardiol.* Apr 17 2007;49(15):1589-1599.
130. Yeh HI, Chou Y, Liu HF, et al. Connexin37 gene polymorphism and coronary artery disease in Taiwan. *Int J Cardiol.* Dec 2001;81(2-3):251-255.
131. Wong CW, Christen T, Pfenniger A, et al. Do allelic variants of the connexin37 1019 gene polymorphism differentially predict for coronary artery disease and myocardial infarction? *Atherosclerosis.* Apr 2007;191(2):355-361.
132. Eriksson EE. Mechanisms of leukocyte recruitment to atherosclerotic lesions: future prospects. *Curr Opin Lipidol.* Oct 2004;15(5):553-558.
133. Galkina E, Ley K. Vascular adhesion molecules in atherosclerosis. *Arterioscler Thromb Vasc Biol.* Nov 2007;27(11):2292-2301.
134. Laird DW. Life cycle of connexins in health and disease. *Biochem J.* Mar 15 2006;394(Pt 3):527-543.
135. Koval M. Pathways and control of connexin oligomerization. *Trends Cell Biol.* Mar 2006;16(3):159-166.
136. Goodenough DA, Paul DL. Beyond the gap: functions of unpaired connexon channels. *Nat Rev Mol Cell Biol.* Apr 2003;4(4):285-294.
137. Thomas MA, Huang S, Cokoja A, et al. Interaction of connexins with protein partners in the control of channel turnover and gating. *Biol Cell.* Nov 2002;94(7-8):445-456.

138. Duffy HS, Delmar M, Spray DC. Formation of the gap junction nexus: binding partners for connexins. *J Physiol Paris.* Apr-Jun 2002;96(3-4):243-249.
139. Chanson M, Kwak BR. Connexin37: a potential modifier gene of inflammatory disease. *J Mol Med.* Aug 2007;85(8):787-795.
140. Kwak BR, Pepper MS, Gros DB, et al. Inhibition of endothelial wound repair by dominant negative connexin inhibitors. *Mol Biol Cell.* Apr 2001;12(4):831-845.
141. Bader P, Weingart R. Pitfalls when examining gap junction hemichannels: interference from volume-regulated anion channels. *Pflugers Arch.* Jul 2006;452(4):396-406.
142. Bader P, Weingart R. Conductive and kinetic properties of connexin45 hemichannels expressed in transfected HeLa cells. *J Membr Biol.* Jun 1 2004;199(3):143-154.
143. Desplantez T, Halliday D, Dupont E, et al. Cardiac connexins Cx43 and Cx45: formation of diverse gap junction channels with diverse electrical properties. *Pflugers Arch.* Jul 2004;448(4):363-375.
144. Bukauskas FF, Elfgang C, Willecke K, et al. Biophysical properties of gap junction channels formed by mouse connexin40 in induced pairs of transfected human HeLa cells. *Biophys J.* Jun 1995;68(6):2289-2298.
145. Ikehara T, Yamaguchi H, Hosokawa K, et al. Kinetic mechanism of ATP action in Na(+)-K(+)-Cl- cotransport of HeLa cells determined by Rb+ influx studies. *Am J Physiol.* Apr 1990;258(4 Pt 1):C599-609.
146. Chadjichristos CE, Matter CM, Roth I, et al. Reduced connexin43 expression limits neointima formation after balloon distension injury in hypercholesterolemic mice. *Circulation.* Jun 20 2006;113(24):2835-2843.
147. Jiang JX, Siller-Jackson AJ, Burra S. Roles of gap junctions and hemichannels in bone cell functions and in signal transmission of mechanical stress. *Front Biosci.* 2007;12:1450-1462.
148. Rodriguez-Sinovas A, Cabestrero A, Lopez D, et al. The modulatory effects of connexin 43 on cell death/survival beyond cell coupling. *Prog Biophys Mol Biol.* May-Jun 2007;94(1-2):219-232.
149. Pointis G, Fiorini C, Gilleron J, et al. Connexins as precocious markers and molecular targets for chemical and pharmacological agents in carcinogenesis. *Curr Med Chem.* 2007;14(21):2288-2303.
150. Cotrina ML, Lin JH, Alves-Rodrigues A, et al. Connexins regulate calcium signaling by controlling ATP release. *Proc Natl Acad Sci U S A.* Dec 22 1998;95(26):15735-15740.
151. Trexler EB, Bukauskas FF, Bennett MV, et al. Rapid and direct effects of pH on connexins revealed by the connexin46 hemichannel preparation. *J Gen Physiol.* May 1999;113(5):721-742.
152. Bukauskas FF, Verselis VK. Gap junction channel gating. *Biochim Biophys Acta.* Mar 23 2004;1662(1-2):42-60.

153. Banach K, Weingart R. Voltage gating of Cx43 gap junction channels involves fast and slow current transitions. *Pflugers Arch.* Jan 2000;439(3):248-250.
154. Trexler EB, Bennett MV, Bargiello TA, et al. Voltage gating and permeation in a gap junction hemichannel. *Proc Natl Acad Sci U S A.* Jun 11 1996;93(12):5836-5841.
155. Valiunas V, Weingart R. Electrical properties of gap junction hemichannels identified in transfected HeLa cells. *Pflugers Arch.* Jul 2000;440(3):366-379.
156. Lampe PD, Cooper CD, King TJ, et al. Analysis of Connexin43 phosphorylated at S325, S328 and S330 in normoxic and ischemic heart. *J Cell Sci.* Aug 15 2006;119(Pt 16):3435-3442.
157. Puljung MC, Berthoud VM, Beyer EC, et al. Polyvalent cations constitute the voltage gating particle in human connexin37 hemichannels. *J Gen Physiol.* Nov 2004;124(5):587-603.
158. Kumari SS, Varadaraj K, Valiunas V, et al. Functional expression and biophysical properties of polymorphic variants of the human gap junction protein connexin37. *Biochem Biophys Res Commun.* Jul 21 2000;274(1):216-224.
159. Lanfear DE, Jones PG, Marsh S, et al. Connexin37 (GJA4) genotype predicts survival after an acute coronary syndrome. *Am Heart J.* Sep 2007;154(3):561-566.
160. Willecke K, Heynkes R, Dahl E, et al. Mouse connexin37: cloning and functional expression of a gap junction gene highly expressed in lung. *J Cell Biol.* Sep 1991;114(5):1049-1057.
161. Reed KE, Westphale EM, Larson DM, et al. Molecular cloning and functional expression of human connexin37, an endothelial cell gap junction protein. *J Clin Invest.* Mar 1993;91(3):997-1004.
162. Pohl U, de Wit C. A Unique Role of NO in the Control of Blood Flow. *News Physiol Sci.* Apr 1999;14:74-80.
163. Yang Z, Ming XF. Recent advances in understanding endothelial dysfunction in atherosclerosis. *Clin Med Res.* Mar 2006;4(1):53-65.
164. Liu VW, Huang PL. Cardiovascular roles of nitric oxide: a review of insights from nitric oxide synthase gene disrupted mice. *Cardiovasc Res.* Jan 2008;77(1):19-29.
165. Duffy HS, Sorgen PL, Girvin ME, et al. pH-dependent intramolecular binding and structure involving Cx43 cytoplasmic domains. *J Biol Chem.* Sep 27 2002;277(39):36706-36714.
166. Shibayama J, Lewandowski R, Kieken F, et al. Identification of a novel peptide that interferes with the chemical regulation of connexin43. *Circ Res.* Jun 9 2006;98(11):1365-1372.
167. Salamon Z, Macleod HA, Tollin G. Surface plasmon resonance spectroscopy as a tool for investigating the biochemical and biophysical

properties of membrane protein systems. II: Applications to biological systems. *Biochim Biophys Acta.* Sep 8 1997;1331(2):131-152.

168. Lang BD DM, Coombs W. . Surface plasmon resonance as a method to study the kinetics and amplitude of protein-protein binding. *Practical Methods in Cardiovasc Research.* 2005:936-947.

169. Hirst-Jensen BJ, Sahoo P, Kieken F, et al. Characterization of the pH-dependent interaction between the gap junction protein connexin43 carboxyl terminus and cytoplasmic loop domains. *J Biol Chem.* Feb 23 2007;282(8):5801-5813.

170. Sorgen PL, Duffy HS, Spray DC, et al. pH-dependent dimerization of the carboxyl terminal domain of Cx43. *Biophys J.* Jul 2004;87(1):574-581.

171. Alderton WK, Cooper CE, Knowles RG. Nitric oxide synthases: structure, function and inhibition. *Biochem J.* Aug 1 2001;357(Pt 3):593-615.

172. Fleming I, Busse R. Molecular mechanisms involved in the regulation of the endothelial nitric oxide synthase. *Am J Physiol Regul Integr Comp Physiol.* Jan 2003;284(1):R1-12.

173. van Rijen HV, van Kempen MJ, Postma S, et al. Tumour necrosis factor alpha alters the expression of connexin43, connexin40, and connexin37 in human umbilical vein endothelial cells. *Cytokine.* Apr 1998;10(4):258-264.

174. Yeh HI, Lu CS, Wu YJ, et al. Reduced expression of endothelial connexin37 and connexin40 in hyperlipidemic mice: recovery of connexin37 after 7-day simvastatin treatment. *Arterioscler Thromb Vasc Biol.* Aug 1 2003;23(8):1391-1397.

175. Yeh HI, Lee PY, Su CH, et al. Reduced expression of endothelial connexins 43 and 37 in hypertensive rats is rectified after 7-day carvedilol treatment. *Am J Hypertens.* Feb 2006;19(2):129-135.

176. Isakson BE, Kronke G, Kadl A, et al. Oxidized phospholipids alter vascular connexin expression, phosphorylation, and heterocellular communication. *Arterioscler Thromb Vasc Biol.* Oct 2006;26(10):2216-2221.

177. Kwak BR, Hermans MM, De Jonge HR, et al. Differential regulation of distinct types of gap junction channels by similar phosphorylating conditions. *Mol Biol Cell.* Dec 1995;6(12):1707-1719.

178. Van Rijen H, van Kempen MJ, Analbers LJ, et al. Gap junctions in human umbilical cord endothelial cells contain multiple connexins. *Am J Physiol.* Jan 1997;272(1 Pt 1):C117-130.

179. Ghosh S, Jain A, Mukherjee B, et al. The host factor polyhedrin promoter binding protein (PPBP) is involved in transcription from the baculovirus polyhedrin gene promoter. *J Virol.* Sep 1998;72(9):7484-7493.

180. Virmani R, Kolodgie FD, Burke AP, et al. Atherosclerotic plaque progression and vulnerability to rupture: angiogenesis as a source of

intraplaque hemorrhage. *Arterioscler Thromb Vasc Biol.* Oct 2005;25(10):2054-2061.

181. Libby P, Theroux P. Pathophysiology of coronary artery disease. *Circulation.* Jun 28 2005;111(25):3481-3488.

182. Tedgui A, Mallat Z. Cytokines in atherosclerosis: pathogenic and regulatory pathways. *Physiol Rev.* Apr 2006;86(2):515-581.

183. Newby AC. Dual role of matrix metalloproteinases (matrixins) in intimal thickening and atherosclerotic plaque rupture. *Physiol Rev.* Jan 2005;85(1):1-31.

184. Wayhs R, Zelinger A, Raggi P. High coronary artery calcium scores pose an extremely elevated risk for hard events. *J Am Coll Cardiol.* Jan 16 2002;39(2):225-230.

185. Budoff MJ, Ahmed V, Gul KM, et al. Coronary anomalies by cardiac computed tomographic angiography. *Clin Cardiol.* Nov 2006;29(11):489-493.

186. Shao JS, Cai J, Towler DA. Molecular mechanisms of vascular calcification: lessons learned from the aorta. *Arterioscler Thromb Vasc Biol.* Jul 2006;26(7):1423-1430.

187. Hsu JJ, Tintut Y, Demer LL. Murine models of atherosclerotic calcification. *Curr Drug Targets.* Mar 2008;9(3):224-228.

188. Danilevicius CF, Lopes JB, Pereira RM. Bone metabolism and vascular calcification. *Braz J Med Biol Res.* Apr 2007;40(4):435-442.

189. Yang YH, Dudoit S, Luu P, et al. Normalization for cDNA microarray data: a robust composite method addressing single and multiple slide systematic variation. *Nucleic Acids Res.* Feb 15 2002;30(4):e15.

190. Cope LM, Irizarry RA, Jaffee HA, et al. A benchmark for Affymetrix GeneChip expression measures. *Bioinformatics.* Feb 12 2004;20(3):323-331.

191. Smyth GK. Linear models and empirical bayes methods for assessing differential expression in microarray experiments. *Stat Appl Genet Mol Biol.* 2004;3:Article3.

192. Bobik A. Transforming growth factor-betas and vascular disorders. *Arterioscler Thromb Vasc Biol.* Aug 2006;26(8):1712-1720.

193. Shao JS, Aly ZA, Lai CF, et al. Vascular Bmp Msx2 Wnt signaling and oxidative stress in arterial calcification. *Ann N Y Acad Sci.* Nov 2007;1117:40-50.

194. Davies MR, Lund RJ, Hruska KA. BMP-7 is an efficacious treatment of vascular calcification in a murine model of atherosclerosis and chronic renal failure. *J Am Soc Nephrol.* Jun 2003;14(6):1559-1567.

195. Chadjichristos CE, Morel S, Derouette JP, et al. Targeting connexin 43 prevents platelet-derived growth factor-BB-induced phenotypic change in porcine coronary artery smooth muscle cells. *Circ Res.* Mar 28 2008;102(6):653-660.

196. Healy AM, Pickard MD, Pradhan AD, et al. Platelet expression profiling and clinical validation of myeloid-related protein-14 as a novel determinant of cardiovascular events. *Circulation.* May 16 2006;113(19):2278-2284.
197. Wall ST, Walker JC, Healy KE, et al. Theoretical impact of the injection of material into the myocardium: a finite element model simulation. *Circulation.* Dec 12 2006;114(24):2627-2635.
198. Jeng AY, Chou M, Sawyer WK, et al. Enhanced expression of matrix metalloproteinase-3, -12, and -13 mRNAs in the aortas of apolipoprotein E-deficient mice with advanced atherosclerosis. *Ann N Y Acad Sci.* Jun 30 1999;878:555-558.
199. Deguchi JO, Aikawa E, Libby P, et al. Matrix metalloproteinase-13/collagenase-3 deletion promotes collagen accumulation and organization in mouse atherosclerotic plaques. *Circulation.* Oct 25 2005;112(17):2708-2715.
200. Ye S. Influence of matrix metalloproteinase genotype on cardiovascular disease susceptibility and outcome. *Cardiovasc Res.* Feb 15 2006;69(3):636-645.
201. Yoon S, Kuivaniemi H, Gatalica Z, et al. MMP13 promoter polymorphism is associated with atherosclerosis in the abdominal aorta of young black males. *Matrix Biol.* Oct 2002;21(6):487-498.
202. Brinckerhoff CE, Matrisian LM. Matrix metalloproteinases: a tail of a frog that became a prince. *Nat Rev Mol Cell Biol.* Mar 2002;3(3):207-214.
203. Visse R, Nagase H. Matrix metalloproteinases and tissue inhibitors of metalloproteinases: structure, function, and biochemistry. *Circ Res.* May 2 2003;92(8):827-839.
204. Luttun A, Lutgens E, Manderveld A, et al. Loss of matrix metalloproteinase-9 or matrix metalloproteinase-12 protects apolipoprotein E-deficient mice against atherosclerotic media destruction but differentially affects plaque growth. *Circulation.* Mar 23 2004;109(11):1408-1414.
205. Gough PJ, Gomez IG, Wille PT, et al. Macrophage expression of active MMP-9 induces acute plaque disruption in apoE-deficient mice. *J Clin Invest.* Jan 2006;116(1):59-69.
206. McCormick MM, Rahimi F, Bobryshev YV, et al. S100A8 and S100A9 in human arterial wall. Implications for atherogenesis. *J Biol Chem.* Dec 16 2005;280(50):41521-41529.
207. Elfgang C, Eckert R, Lichtenberg-Frate H, et al. Specific permeability and selective formation of gap junction channels in connexin-transfected HeLa cells. *J Cell Biol.* May 1995;129(3):805-817.
208. Steinberg TH, Civitelli R, Geist ST, et al. Connexin43 and connexin45 form gap junctions with different molecular permeabilities in osteoblastic cells. *Embo J.* Feb 15 1994;13(4):744-750.

209. Kruger O, Beny JL, Chabaud F, et al. Altered dye diffusion and upregulation of connexin37 in mouse aortic endothelium deficient in connexin40. *J Vasc Res.* Mar-Apr 2002;39(2):160-172.
210. Seul KH, Kang KY, Lee KS, et al. Adenoviral delivery of human connexin37 induces endothelial cell death through apoptosis. *Biochem Biophys Res Commun.* Jul 9 2004;319(4):1144-1151.
211. Wang M, Martinez AD, Berthoud VM, et al. Connexin43 with a cytoplasmic loop deletion inhibits the function of several connexins. *Biochem Biophys Res Commun.* Aug 12 2005;333(4):1185-1193.
212. Kyle JW, Minogue PJ, Thomas BC, et al. An intact connexin N-terminus is required for function but not gap junction formation. *J Cell Sci.* Aug 15 2008;121(Pt 16):2744-2750.
213. Flagg-Newton J, Simpson I, Loewenstein WR. Permeability of the cell-to-cell membrane channels in mammalian cell juncton. *Science.* Jul 27 1979;205(4404):404-407.
214. Neyton J, Trautmann A. Single-channel currents of an intercellular junction. *Nature.* Sep 26-Oct 2 1985;317(6035):331-335.
215. Imanaga I, Kameyama M, Irisawa H. Cell-to-cell diffusion of fluorescent dyes in paired ventricular cells. *Am J Physiol.* Jan 1987;252(1 Pt 2):H223-232.
216. Weber PA, Chang HC, Spaeth KE, et al. The permeability of gap junction channels to probes of different size is dependent on connexin composition and permeant-pore affinities. *Biophys J.* Aug 2004;87(2):958-973.
217. Takens-Kwak BR, Jongsma HJ. Cardiac gap junctions: three distinct single channel conductances and their modulation by phosphorylating treatments. *Pflugers Arch.* Nov 1992;422(2):198-200.
218. Kwak BR, Saez JC, Wilders R, et al. Effects of cGMP-dependent phosphorylation on rat and human connexin43 gap junction channels. *Pflugers Arch.* Sep 1995;430(5):770-778.
219. van Veen AA, van Rijen HV, Opthof T. Cardiac gap junction channels: modulation of expression and channel properties. *Cardiovasc Res.* Aug 1 2001;51(2):217-229.
220. Moreno AP, Fishman GI, Spray DC. Phosphorylation shifts unitary conductance and modifies voltage dependent kinetics of human connexin43 gap junction channels. *Biophys J.* Apr 1992;62(1):51-53.
221. Zaragosi LE, Wdziekonski B, Fontaine C, et al. Effects of GSK3 inhibitors on in vitro expansion and differentiation of human adipose-derived stem cells into adipocytes. *BMC Cell Biol.* 2008;9:11.
222. Ramanan SV, Valiunas V, Brink PR. Non-stationary fluctuation analysis of macroscopic gap junction channel records. *J Membr Biol.* May 2005;205(2):81-88.
223. Ramanan SV, Brink PR, Varadaraj K, et al. A three-state model for connexin37 gating kinetics. *Biophys J.* May 1999;76(5):2520-2529.

224. Spray DC, Ye ZC, Ransom BR. Functional connexin "hemichannels": a critical appraisal. *Glia.* Nov 15 2006;54(7):758-773.
225. Arcuino G, Lin JH, Takano T, et al. Intercellular calcium signaling mediated by point-source burst release of ATP. *Proc Natl Acad Sci U S A.* Jul 23 2002;99(15):9840-9845.
226. Stout CE, Costantin JL, Naus CC, et al. Intercellular calcium signaling in astrocytes via ATP release through connexin hemichannels. *J Biol Chem.* Mar 22 2002;277(12):10482-10488.
227. Gomes P, Srinivas SP, Van Driessche W, et al. ATP release through connexin hemichannels in corneal endothelial cells. *Invest Ophthalmol Vis Sci.* Apr 2005;46(4):1208-1218.
228. Zhao HB, Yu N, Fleming CR. Gap junctional hemichannel-mediated ATP release and hearing controls in the inner ear. *Proc Natl Acad Sci U S A.* Dec 20 2005;102(51):18724-18729.
229. Ye ZC, Wyeth MS, Baltan-Tekkok S, et al. Functional hemichannels in astrocytes: a novel mechanism of glutamate release. *J Neurosci.* May 1 2003;23(9):3588-3596.
230. Sabirov RZ, Dutta AK, Okada Y. Volume-dependent ATP-conductive large-conductance anion channel as a pathway for swelling-induced ATP release. *J Gen Physiol.* Sep 2001;118(3):251-266.
231. Suadicani SO, Brosnan CF, Scemes E. P2X7 receptors mediate ATP release and amplification of astrocytic intercellular Ca2+ signaling. *J Neurosci.* Feb 1 2006;26(5):1378-1385.
232. Pangrsic T, Potokar M, Stenovec M, et al. Exocytotic release of ATP from cultured astrocytes. *J Biol Chem.* Sep 28 2007;282(39):28749-28758.
233. Haussig S, Schubert A, Mohr FW, et al. Sub-chronic nicotine exposure induces intercellular communication failure and differential down-regulation of connexins in cultured human endothelial cells. *Atherosclerosis.* Jan 2008;196(1):210-218.
234. Muscella A, Elia MG, Greco S, et al. Activation of P2Y2 purinoceptor inhibits the activity of the Na+/K+-ATPase in HeLa cells. *Cell Signal.* Jan 2003;15(1):115-121.
235. Ming Yi JDH, Jonathan C Cohen, Helen H Hobbsand and Robert M Stephens. WholePathwayScope: a comprehensive pathway-based analysis tool for high-throughput data. *BMC Bioinformatics.* 19 January 2006 2006;7.